

**December 3, 2021**

**ICE, CLOUD, and Land Height Satellite  
(ICESat-2) Project**

**Algorithm Theoretical Basis Document  
(ATBD)  
for  
Ocean Surface Height  
Release 5**

**Prepared By:  
ICESat-2 Science Definition Team Ocean Working Group**

**Contributors**

**James Morison  
David Hancock  
Suzanne Dickinson  
John Robbins  
Leeanne Roberts  
Ron Kwok  
Steve Palm  
Ben Smith  
Mike Jasinski  
Bill Plant  
Tim Urban**

**/Code:**



---

**Goddard Space Flight Center  
Greenbelt, Maryland**

## **Abstract**

This document describes the theoretical basis of the ocean processing algorithms and the products that are produced by the ICESat-2 mission. It includes descriptions of the parameters that are provided in each product as well as ancillary geophysical parameters, which are used in the derivation of these ICESat-2 products.

*ICESat-2 Algorithm Theoretical Basis Document for Ocean Surface Height  
Release 005*

## **CM Foreword**

This document is an Ice, Cloud, and Land Height (ICESat-2) Project Science Office controlled document. Changes to this document require prior approval of the Science Development Team ATBD Lead or designee. Proposed changes shall be submitted in the ICESat-II Management Information System (MIS) via a Signature Controlled Request (SCoRe), along with supportive material justifying the proposed change.

In this document, a requirement is identified by “shall,” a good practice by “should,” permission by “may” or “can,” expectation by “will,” and descriptive material by “is.”

Questions or comments concerning this document should be addressed to:

ICESat-2 Project Science Office

Mail Stop 615

Goddard Space Flight Center

Greenbelt, Maryland 20771

*ICESat-2 Algorithm Theoretical Basis Document for Ocean Surface Height*

*Release 005*

## **Preface**

This document is the Algorithm Theoretical Basis Document for the processing open ocean data to be implemented at the ICESat-2 Science Investigator-led Processing System (SIPS). The SIPS supports the ATLAS (Advance Topographic Laser Altimeter System) instrument on the ICESat-2 Spacecraft and encompasses the ATLAS Science Algorithm Software (ASAS) and the Scheduling and Data Management System (SDMS). The science algorithm software will produce Level 0 through Level 4 standard data products as well as the associated product quality assessments and metadata information.

The ICESat-2 Science Development Team, in support of the ICESat-2 Project Science Office (PSO), assumes responsibility for this document and updates it, as required, as algorithms are refined or to meet the needs of the ICESat-2 SIPS. Reviews of this document are performed when appropriate and as needed updates to this document are made. Changes to this document will be made by complete revision.

Changes to this document require prior approval of the Change Authority listed on the signature page. Proposed changes shall be submitted to the ICESat-2 PSO, along with supportive material justifying the proposed change.

Questions or comments concerning this document should be addressed to:

Tom Neumann, ICESat-2 Project Scientist  
Mail Stop 615  
Goddard Space Flight Center  
Greenbelt, Maryland 20771

*ICESat-2 Algorithm Theoretical Basis Document for Ocean Surface Height*

*Release 005*

## **Review/Approval Page**

**Prepared by:**

*Jamie*  
<Enter Position Title Here>  
Org/Address

**Reviewed by:**

*Bea*  
<Enter Position Title Here>  
<Enter Org/Code Here>

*Tom*  
<Enter Position Title Here>  
<Enter Org/Code Here>

**Approved by:**

*Thorsten*  
<Enter Position Title Here>  
<Enter Org/Code Here>

**\*\*\* Signatures are available on-line at: [https:// /icesatiimis.gsfc.nasa.gov](https://icesatiimis.gsfc.nasa.gov) \*\*\***

### Change History Log

| Revision Level | Description of Change   | SCoRe No.       | Date Approved |
|----------------|---|-----------------|---------------|
|                | <p>Initial Release<br/>7/27/2019 Section 5.3.4.1 code steps A: replace <i>snoothrechist</i> with <i>smoothrechist</i></p> <p>7/30/2019 – globally replace term Maximum Likelihood with Expectation Maximization to clarify that the Matlab developmental code and the ASAS FORTRAN code both use expectation maximization.</p> <p>7/30/2019 Change the third paragraph of 5.3.4.2 (H) to:<br/>- To apply the expectation maximization approach, we first derive a sea surface height spatial series from the height distribution <math>Y</math>, which is defined over a range of heights the same as the received height histogram (i.e., <i>jlow</i> to <i>jhigh</i> from surface finding). This is accomplished by first multiplying <math>Y</math> by 10,000, rounding and deleting any values less than or equal to zero (a few unrealistic weakly negative values to occur in <math>Y</math> associated with the Weiner deconvolution process) to produce an integer distribution, <math>YI</math>. A series, <math>XY</math>, is assembled by concatenating for each value of <math>YI(i)</math> for index <math>i</math> corresponding to height <i>sshx(i)</i>, <math>YI(i)</math> values equal to <i>sshx(i)</i>. The shift to heights including <i>meanoffit2</i> was accomplished in developmental code by adding <i>meanoffit2</i> to each value in <math>XY</math>. (ASAS FORTRAN code does not add <i>meanoffit2</i> at this point but after the Gaussian Mixture calculation.)</p> <p>7/30/2019 Add <i>xbind</i> as an output variable in 5.3.3 (14) and at the end of 5.3.3<br/>To Table 6 add:<br/><i>xbind</i> = 1 x 710 element array of 10-m bin averages of along-track distance<br/>And change the description of <i>xbin</i> to:<br/>“Center of 1 x 710 element array of 10-m bins. Note this may be included as a data description or other static array equal to [5, 15, 25, 35 ..... 7095 m]</p> <p>7/30/2019 In Table 6 changed from 700 10-m bins to 710 10-m bins to account for ocean segments longer than 7,000 m</p> | <p>GG<br/>G</p> |               |

|   |  |  |
|---|--|--|
| <p>7/30/2019 Change 5.3.4.1 (G) points 1-4 to:</p> <p>“The surface histogram should be the same length and have the same horizontal (height) axis as the received histogram, <i>rechist</i>. In this we compute the distribution of surface height as a probability density function (PDF), <i>Y</i>, starting with the Fourier transform of that PDF output by the Weiner deconvolution. The steps are:</p> <ol style="list-style-type: none"> <li>1. Compute <i>Yfi</i>, as the inverse Fourier Transform of <i>Yf</i> divided by <i>binsize</i>. <i>Yfi</i> as it comes from the inverse Fourier transform is <i>NFFT</i> points long with the first half appearing displaced to the end of the array. We reorder this by first putting the last <i>NFFT/2</i> points ahead of the first <i>NFFT/2</i> points. To establish the surface height probability density function, <i>Y</i>, we then remove the first (<i>rzbin-1</i>) points where <i>rzbin</i> is the index of the centroid (height equals zero) index of the received histogram. We keep as <i>Y</i> the remaining points equal to the length of the <i>rechist</i>. In the case of the ASAS FORTRAN code, which pads each end of <i>rechist</i> to reach heights of <math>\pm 15</math> m, <i>rzbin</i> is the center bin of <i>rechist</i>.</li> <li>2. Set the x-axis of <i>Y</i>, <i>derivedsshx</i> equal to the x-axis, <i>xrechist</i>, of the received histogram <i>rechist</i>.”</li> </ol> <p>7/30/2019 Clarify bin centering in 5.3.1 (B) by changing (B) to:</p> <p>“Establish an initial coarse histogram array, <i>H<sub>c</sub></i>, spanning <math>\pm 15</math> m with bin size <i>B<sub>1</sub></i> equal to 0.01 m with center bin centered at zero and bin centers at whole centimeters. Also establish a data array, <i>A<sub>coarse</sub></i>, for up to 10,000 photon heights and associated information (index, geolocation, time) plus noise photon counts. This will be populated with data as we step through 14-geobin segments searching for an adequate number of surface photon candidates.”</p> <p>and change 5.3.2 (A) to:</p> <p>“Set up for the surface finding histogram, <i>N</i>, by establishing the vector, <i>Edges</i>, (with a length one greater than <i>N</i>) of histogram bin edges with bins <i>Bf</i> wide between -15 m to +15 m. Also establish the vector, <i>Ctrpt</i>, of bin center points with length equal to <i>N</i>. In practice <i>Bf</i> equals 1 cm, <i>Ctrpt</i> values are whole centimeters, and <i>Edges</i> are at half centimeter values. Also establish a vector array, <i>BinB</i>, as long as <i>ht_initial</i> for bin assignments.”</p> |  |  |
|---|--|--|

|  |   |  |  |
|--|---|--|--|
|  | <p>8/6/2019 Change 5.3.4.1 (G) near the end from</p> <p>“<b>Y</b> is defined over a vector of bin centers, <b>sshx</b>, but <b>Y</b> will be output as a 1001 element vector for every segment with the 501<sup>st</sup> center bin being for height zero, bin <math>501 - Y_{low}X/binsize</math> being the lowest bin with nonzero <b>Y</b> and bin <math>501 + Y_{low}X/binsize</math> being the highest bin with nonzero <b>Y</b>.”</p> <p>To</p> <p>“<b>Y</b> is defined over a vector of bin centers, <b>sshx</b>, but for <b>binsize</b> = 1 cm <b>Y</b> will be output as a 3001-element vector from -15 m to +15 m for every segment with the 1,501<sup>st</sup> center bin being for height zero. Values will be zero for bins outside the range of <b>sshx</b>. Owing to noise and the effect of the FFT-deconvolution-inverse-FFT process, small negative values occur in <b>Y</b> within the range of <b>sshx</b>. These will be set to zero in the output <b>Y</b> vector.”</p> <p>8/28/2019 Replace section 5.3.3 to use simplified and more robust method of computing photon return rate in SSB calculation: <math>xrbin = nbind/10</math></p> <p>9/9/2019 in 5.3.3 7. - Add clause to end of sentence to clarify using only bins with photons for ssb calculation, i.e.,</p> <p>7. Compute, <b>binAVG_Xr</b>, the average of binned data rate, <b>xrbin</b>, over the 10-m bins with photons.</p> <p>11/5/2019 Modified 5.3.2 to change surface finding based on the distribution of photon heights to surface finding based on the photon height anomaly relative to a moving bin average of high confidence photon heights. This is done to exclude subsurface returns under the crests of surface waves that otherwise fall inside the histogram of true surface heights. Added to Table 5 <b>conf_lim</b>, the limiting confidence level to be included in the moving bin average, <b>nphoton</b>, the number of photons either side of a central photon to be included in the moving bin average, e.g., for <b>nphoton</b>=10, a 21 point average is used</p> <p>11/18/2019 Added section 5.3.3.2 to compute <b>nharms+1</b> harmonic coefficients, <b>a</b>, of surface height for surface waves and possible relation to degrees of freedom and uncertainty. Added to Table 5 <b>nharms</b> and added to Table 6 <b>wn</b> and <b>a.wn</b> is a vector of <b>nharms</b> wavenumbers. <b>a(1)</b> is the coefficient for the zero</p> |  |  |
|--|---|--|--|

|  |  |  |  |
|--|--|--|--|
|  | <p>wavenumber component of the fit to test if this is a more stable estimate of average heights. <math>a(3,5,7,..2*nharms+1)</math> are sine coefficients for <math>wn(1,2,3,..nharms)</math>. <math>a(2,4,6,..2*nharms+1)</math> are cosine coefficients for <math>wn(1,2,3,..nharms)</math>.</p> <p><b>11/27/2019</b> Added a section to the end of 5.3.6.1 to estimate the effective number of degrees of freedom, <b><i>NP_effect</i></b>, and associated uncertainty, <b><i>h_uncrtn</i></b>, in sea surface height over an ocean segment. The estimates are based on the integral of autocorrelation of 10-m bin average surface height. Added <b><i>h_uncrtn</i></b> and <b><i>NP_effect</i></b> to Table 6.</p> <p>12/19/2019 Removed (or corresponding <b><i>ht_initial, really?</i></b>) from 5.3.2(D)</p> <p>12/19/2019 Added the sentence: “The received histogram, <b><i>Nrs</i></b>, is then the histogram of <b><i>ht_initial2_surf</i></b> only including from the lowest height with count&gt;0 to the highest height with count&gt;0.” to 5.3.2 (P) to clarify that though the histogram of height anomalies, <b><i>N</i></b>, is used for surface finding, we look to the corresponding histogram of heights, <b><i>Nrs</i></b>, for the rest of the analysis. In a later section we form the probability density function, <b><i>rechist</i></b>, from <b><i>Nrs</i></b> and pass it on to have the instrument impulse response removed and statistics of sea surface height computed.</p> <p>12/19/2019 Pursuant to the change immediately above we changed the first sentence of 5.3.4.1 (A) “Start with the histogram of surface reflected photons heights, <b><i>N</i></b>, from section (5.3.2 (M)) versus the ...”<br/>to,<br/>” Start with the histogram of surface reflected photons heights, <b><i>Nrs</i></b>, from section (5.3.2 (P)) versus the ...”</p> <p>02/06/2020: Corrected 5.3.3.2 paragraph 4) to properly include <b><i>ht_initial2_surf</i></b> in the derivation of harmonic coefficients:</p> <p>4) For <b><i>y</i></b> equal to the column vector of <b><i>ht_initial2_surf</i></b> with <b><i>meanoffit2</i></b> added to it, compute the vector of harmonic coefficients, <b><i>a</i></b>, by the Vericek least squared error or left pseudo inverse method, where</p> <p><math>a = F'F \backslash F'y</math>. The <b><i>m</i></b> x 1 vector of harmonic coefficients, <b><i>a</i></b>, for</p> |  |  |
|--|--|--|--|



|  |  |  |
|--|--|--|
| <p>“Start with <math>Lscale = 0</math> and at <math>i = 1</math> where the corresponding lag, <math>l</math>, is zero, and <math>R_L(i)=1</math>. Increment <math>i</math> and the corresponding <math>l</math> by 1 and keep adding to <math>Lscale</math> while <math>R_L(i+1)</math> is greater than zero, i.e.,</p> $Lscale=Lscale + ( (1-l/Nbin10)*R_L(i) + (1-(l+1)/Nbin10)*R_L(i+1))/2$ <p>When <math>R_L(i+1)</math> becomes less than zero, terminate the integration by essentially assuming <math>R_L(i+1)</math> is zero, i.e.,</p> $Lscale=Lscale + (1-l/Nbin10)*R_L(i))/2$ “ <p>Also added <math>Lscale</math> and <math>Nbin10</math> to Output Table 6.</p> <p>4/17/2020 – Modified 3.2 Grif=ded Sea Surface Height (ATL19) to allow for merging ATL10 with ATL12 data in the polar oceans.</p> <p>4/17/2020 – Modified 4.5 and Figure 13 to add computing averages of SSH moments weighted by degrees of freedom.</p> <p>4/20/2020 – In Table 6 ATL12 Outputs, change the name of photon noise rate, <i>photonns_rate</i>, to <i>photon_noise_rate</i> to avoid confusion with photon rate, <i>Photon_rate</i>.</p> <p>4/20/2020 – Inserted as section 5.5, a description the gridding process including 5.6.1 Grids 5.6.2 Inputs bto Gridding, and Table 7 of inputs from ATL12.</p> <p>5/2/2020 Edited 5.3.6.1 paragraphs a) and b) to make it clear that we use the lagged covariance <math>COV_L</math>, and lagged autocorrelation, <math>R_L</math>, of binned surface height are used from lag, <math>l</math>, equal to 0 to the length of the record. This included standardizing the spelling the lag=dependent variables as <math>COV_L</math> and <math>R_L</math>.</p> <p>5/7/2020 Changed Section 5.3.2 (B) <i>conf_lim</i> from 4 to 3. Now it reads “For example, in testing we used <i>nphotons</i> = 5 and <i>conf_lim</i> = 3 to make an 11-point running average centered on each photon height, and included in each average, only heights with confidence level 3 and 4.</p> <p>5/7/2020 and 5/8/2020 Edited section 5.6 Gridding to include missing variables, regularize variable naming for averaged</p> |  |  |
|--|--|--|

|  |   |  |  |
|--|---|--|--|
|  | <p>(<i>_avg</i>) and degree-of-freedom weighted averaged (<i>_dfw</i>) variables. Added Appendix, a hierarchy of ATL12 and ATL19 variables.</p> <p>5/19/2020 In the ATL19 section changed <i>dot_sig_albm</i> to <i>dot_sigma_dfwalbm</i> as a better descriptor.</p> <p>5/19/2020 Substituted Dickenson’s Table 6 edited to have correct folder labels and to be consistent with ATL12 output names and folders.</p> <p>5/19/2020 Added folder headings to Table 7 to be consistent with edited Table 6 and made small edits to ATL19 to emphasize we would perform analyses er each strong beam until the all-beam combination.</p> <p>6/6/2020 added <i>n_ttl_photon</i> to Table 7 inputs to ATL-19 gridding.</p> <p>6/6/2020, added a paragraph to 5.19.4.1 to explain computation of grid cell-total surface photons, total photons, surface photon rate and noise photon rate. Also added a paragraph to 5.19.5 to explain computation of all-beam-total surface photons, total photons, surface photon rate and noise photon rate.</p> <p>6/6/2020, added the grid cell total and all-beam grid cell total surface photon and all photon counts and photon rate and noise photon rate to Table 8 ATL19 Outputs.</p> <p>6/6/2020 In response to Hancock “Photo select” email June 3, 2020, edited 4.2.1.1 on page 57 to clear up ambiguities in the use of the downlink band and confidence level from ATL03 to select candidate photons for the ATL12 surface finding routine.</p> <p>6/29/2020 Edit 3.1.3.4 to distinguish between tide corrections already in ATL03 photon heights and those to be made in ATL12, Also emphasized the ATL03 solid earth tides are in a tide-free reference system as opposed to a mean-tide system, and for ATL12 this is appropriate when the ocean tides are added.</p> <p>6/29/2020 Added to 4.2.1.1 and 5.2.1 sentences to include exclusion of data for which the pointing and orbit determination are suspect: “As of Release 3, the ATL03 includes a flag for each</p> |  |  |
|--|---|--|--|

|   |  |  |
|---|--|--|
| <p>ground tract indicating the quality of the precision orbit and pointing determination: <i>gtx/geolocation/podppd_flag</i>, and we have found unrealistic values for ocean segments when this flag is non-zero indicating degraded orbit and/or pointing data. Consequently ATL12 processing should only be done with data for which <i>gtx/geolocation/podppd_flag=0</i>.” Also added which <i>podppd_flag</i> to Table 2.</p> <p>6/29/2020 Added to 5.3.3.1 (5) averaged variables</p> <ul style="list-style-type: none"> <li>- Set <i>latbind</i> to the mean of photon latitude in each 10-m bin.</li> <li>- Set <i>lonbind</i> to the mean of photon longitude in each 10-m bin</li> </ul> <p>Also added <i>latbind</i> and <i>lonbind</i> to Table 6, ATL12 Outputs</p> <p>6/29/2020 Added a data editing paragraph to 5.19.2</p> <p>“We find that for reasons that we are investigating, ATL12 produces some ocean segment heights that are unrealistic compared to the geoid. Consequently, prior to inclusion in the gridding process, each ATL12 ocean granule is to be edited of ocean segment heights, <i>h</i>, that do not survive a 2-pass 3-sigma filter on dynamic ocean topography equal to <i>h-geoid_seg</i>. For each granule compute the standard deviation and mean of <i>h-geoid_seg</i>. On the first pass any ocean segment for which the magnitude of <i>h-geoid_seg</i> – mean(<i>h-geoid_seg</i>) &gt; 3 x std(<i>h-geoid_seg</i>) should be eliminated from the input data and the standard deviation of the remain <i>h-geoid_seg</i> re-computed from the first-pass edited data. The editing process is then repeated with any ocean segment from the first for which the magnitude of <i>h-geoid_seg</i> minus the re-computed mean(<i>h-geoid_seg</i>) &gt; 3 x re-computed std(<i>h-geoid_seg</i>) should be eliminated from the data to be input to the gridding process. “</p> <p>6/30/2020 - Section 3.1.3.1 Added explanation of ATL03 Release 4 changing the geoid provided to a tide-free EGM2008 in place of the mean-tide EGM2008 provided in earlier releases. Also noted ATL03 all will now include the conversion from tide-free to mean-tide geoid.</p> <p>6/30/2020 Table 2, Inputs from ATL03, Added <i>geoid</i> and <i>geoid_free2mean</i> conversion factor to table</p> <p>6/30/2020 Table 6 Outputs and Table 9, added specification that <i>earth_tide_seg</i> would be in the tide-free system</p> |  |  |
|---|--|--|

|  |  |  |
|--|--|--|
| <p>6/30/2020 Section 4.2.1.2 – Added specification that ATL03 geoid would now be in the tide-free system and require conversion to mean-tide with the provided conversion factor.</p> <p>6/30/2020 Section 5.3.1 (A) 4)– Added specification that ATL03 geoid would now be in the tide-free system and require conversion to mean-tide with the provided conversion factor.</p> <p>6/30/2020 Section 5.4.2– Added <b>geoid_free2mean</b> and <b>tide_earth_free2mean</b> to list of ancillary variables to be averaged over and ocean segment.</p> <p>6/30/2020 Table 6 of ATL12 Outputs– Added <b>geoid_free2mean_seg</b> and <b>tide_earth_free2mean_seg</b> as segment averages of <b>geoid_free2mean</b> and <b>tide_earth_free2mean</b> to list of outputs. Noted that <b>tide_earth_free2mean</b> was not used in ATL12.</p> <p>7/14/2020 (with change of <i>layer_switch</i> default value to 0 on 7/15/2020) Changed 4.2.1.2 as recommended by David Hancock 7/8/2020 concerning editing for <i>layer_flag</i> =1, i.e., 4.2.1.2 1) is now</p> <ol style="list-style-type: none"> <li>1. Examine ocean depth and cloud parameters against control parameters to test for suitability for ocean processing. <ul style="list-style-type: none"> <li>- If control parameter <i>layer_swtrch</i> is equal to 1, then remove the ATL03 segment ids from ocean processing that are associated with the ATL09 segment ids where <i>layer_flag</i> is equal to 1. When <i>layer_swtrch</i> equals 0 (the default value), the software will ignore the cloud cover in accepting data during coarse surface finding.</li> <li>- Ignore data collected over land or too close to land. If ocean depth, <i>depth_ocn</i>, is less than a depth, <i>depth_shore</i>, specifying the effective shoreline of water for which ocean processing is appropriate, then proceed to next 14 geo-bin (400-pulse) segment. The default value for control parameter <i>depth_shore</i> will be 10 m.</li> </ul> </li> </ol> <p>7/14/2020 Changed formatting of lines in Table 7, Input to gridding to “normal” in order for auto formatting of headings of 5.19 not to skip 5.19.3 and jump from 5.1.2 to 5.19.4</p> <p>7/15/2020, Table 3 inputs from ATL09, added <i>layer_flag</i> as Representing presence (1) or absence (0) of significant cloud</p> |  |  |
|--|--|--|

|  |  |  |  |
|--|--|--|--|
|  | <p>layers.</p> <p>7/15/2020, Section 5.4.2 Added description of <b>layer_flag_seg</b> and <b>cloudcover_percent_seg</b>:<br/>         For each ocean segment, we output <b>layer_flag_seg</b> as equal to 1 for ocean segments with more than 50% of geosegs having <b>layer_flag</b> =1, indicating significant cloud layers were present. In addition, we compute <b>cloudcover_percent_seg</b> for each ocean segment as the percentage of geosegs in the ocean segment with <b>layer_flag</b> = 1, i.e., <b>cloudcover_percent_seg</b> = 100*(total number of geosegs used with <b>layer_flag</b>=1)/(total number of geosegs used).</p> <p>7/24/2020 Made numerous small edits and updates suggested by Patricia Vornberger, but with no change in the processing code</p> <p>8/4/2020 Made numerous name updates, corrections, and deletions to variables in Tables 2 and 3 in accordance to Patricia's comments and John Robbin's ATBD_Table_2&amp;3_Notes_JM<br/>         Also substituted <i>asr_cloud_probability</i> for <i>cloud_flag_asr</i> in text in description of ATL09 processing for the <i>layer_flag</i></p> <p>8/11/2020 Corrected error that Leeanne spotted in equation 49. Corrected <b>dot_m</b> to <b>dot_avg</b> i.e.<br/> <math display="block">c = dot\_avg - (a * grid\_lon + b * grid\_lat)</math></p> <p>8/18/2020 Modified equation above 5.6.5 to correct placement of parentheses to read:</p> $dot\_sigma\_dfwalbm = ((Sum [dof\_grid * (dot\_sigma\_dfw)^2]_{beams1,3,5}) / dof\_grid\_albm)^{1/2}$ <p>8/28/2020 Sect 4.2.1.2 Paragraph 4: Add editing for <i>quality_ph</i>=0 i.e., "Select only photon heights for which the signal confidence (<i>gtxx/heights/signal_conf_ph</i>) is greater than or equal to 1 and indicator for saturation <i>gtxx/heights/quality_ph</i> is zero."<br/>         - Similarly, added <i>quality_ph</i> to input Table 2 and<br/>         - Sec 5.3.1 A) 3. Now includes "Select only photon heights for which the signal confidence (<i>gtx/heights/signal_conf_ph</i>) is greater than or equal to 1 and photon quality (<i>gtxx/heights/quality_ph</i>) is equal to zero."</p> |  |  |
|--|--|--|--|

|  |  |  |
|--|--|--|
| <p>8/28/2020 Sect 5.4.2, Added <i>full_sat_fract</i> and <i>near_sat_fract</i> to list of variables to be simply averaged over an ocean segment. And added the corresponding outputs of averaging, <i>full_sat_fract_prct</i> and <i>near_sat_fract_prct</i> to Table 6</p> <p>9/8/2020 In section 5.6.2 we gave the second paragraph on pre-filtering its own subsection:<br/>5.6.2.1 Pre-grid Filtering – Along-Track</p> <p>9/8/2020 In Table 2 Inputs from ATL03, eliminated reference to <i>signal_conf_ph</i> = -1, -3, -4 and substituted, “ With release 4 <b><i>signal_conf_ph</i></b> equal = -2 indicates possible TEP photon”</p> <p>9/10/2020 In Table 6, ATL12 Outputs, changed <i>full_sat_fract_prct</i> to <i>full_sat_fract_seg</i> and <i>near_sat_fract_prct</i> to <i>near_sat_fract_seg</i>. In the variable descriptions “percentage” is changed to “fraction”.</p> <p>9/15/2020 In 4.2.1.2 5) corrected typo EGM208 to EGM2008 and<br/>Happy 2<sup>nd</sup> Birthday ICESat-2 and Happy 100<sup>th</sup> Birthday W. H. Morison</p> <p>10/14/2020 - In Table 9 ATL12 outputs per orbit change the name of photon noise rate, <i>photonns_rate</i>, to <i>photon_noise_rate</i> to avoid confusion with photon rate, <i>Photon_rate</i>.</p> <p>10/14/2020 – In Section 5.3.2 (Q) change the last sentence to:<br/>“The surface reflected photon rate per meter, <b><i>photon_rate</i></b> = <math>r_{surf}</math>, is equal to <b><i>n_photons</i></b> divided by <b><i>length_seg</i></b>, and the noise photon rate per meter, <b><i>photon_noise_rate</i></b> = <math>r_{noise}</math>, is equal to the difference of <b><i>n_ttl_photon</i></b> minus <b><i>n_photons</i></b> divided by <b><i>length_seg</i></b>.”</p> <p>11/9/2020 – Section 5.6.3.2.1 regarding equation 48 description, changed “cross product” to “product sum”</p> <p>1/4/2021 –In Table 6 Changed <i>Binsize</i> to <i>binsize</i><br/>Deleted mention of <i>slope_seg</i><br/>Added <b><i>nharms</i></b> (= 32) to description of output variable <i>ds_wn</i>, the vector of wavenumbers<br/>Added <i>last_geoseg</i><br/>Deleted <i>segment_id</i></p> |  |  |
|--|--|--|

|   |  |  |
|---|--|--|
| <p>1/4/2021 – Section 5.4.2 Ancilliary Data – added <b><i>last-geoseg</i></b></p> <p>1/4/2021 – Deleted nearly all of Section 5.6 ATL 19 Gridded Product in favor of a short paragraph referring the reader to the ATL19 ATBD</p> <p>1/4/2021 – In Table 6, changed <i>ds_wn</i> to <i>wn</i> and <i>ds_a</i> to <i>a</i> and moved to segments group.</p> <p>1/5/2021- In Table 6 put <i>da_a</i> and <i>ds_wn</i> back in with corrected descriptions</p> <p>1/5/2021 Table 6 – Put in alphabetical order wim groups and applied a consistent border scheme.</p> <p>1/5/2021 – Deleted nearly all of Section 3.6 about plans for ATL 19 Gridded Product in favor of a short paragraph referring the reader to the ATL19 ATBD.</p> <p>1/15/2021 Section 2.1, paragraph 3 – Updated and corrected the discussion of <u>Tides, Medium-Frequency Changes in Circulation and Aliasing and the fourth paragraph on the Geoid, Narrowing the Window on Photon Returns, and Measuring Mean DOT.</u></p> <p>1/15/2021 Section 2.2.3 - Updated previous sentence and the paragraph under <b><i>A Priori Estimation of SSB Using Only Altimeter Data</i></b></p> <p>1/18/2021 Section 3.1.1.6 – Annotated with output directories and variables e.g., <i>gtx/ssh_segments/heights/bimd, latbin, lonbin,htybin, xrbin, bin_ssbia, swh.</i></p> <p>1/18/2021 Section 3.1.15 – Annotated with output directories and variables, e.g., (<i>gtx/ssh_segments/stas/ n_photons; gtx/ssh_segments/heights/y, ymean, yvar, yskew, ykurt, meanoffit2.</i></p> <p>1/18/2021 Added Section 3.1.1.9 <b>Ocean Segment Statistics</b></p> <p>1/18/2021 Section 4.5 on ATL19 gridded product: Added a reference to ATL19 ATBD and removed a small amount of out of</p> |  |  |
|---|--|--|

|  |  |  |
|--|--|--|
| <p>date text leftover from previous edits.</p> <p>1/18/2021 Section 5.2.3 Control parameters added: “These control parameters are output in <i>ancillary_data/ocean</i> for each granule/file ATL12”</p> <p>1/18/2021 Section 3.1 near the end of the last paragraph, added: “where a geo-bin is the ATL03 geolocation segment and amounts to about 20-m along-track distance”</p> <p>1/18/2020 Section 5.4.2 at end of the first paragraph, added: “variables are locted in <i>/gtx/stats</i> group and include “</p> <p>1/18/2021 Section 5.6 at the end corrected ATL-19 to ATL19</p> <p>1/20/2021 Section 3.1.1.4 – Added an explanation of editing out photons in afterpulses due to saturation as indicarte by the <i>quality_ph</i> flag being nonzero. Also added to Section 5.3.6 a reference to 3.1.1.4. Also in Table 2, noted in description for <i>fpb_param(n)</i> that it was not used at present and refrred to Section 3.1.1.4. In Table 6 descriptions of <i>fpb_corr</i> and <i>fpb_corr_stdev</i> noted that they are “ currently set to INVALID. See 3.1.1.4.”</p> <p>1/21/2021 Section 4.2.1.3 2): Added text describing change to 5.3.2 to change surface finding based on the distribution of photon heights to surface finding based on the photon height anomaly relative to a moving bin average of high confidence photon heights.</p> <p>1/21/2021 Section 3.1.1.3: Added text describing thre latest surface findin including “ starting with Release 4, the surface finding, instead of being based on the distribution of photon heights, is based on the distribution of the photon height anomalies relative to a moving 11-point bin average of high-confidence photon heights. This excludes subsurface returns under the crests of surface waves obviating the immediate need for a subsurface return correction.</p> <p>1/21/2021 Also to 5.6.3 added: “ Also, for Release 4, the surface finding, instead of being based on the distribution of photon heights, is based on the distribution of the photon height anomalies relative to a moving 11-point bin average of high-confidence photon heights. This excludes subsurface returns</p> |  |  |
|--|--|--|

|  |  |  |  |
|--|--|--|--|
|  | <p>under the crests of surface waves obviating the immediate need for a subsurface return correction.”</p> <p>1/21/2021 Table 6: Specified the place-holder variables <i>ss_corr</i> and <i>ss_corr_stddev</i> would have values equal to INVALID pending further developments</p> <p>1/21/2021 Updated Section 5.2.1 summary discussion of the use of quality variables and flags from ATL03, <b><i>quality_ph</i></b>, <b><i>gtx/geolocation/podppd_flag</i></b>, <b><i>signal_conf_ph</i></b>, and <b><i>layer_flag</i></b> in editing and surface finding</p> <p>1/22/2021 Changed previous Table 9 to 7 and Table 10 to 8 because previous Tables 7 and 8 were removed with ATL19 to their own ATBD. Also update the list of Figures and Tables</p> <p>2/23/2021 – In Section 5.2.2 added a paragraph for deriving ice concentration, <b><i>ice_conc</i></b>, from NSIDC daily data. Also added ice concentration, <b><i>gtx/ssh_segments/stats/ice_conc</i></b>, to Table 6 ATL12 Outputs.</p> <p>3/30/2021 – Section 4.2.1.1 Added specification of the data for which <i>podppd_flag</i> value would be processed in Release 5:<br/>         “As of Release 5, the <b><i>podppd_flag</i></b> will have seven possible values: normal operations values: 0=NOMINAL; 1=POD_DEGRADE; 2=PPD_DEGRADE; 3=PODPPD_DEGRADE; plus possible calibration maneuver related “CAL” values: 4=CAL_NOMINAL; 5=CAL_POD_DEGRADE; 6=CAL_PPD_DEGRADE; 7=CAL_PODPPD_DEGRADE. For ATL12, we will only use data when the POP/PPD flag indicates nominal normal operations or nominal CAL maneuvers, <b><i>podppd_flag</i></b> equal to 0 or 4. For each ocean segment processed, we will report the the higher of these two <b><i>podppd_flag</i></b> values, 0 or 4, of data used in the ocean segment.”</p> <p>3/30/2021 – Similar to above, for Section 5.2.1 added:<br/>         “Per Section 4.2.1, for Release 5 with seven possible values of <i>podppd_flag</i>, ATL12 processing should only be done with data for which <b><i>gtx/geolocation/podppd_flag</i></b>=0 indicating nominal operations or <b><i>gtx/geolocation/podppd_flag</i></b>=4 indicating nominal calibration maneuvers”</p> |  |  |
|--|--|--|--|

|  |  |  |
|--|--|--|
| <p>3/30/2021 – Table 2 changed the description of <b>podppd_flag</b> to seven values and added <b>podppd_flag_seg</b> to Tabler 6 Outputs.</p> <p>8/25/2021 – Table 7 change <i>slope_seg</i> to <i>p1</i>.</p> <p>8/25/2021 -4.3.1 – Remove “However, pending further study, it is TBD whether they will be included in the ATL12 data output”</p> <p>11/2/2021 Section 4.2.1 – Added text explaining the rationale for expanding the podppd_flag and changes to ocean scan and RTW scan operations to alleviate the Western Pacific ocean scan ATL12 data gap.</p> <p>12/1/2021 Starting with the ATBD 11/02/2021 version with prior changes accepted we implemented slight changes to Table 6, mostly units, e.g., m in place of meters, for consistency.</p> <p>12/3/2021 Change<br/>         “. Compute the segment latitude, <b>lat_seg</b>, and segment longitude, <b>lon_seg</b>, as the means of <b>lat_initial(ii)</b> and <b>lon_initial(ii)</b>, and the segment length, <b>length_seg</b>, as the <b>last</b> value of <b>trackdist_initial2(ii)</b> - the first value of <b>trackdist_initial2(ii)</b>.”</p> <p>To<br/>         “. Compute the segment latitude, <b>lat_seg</b>, and segment longitude, <b>lon_seg</b>, as the means of <b>lat_initial(ii)</b> and <b>lon_initial(ii)</b>, and the segment length, <b>length_seg</b>, as the maximum value of <b>trackdist_initial2(ii)</b> - the minimum value of <b>trackdist_initial2(ii)</b>.”</p> <p>12/3/2021 Correcting <b>trackdist_initial_surf</b> to <b>trackdist_initial2_surf</b> as follows:</p> <p>In 5.3.2 (P) we define <b>trackdist_initial2_surf</b>, as the along track distances of the final selected surface photons:</p> <p>Identify the corresponding track distances, <b>trackdist_initial2_surf</b>, in <b>trackdist2_initial</b> at the indices in <b>ii</b>, [i.e., in Matlab code <b>trackdist_initial2_surf = trackdist2_initial(ii)</b>].</p> <p>But as of 12/3/20212 David Hancock and Suzanne Dickinson discovered that the 2 had been dropped from subsequent usage</p> |  |  |
|--|--|--|

|  |  |  |  |
|--|--|--|--|
|  | <p>of the along track distance, i.e., <i>trackdist_initial_surf</i> was used instead.</p> <p>Corrections are made at the following subsequent places in the ATBD:</p> <p>In 5.3.3.1 :</p> <ol style="list-style-type: none"> <li>1. Add <i>meanoffit2</i> to <i>ht_initial2_surf</i>.</li> <li>2. Convert <i>trackdist_initial2_surf</i> to meters if necessary and subtract the minimum of <i>trackdist_initial2_surf</i> to obtain distance from start of the ocean segment.</li> <li>3. Sort height data in ascending order of along-track distance, <i>trackdist_initial2_surf</i>, to allow calculation of photon return rate per meter</li> <li>4. Define <i>x</i> as the sorted <i>trackdist_initial2_surf</i> and define <i>hty</i> the associated heights from <i>ht_initial2_surf</i>.</li> </ol> <p>and</p> <p><u>Estimating sea state bias over ocean segments</u></p> <p>At this point, if not earlier, because we want to estimate the properties of waves typically hundreds of meters long, it will be necessary to aggregate <i>ht_initial2_surf</i> and <i>trackdist_initial2_surf</i> along each ocean segment found during the coarse signal finding step. Section 5.3.1</p> <p><u>Add mean from detrending used after first cut surface finding</u></p> <p>The means from the first cut of surface finding are computed from photon heights over surface waves and are therefore contaminated by the correlation of photon return rate with height of the surface over surface waves. If these are not added back into the height record, that contamination by SSB will be lost. Therefore, we add <i>meanoffit2</i>, the mean of <math>P0 + P1 \times trackdist\_initial2\_surf</math> (the along-track position of 2<sup>nd</sup> iteration surface photons), back into the photon height record, <math>hty = ht\_initial2\_surf + meanoffit2</math></p> <p>In 5.4.3.2 (I)</p> <p>- The first moment or mean of the mixture, <math>\mu_{mix} = m_1\mu_1 + m_2\mu_2</math> is the mean of the detrended surface photon heights relative to the geoid with the mean of the detrending process, <i>meanoffit2</i> (equal the mean of <math>P0+P1*trackdist\_initial2\_surf</math>), added back in prior t</p> |  |  |
|--|--|--|--|

|  |  |  |  |
|--|--|--|--|
|  | <p>Gaussian mixture determination. Thus, it represents the mean DO1 uncorrected for sea state bias, along the ocean segment. Therefore mean sea surface height, <b>SSH</b>, for the segment to be output in ATL1 equal to the mean of the mixture, <math>\bar{\mu}_{mix}</math>, plus <b>meangdht</b> equal to the mean of geoid height, <b>geoid</b>, over the segment:</p> |  |  |
|--|--|--|--|

*ICESat-2 Algorithm Theoretical Basis Document for Ocean Surface Height*

*Release 005*

**List of TBDs/TBRs**

| Item No. | Location      | Summary   | Ind./Org. | Due Date |
|----------|---------------|---|-----------|----------|
| 1        | 3.1, p52      | The possible methods of distinguishing open ocean from sea ice and land and setting the ocean segment lengths in these mixed regions are TBD.   |           |          |
| 2        | 3.2, p54      | Applying a TBD first-photon-bias correction where photon rates are high   |           |          |
| 3        | 4.2.1.3, p65  | $Th_{Nc_f}$ is TBD, but we have used $Th_{Nc_f} = 1.5$  |           |          |
| 4        | 5.3.1(D), p79 | $Th_{Nc_c}$ is TBD, but we have been using $Th_{Nc_c} = 1$ in our tests with early ICESat-2 data  |           |          |
| 5        | 5.3.5 P107    | The <i>a priori</i> SSB estimate of Section 5.3.3 can be applied to the mean SSH and DOT (=SSH-EGM2008 Geoid) for comparison to in situ cal/val or other altimeters. The impact of this SSB on the other moments is TBD |           |          |
| 6        | Appendix A    | Various parameters in other ICESat-2 data products  |           |          |
|          |               |   |           |          |
|          |               |   |           |          |
|          |               |   |           |          |
|          |               |   |           |          |
|          |               |   |           |          |
|          |               |   |           |          |

## Table of Contents

|  |     |
|--|-----|
| Abstract .....   | 2-i |
| CM Foreword.....   | ii  |
| Preface .....  | iv  |
| Review/Approval Page .....   | vi  |
| Change History Log .....   | vii |
| List of TBDs/TBRs.....   | xxv |
| Table of Contents .....  | 26  |
| List of Figures.....   | 30  |
| List of Tables.....  | 33  |
| 1.0 INTRODUCTION .....   | 36  |
| 2.0 OVERVIEW AND BACKGROUND INFORMATION.....   | 39  |
| 2.1 Open Ocean Background .....  | 40  |
| 2.2 The Importance of Waves .....  | 42  |
| 2.2.1 Waves and Reflectance .....  | 42  |
| 2.2.2 Waves and Sea State Bias .....   | 44  |
| 2.2.3 ICESat-2 Height Statistics and Sea State Bias .....                            | 49  |
| 3.0 Open Ocean Products.....   | 54  |
| 3.1 Open Ocean Surface Height (ATL12/L3A) .....                                      | 54  |
| 3.1.1 Height Segment Parameters (output group <i>gtx/ssh_segments/heights/</i> ).... | 55  |
| 3.1.2 Input from IS-2 Products .....   | 57  |
| 3.1.3 Corrections to height (based on external inputs).....                          | 57  |
| 3.2 Gridded Sea Surface Height (ATL19/ L3B).....                                     | 59  |
| 4.0 ALGORITHM THEORY .....   | 61  |
| 4.1 Introduction .....   | 61  |
| 4.2 ATL12: Finding the surface-reflected photon heights in the photon cloud .....    | 61  |
| 4.2.1 Selection of Signal Photon Heights .....                                       | 63  |
| 4.2.2 A Priori Sea State Bias Estimation and Significant Wave Height.....            | 68  |
| 4.3 ATL12: Correction and Interpretation of the Surface Height Distribution .....    | 69  |
| 4.3.1 Separating the Uncertainty due to Instrument impulse response.....             | 69  |
| 4.3.2 Characterizing the Random Sea Surface .....                                    | 71  |

|       |   |     |
|-------|---|-----|
| 4.3.3 | Expectation Maximization.....   | 73  |
| 4.4   | Calculation of Uncertainty .....  | 73  |
| 4.5   | ATL19: Gridding the DOT and SSH.....  | 74  |
| 5.0   | Algorithm Implementation.....   | 75  |
| 5.1   | Outline of Procedure .....  | 75  |
| 5.2   | Input Parameters .....  | 75  |
| 5.2.1 | Parameters Required from ICESat-2 Data.....   | 75  |
| 5.2.3 | Parameters Required from Other Sources.....   | 78  |
| 5.2.4 | Control Parameters for ATL12 Processing.....  | 79  |
| 5.3   | Processing Procedure.....   | 79  |
| 5.3.1 | Coarse Surface Finding and Setting of Segment Length .....  | 79  |
| 5.3.2 | Processing Procedure for Classifying Ocean Surface Photons, Detrending,<br>and Generating a Refined Histogram of Sea Surface Heights .....            | 82  |
| 5.3.3 | Processing to Characterize Long Wavelength Waves, Dependence of<br>Sample Rate on Long Wave Displacement, and <i>A Priori</i> Sea State Bias Estimate | 88  |
| 5.3.4 | Processing Procedure for Correction and Interpretation of the Surface<br>Height Distribution.....   | 93  |
| 5.3.5 | Applying <i>a priori</i> SSB Estimate .....   | 108 |
| 5.3.6 | Expected Uncertainties in Means of Sea Surface Height.....  | 108 |
| 5.4   | Ancillary Information .....   | 113 |
| 5.4.1 | Solar Background Photon Rate and Apparent Surface Reflectance (ASR)<br>113  |     |
| 5.4.2 | Additional Ancillary Data .....   | 113 |
| 5.5   | Output Parameters.....  | 115 |
| 5.6   | Gridding DOT for ATL19. ....  | 121 |
| 5.7   | Synthetic Test Data.....  | 121 |
| 5.8   | Numerical Computation Considerations .....  | 128 |
| 5.9   | Programmer/Procedural Considerations.....   | 128 |
| 5.10  | Calibration and Validation .....  | 128 |
| 6.0   | Browse Products .....   | 129 |
| 6.1   | Data Quality Monitoring .....   | 129 |
| 6.1.1 | Line plots (each strong beam).....  | 129 |
| 6.1.2 | Histograms (each strong beam).....  | 129 |

|       |  |     |
|-------|--|-----|
| 7.0   | Data Quality.....  | 130 |
| 7.1   | Statistics.....  | 130 |
| 7.1.1 | Per orbit statistics .....   | 130 |
| 8.0   | TEST DATA.....   | 133 |
| 8.1   | In Situ Data Sets .....  | 133 |
| 8.2   | Simulated Test Data .....  | 133 |
| 9.0   | CONSTRAINTS, LIMITATIONS, AND ASSUMPTIONS .....                          | 134 |
| 9.1   | Constraints.....   | 134 |
| 9.2   | Limitations.....   | 134 |
| 9.3   | Assumptions .....  | 135 |
| 10.0  | References .....   | 136 |
|       | ACRONYMS.....  | 137 |
|       | GLOSSARY.....  | 138 |
|       | APPENDIX A: ICESat-2 Data Products .....                                 | 139 |
|       | APPENDIX B: Sea State Bias Computations for a Photon Counting Lidar..... | 143 |
|       | APPENDIX C: Expectation-Maximization (EM) Procedure .....                | 149 |
|       | APPENDIX D: Fitting a Plane to Spatially Distributed Data .....          | 150 |
|       | APPENDIX E: Hierarchy of ATL12 and ATL10 Variables .....                 | 152 |
| 11.0  | References .....   | 153 |



## List of Figures

| <u>Figure</u>   | <u>Page</u> |
|---|-------------|
| Figure 1 - Characteristics of an idealized distribution .....         | 37          |
| Figure 2. Geodetic height.....  | 39          |
| Figure 3. Reflectance as modeled .....                                | 41          |
| Figure 4. Typical Gram-Charlier distribution .....                    | 42          |
| Figure 5. Trochoidal shape of surface waves .....                     | 43          |
| Figure 6. Short wave MSS & standard deviation MSS.....                | 44          |
| Figure 7. Simulated surface displacement and MSS.....                 | 45          |
| Figure 8. Height due to long-waves & MSS.....                         | 45          |
| Figure 9. Height due to long-waves & probability .....                | 46          |
| Figure 10. Surface return heights from MABEL .....                    | 50          |
| Figure 11. ATL 12 processing block diagram.....                       | 60          |
| Figure 12 Coarse, smoothed, and fine histograms .....                 | 64          |
| Figure 13. Block diagram for the ATL19 gridding.....                  | 71          |
| Figure 14. Coarse, smoothed, final Mabel histograms .....             | 83          |
| Figure 15. Instrument impulse response histogram .....                | 92          |
| Figure 16. Probability density functions of the synthetic SSH .....   | 93          |
| Figure 17. Synthesized received probability density functions .....   | 94          |
| Figure 18. Single-sided spectra of the received PDFs .....            | 97          |
| Figure 19. Single-sided spectrum of impulse response .....            | 98          |
| Figure 20. Single-sided amplitude spectra of the Wiener filters ..... | 98          |
| Figure 21. Single-sided amplitude spectra of the surface PDF .....    | 99          |
| Figure 22. PDF of SSH and calculated PDF for 8000 photons.....        | 102         |
| Figure 22. PDF of SSH and calculated PDF for 800 photons.....         | 104         |





## List of Tables

| <u>Table</u>   | <u>Page</u> |
|--|-------------|
| Table 1 Reflectance.....   | 41          |
| Table 2 Input parameters (Source: ATL03).....                            | 78          |
| Table 3 Input parameters (Source: ATL09) .....                           | 76          |
| Table 4 Control Parameters - Surface Finding.....                        | 77          |
| Table 5 Control Parameters for Refined Surface Finding and Analysis..... | 79          |
| Table 6 Output (See Appendix A for full product specifications).....     | 114         |
| Table 7 ATL12 Output Variables for per Orbit Statistics.....             | 129         |
| Table 8 ATL12 Test Data .....  | 132         |





## **1.0 INTRODUCTION**

This ATBD will cover the retrieval of Sea Surface Height (SSH) from ICESat-2 ATLAS laser returns. For the purpose of this early draft, the levels of spatial and temporal averaging to be included are still to be definitively decided, as is the amount of high-level data processing to produce gridded fields of SSH and such things as Dynamic Ocean Topography (equal to SSH minus the geoid).

Other ICESat-2 ATBDs describe the products for ice sheets, vegetation, sea ice and inland water, the latter two having close relations with the ocean ATBD. Technical ATBDs include orbit and attitude calculations, corrections for atmospheric path-length delays, and corrections for changes in the surface heights due to tidal effects; these other data are needed to convert ranges into absolute surface heights with respect to the geoid.

This document will address sampling the ice-free world ocean, but not ice-covered or inland waters, because the ICESat-2 sampling scheme is different for the open ocean, generally sampling strong beams only, and because the defining characteristics, (e.g., well developed surface waves) are unique to the open ocean. It will include coastal ocean waters. Because of the increasing seasonal variation in the sea ice cover, the boundary between the open-ocean and ice-covered ocean domains will vary seasonally. This ATBD will share some considerations and features with the sea ice ATBD (surface finding algorithm, concern for tides and the geoid) and the vegetation and inland water ATBD (concern with waves in large bodies of inland water). We consider as input data level 2 photon heights for each of the three strong beams along the satellite track along with the required navigation information. (In certain ocean regions near land or sea ice, the weak beams may be also be active. In these cases the weak beam data over the ocean should be processed the same way as the strong beams.) As output, the processing to be described will produce ATL12/L3A (Appendix A), the height of the open ocean surface at a length scales between 70 m (100 Hz) and 7 km (1 Hz), determined by an adaptive surface finding algorithm. Output will include estimates of height distributions (decile bins), significant wave height, surface slope, and apparent reflectance.

Section 2 provides an overview of the ocean altimetry issues,

Section 3 discusses the ocean products the parameters that reside in each product as well as ancillary geophysical parameters, of interest to science users, which are used in the derivation of these ICESat-2 products.

Section 4 provides a theoretical description of the algorithms used in the derivation of the ocean products.

Section 5 describes the specific implementations of the algorithms that are relevant to the development of the processing code. Included here are both algorithmic details and some software architecture details on throughput optimization and computational loading.

Section 6 provides the processing requirements for data quality monitoring and control. These are provided to users as quality assessments of the individual parameters on each file and to provide criteria for automatic quality control to facilitate timely distribution of the product to the users. Summary statistics or images are provided that

allow users to easily evaluate (or Browse) whether the data would be useful and of adequate quality for their research, and as needed to aid in the quick approval or disapproval of products prior to public distribution.

Section 7 describes the testing and validation procedures that are planned.

This page intentionally left blank

## 2.0 OVERVIEW AND BACKGROUND INFORMATION

The Advanced Topographic Laser Altimeter System (ATLAS) consists of both LIDAR and altimetry subsystems that will fly on the dedicated platform comprising the mission referred to as ICESat-2, the Ice, Cloud, and Land Height Satellite. The following subsections discuss the basic concepts of how ATLAS works and the Level 2 data that we will turn into sea surface height. It then describes the basic properties of the sea surface and how these relate to processing the ICESat-2 data.

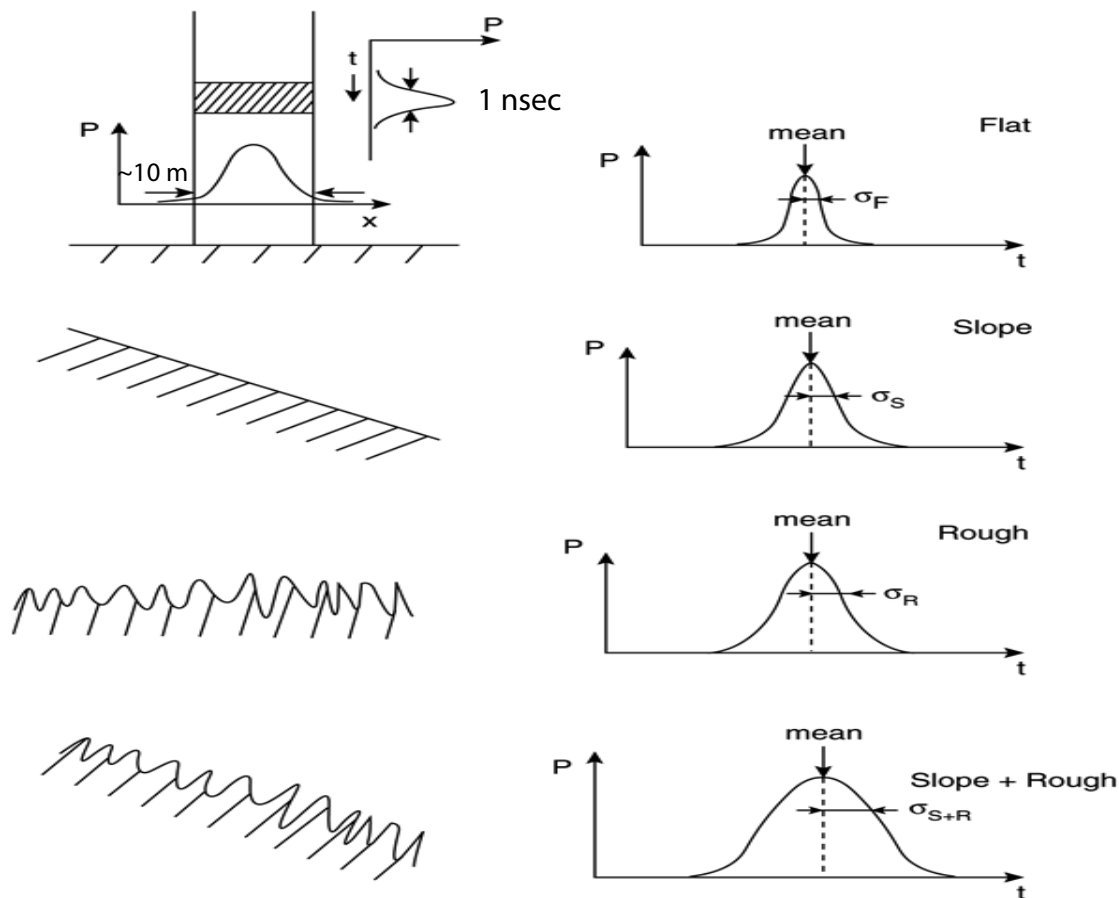


Figure 1 - Characteristics of an idealized distribution of ATLAS return photon arrival times assuming a Gaussian instrument impulse response and a reflective surface with Gaussian roughness. In general surface slope and roughness both broaden the return distribution. For the open ocean the slope effect is likely negligible compared the effect of roughness due to surface waves. An important complication is that surface waves produce a non-Gaussian surface due to their broad troughs and narrow peaks.

The primary purpose of the ATLAS instrument on the ICESat-2 mission is to detect surface height changes. With respect to the ocean, these represent Sea Surface Height

(SSH). By way of technical history, the predecessor of ICESat-2 ATLAS, the ICESat GLAS instrument, used a laser altimeter to measure the range to the surface. Ranges were determined from the measured time between transmission of the laser pulse and detection of the pulse reflected from the surface and received by the instrument. The GLAS laser footprint diameter on the surface due to beam spreading was nominally 70 m, and the duration of the transmitted pulse was 4 ns.

The ICESat-2 ATLAS instrument will sample at a higher rate, 10 kHz with 1-2 ns pulse width, with a smaller intrinsic footprint, ~10 m (Fig. 1), and will rely on detecting the range traveled by individual photons. Experience with MABEL suggests that the instrument impulse response distribution, due largely to the variation in transmit times for the photons of each pulse, will be non-Gaussian with significant skewness. Consequently, four points will be measured on the out going pulse distribution and these will be part of the ICESat-2 raw data stream. The distribution of receive times of the surface-reflected photons, and hence photon heights, will be broadened by the distribution of surface heights within the footprint as depicted in Figure 1 for an idealized Gaussian distribution of photon return times or heights. Photon return-times will be digitized in 200 ps (3 cm) range bins. However, the origination time of a photon within a pulse is unknown, and the uncertainty in the time of flight of a single photon will be between 1 and 1.5 ns RMS (30-45 cm flight time) due mostly to the laser pulse width, with smaller contributions from other effects within the instrument. This time uncertainty corresponds to between 15 and 22 cm RMS in range.

Return photon arrivals will be aggregated at a scale depending on the surface type being over flown. Over the open ocean, short segment aggregates will be retrieved at 100 Hz (100 pulses over 70 m of track) and long segment aggregates retrieved up to 1 Hz (10,000 pulses over 7 km corresponding to 25 times the atmospheric sample rate. In contrast, to ensure adequate detection of leads, over sea ice return photons may be taken at the maximum rate of 10 kHz (each pulse every 0.7m).

## **2.1 Open Ocean Background**

Over distances of cm to a few hundred meters, the sea surface is roughened by waves and ocean swell, but over distances of many km, the sea surface is almost flat. Nevertheless, surface slopes and long-wavelength undulations are present, caused by variations in Earth's gravity field represented by the geoid, ocean currents, and variations in atmospheric pressure and seawater density. Satellite radar altimeters have shown remarkable success in measuring sea-surface height and tracking changes in circulation and mean sea level. However, the major satellite radar altimeters, TOPEX/Poseidon/Jason do not go beyond about 62° latitude, and thus miss the sub-Arctic seas and southern parts of the Southern Ocean that are critical to the global overturning circulation and the fate of sea ice in the ice covered Arctic Ocean. ICESat-2 over the open ocean will cover this gap between the temperate lower-latitude ocean and the sea ice covered regions of the Arctic and Antarctic

As discussed above, the distribution of ICESat photon return times, or apparent heights

from Level 2 processing, will be determined by the mean SSH, the mean surface slope and a surface roughness within the footprint. Among these, the effect of sea surface slope on the photon height distributions should be small compared to the effect of roughness due to surface waves. For the aggregation scales above, the SSH is the sum of the geoid height (fixed in time and on the order of meters amplitude), the dynamic ocean topography (DOT, on the order of centimeters to tens of centimeters amplitude) associated with mean surface currents, tides (mainly diurnal to semidiurnal periods with amplitudes of up to meters), and sea surface atmospheric pressure (SAP, as much as 10s of cm). As a first approximation, SSH can be estimated as the mean of the distribution of photon heights within a vertical window about the ellipsoid or an approximated canonical sea surface height (e.g., 30 m from the estimated geoid) and over the along track aggregation scales to be decided as above. However, the special and rapidly varying nature of the sea surface

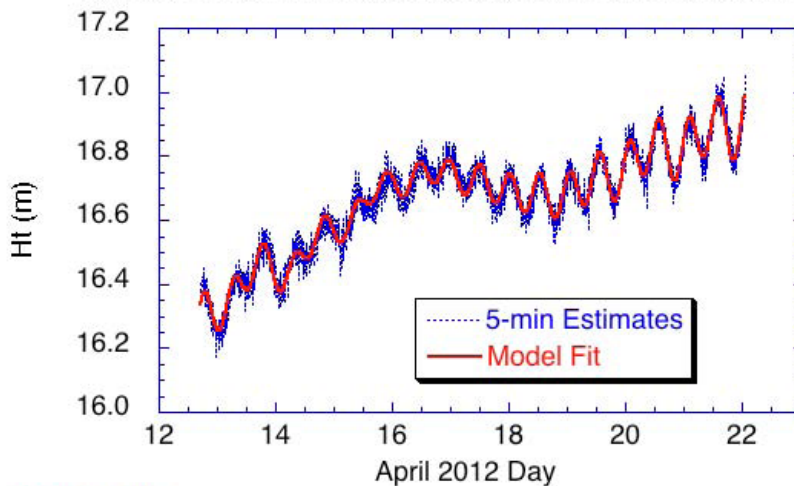


Figure 2. Geodetic height measured with a geodetic grade dual-frequency GPS with PPP processing at a drifting ice camp near the North Pole plotted with an *ad hoc* model of ocean tides and longer variations assumed due to the geoid and DOT variations. The geoid variations over the 60 km drift are estimated to be 60 cm, tides 10 cm peak to peak, and DOT only a few cm.

latitudes, a 25-km grid cell in a grid-average of ICESat-2 might only have a few satellite passes per month. Consequently, tides and medium to high-frequency changes in circulation will seriously alias into slowly sampled regions, making aggregation into valid long-term means difficult. This is addressed by correcting the photon heights to the SSH relative to the WGS84 ellipsoid using models of tides and the response of the ocean to atmospheric forcing including the inverse barometer effect. With the predicted tidal and circulation contributions to SSH, the residual can be averaged, and only the error in the modeled response is aliased. As we will show, for ATL12 processing we reduce the size of the signal we process by subtracting the EGM2008 mean tide geoid to process for dynamic ocean topography.

The Geoid, Narrowing the Window on Photon Returns, and Measuring Mean DOT: ICESat-2

pose challenges with the interpretation and aggregation of meaningful SSH from ICESat-2 photon heights. It is useful to outline these issues here, keeping in mind that the magnitude of the most sought after components of the SSH signal, changes in DOT and mean SSH, are significantly smaller than most of the other components of SSH.

Tides, Medium-Frequency Changes in Circulation and Aliasing: ICESat-2 will complete one orbit of the earth in about 1.5 hours. The repeat period is 91 days, and commonly, especially at low

photon heights will be heavily influenced by the geoid. An example of this for the Arctic Ocean near the North Pole (Fig. 2) shows changes in SSH associated with geoid height variations of about 1 cm per km of horizontal distance. Globally, variations in SSH and the geoid are hundreds of meters, while variations in DOT, equal to SSH minus the geoid, are only a couple of meters. Given the potentially sparse character of ICESat-2 ocean returns, the variations in the geoid from EGM2008 will be extracted from the photon heights to remove the inherent variability not due to ocean processes and reduce the range of variability we have to deal with in our signal processing. As a final step in processing, the EGM2008 geoid will be added back to DOT to yield SSH relative to the WGS84 ellipsoid as the primary AT L12 output.

Surface Atmospheric Pressure and the Inverse Barometer Effect: Changes in surface atmospheric pressure on short time scales directly cause an inverse deflection of SSH. As with tides, ocean circulation changes, and the geoid, these direct pressure disturbances at the time and place of each ICESat-2 photon retrieval should be estimated and removed from estimated SSH before aggregation to avoid spatial and temporal aliasing. This will require bringing atmospheric reanalysis products or direct SAP observations into the processing stream. Knowledge of the likely inverted barometer effect will also help in narrowing the range of return photon heights and thus identifying photons returning from the sea surface.

## 2.2 The Importance of Waves

### 2.2.1 Waves and Reflectance

Surface Waves Reflectance, Scattering, and the Sea State Bias: We expect surface waves to have dominant effects on the ICESat-2 returns from the open ocean.

Reflectance: Surface waves and wind speed have a critical effect on reflectance. Menzies et al. [Menzies et al., 1998] indicate reflectance is given by:

$$R = W R_f + (1-W) R_s + (1-W R_f) R_u \quad (1)$$

where  $R$  is the total backscatter or retro-reflectance,  
 $W$  is the fraction of the ocean covered by foam (up to 0[1] for winds above about 7 m/s),  
 $R_f$  is the reflectance of foam,  
 $R_s$  is reflectance due to specular reflection from the wave roughened surface, and  
 $R_u$  is the apparent reflectance due to light that penetrates and comes back up through the surface anywhere it is not reflected downward by surface foam.

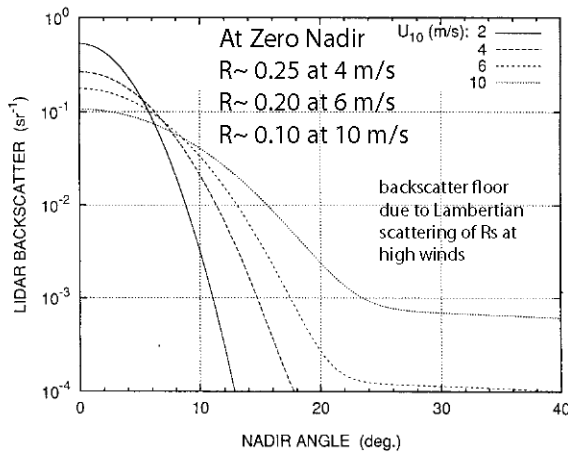


Figure 3. Reflectance as modeled by *Menzies et al.* [1998] as a function of wind speed and nadir angle.

$R_f$  is considered diffuse Lambertian scattering independent of incidence angle. As we would expect,  $R_s$  is highly dependent on incidence angle and is the dominant form of backscatter.  $R_u$  is Lambertian but it is usually small, about 0.0075 maximum. Menzies et al, model the reflectance owing to  $R_s$  and  $R_f$ . The main part is an inverse relation between  $R_s$  and the variance in surface slope,  $R_s \sim 1 / \langle S^2 \rangle$ , due to wind generated surface waves. They use a relation between wind speed,  $U_{10}$ , and  $\langle S^2 \rangle$  by Wu [Wu, 1972] based on results of Cox and Munk [Cox and Munk, 1954];  $\langle S^2 \rangle$  goes up as the log of wind speed. The model

results are given in Figure 3, wherein the strong dependence on nadir angle is apparent. The exception is at high wind speeds where the backscatter from foam starts to become important, flattening the  $R$  curves for nadir angles greater than  $30^\circ$ . Other results in [Menzies et al., 1998] show good agreement between the model and data from the Lidar In-

Table 1

| <u>Case</u> | <u>Description</u>        | <u>Water Reflectance, Lambertian, Green</u> | <u>Water Reflectance, Lambertian, IR</u> |
|-------------|---------------------------|---|--|
| 10a         | Conical Scan, low wind    | 0.28  |  |
| 10b         | Conical Scan, medium wind | 0.12  |  |
| 10c         | Conical Scan, high wind   | 0.07  |  |

Modeled Reflectance for Zero Nadir Angle from Figure 4, *Menzies et al.* [1998] Figure 1

| <u>Case</u> | <u>Description</u> | <u>Water Reflectance, Green</u> |
|-------------|--------------------|---------------------------------|
| 10a         | Wind = 4 m/s       | 0.25                            |
| 10b         | Wind = 6 m/s       | 0.20                            |
| 10c         | Wind = 10 m/s      | 0.1                             |

space Technology Experiment (LITE) shuttle lidar mission of September 1994. The modeled reflectance essentially agrees with the values for reflectance used in the design performance study for ATLAS (Table 1). However, most important with respect to this ATBD, the dependence of sea surface directional reflectance on surface wind stress suggests a method for deriving surface wind speed from ICESat-2 measurements of sea surface backscatter. Working solely with ICESat-2 observations, we can conceivably

estimate  $U_{10}$  from reflectance. As we discuss below this estimate of  $U_{10}$  may be used with SWH, estimated from the variance of the photon height distributions, to calculate the Sea State Bias in ICESat-2 SSH measurements.

### 2.2.2 Waves and Sea State Bias

Sea state bias is a critical issue that has been found to relate to the amplitude of waves and to wind forcing. The SSB problem is fundamental and has received considerable attention with respect to radar altimetry [Elfouhaily et al., 2000; Gaspar et al., 1994]. Improved corrections for SSB in the TOPEX altimeters have been developed [Chambers et al., 2003] relating SSB to wind speed,  $U_{10}$ , and significant wave height (SWH, the trough-to-crest height of the highest third of ocean waves) measured with the radar altimeter. Studies using both laser and radar instruments find a fair degree of commonality [Chapron et al., 2000; Vandemark et al., 2005]. Urban and Schutz [Urban and Schutz, 2005] compare ICESat-derived SSH with TOPEX/Poseidon SSH and find a negative 10 cm bias in ICESat relative to the radar altimeters. They indicate that the bias is unknown, but that it may be

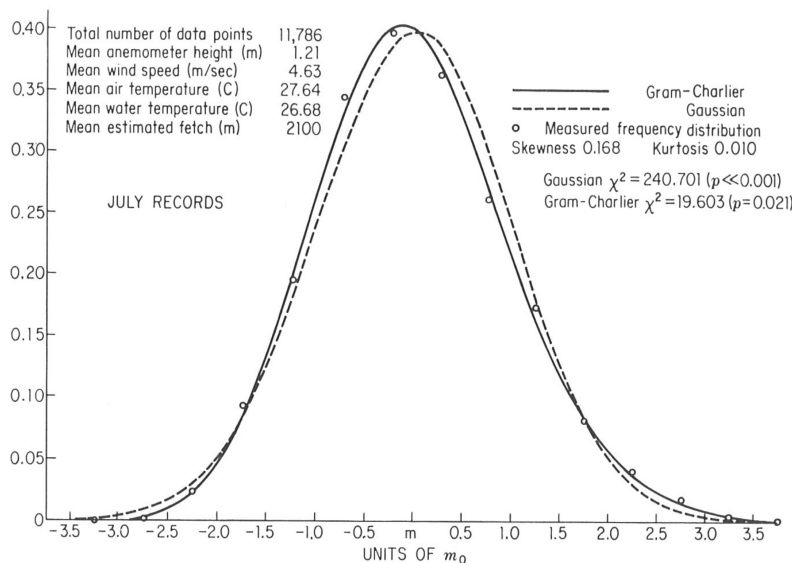


Figure 4. Typical Gram-Charlier distribution sea surface height in a wave environment. The positive skewness and excess kurtosis (Gaussian skewness and excess kurtosis = 0) is due to truncation at low heights and a long tail at high heights. Fig. 7.4-1 of Kinsman [1965].

The distribution of surface height in a wave-covered ocean (Fig. 4) is typically given by the Gram-Charlier distribution [Kinsman, 1965]. For this the third and fourth moments of the distribution expressed as skewness and kurtosis (or excess kurtosis = kurtosis-3) are important and indicate truncation of the distribution at low heights with a long tail at high heights. This reflects the shape of surface waves.

related in part to sea state, and they recognize that the radar altimeter is corrected for SSB using a relation with SWH. Unfortunately, a SWH parameter was not provided with the ICESat GLAS data, a shortcoming we cannot repeat with ICESat-2.

The ICESat ATBD document made the assumption that sea surface heights are Gaussian distributed, so that with a Gaussian transmission pulse, the reflected pulse received by ICESat could be assumed to be Gaussian also. In fact, the ocean surface is not Gaussian and this affects the reflection of either radar or light from the surface. The

In general, surface waves have trochoidal shape, with narrow, steep sided peaks and relatively broad flat troughs (Fig. 5). This applies particularly to the short-wavelength

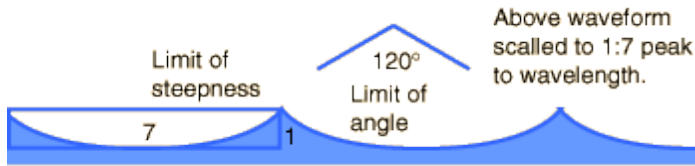


Figure 5. Trochoidal shape of surface waves at the limit of steepness, wavelength equal to seven times height. The sharply peaked trochoidal shape is common to all surface waves longer than capillary waves, which have an inverted trochoidal shape. At the steepness limit the waves begin to break. (Figure from <http://hyperphysics.phy-astr.gsu.edu/hbase/waves/watwav2.html>)

surface is composed of swell and wind waves. Swell is the manifestation of large long-wavelength waves that are mature and forced elsewhere. The wavelengths are long enough that in spite of significant amplitude, the slopes are small and the waves are linear and well represented by sine waves. The wind waves, forced by local wind, are shorter (down to capillary wavelengths) and steeper with trochoidal shape. In the extreme, when they reach the limit of steepness (Figure 5), they break and form white caps. As such, these waves can by their shape affect sea state bias in altimetry returns, but their direct bias is small because their amplitudes are small. However, several studies including one done for the development of this ATBD, suggest the character of the short waves varies with position on the larger linear waves and thus can contribute to large SSB.

We have performed a study of the effect of long waves on short waves and their implications for ICESat-2 sea state bias. We have sought a model sea surface suitable for driving the NASA GSFC numerical ATLAS simulator. With this we will be able to test the performance ATLAS over the open ocean and evaluate such things as the sea state bias in mean sea surface height measurements. There are two elements to our artificial sea surface. The first is a realistic representation of the height and surface slope due to waves with wavelengths greater than the 10-m footprint of an ATLAS laser pulse. This captures the bulk of the energy in the wave field. Because the waves are long, a linear model of them can be used. The second component is a measure of the distribution of surface slopes due to the waves with wavelengths less than 10-m laser pulse footprint of ATLAS. The distribution of surface slopes, shifted by the instantaneous slope of the long wave component determines the probability of ATLAS finding a specular return resulting from a photon laser pulse. Knowing this as a function of surface height and slope due to the long-wave will allow us to predict SSB in the ICESat-2 measurements.

waves proximally forced by wind. Photons striking the upper portions of these wave are less likely to be returned to ICESat-2 than photons striking the lower portions of wave surfaces; peaks are undersampled relative to troughs resulting in a sea state bias (SSB) in estimates of SSH based on the mean of an ICESat-2 photon height distribution or, in the case of ICESat, mean arrival time of a return pulse.

However, commonly the sea surface is composed of swell and wind waves. Swell is the manifestation of large long-wavelength waves that are mature and forced elsewhere. The wavelengths are long enough that in spite of significant amplitude, the slopes are small and the waves are linear and well represented by sine waves. The wind waves, forced by local wind, are shorter (down to capillary wavelengths) and steeper with trochoidal shape. In the extreme, when they reach the limit of steepness (Figure 5), they break and form white caps. As such, these waves can by their shape affect sea state bias in altimetry returns, but their direct bias is small because their amplitudes are small. However, several studies including one done for the development of this ATBD, suggest the character of the short waves varies with position on the larger linear waves and thus can contribute to large SSB.

We have taken advantage of a code simulating long-wave surface height based on a long-wave spectrum developed by Donelan et al. (1985) to model the long wave component of our ATLAS ocean surface model (AOSM).

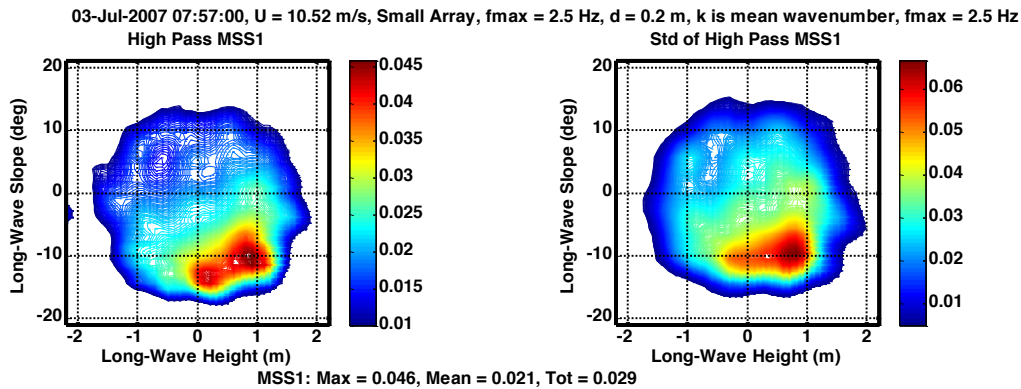


Figure 6. Left – Short wave MSS as a function of long-wave height and slope. Right – the standard deviation of short wave MMS as a function of the same variables.

Our main challenge has been determining the mean square slope (MSS) representing short-wave roughness and its dependence on long-wave height and slope. We had thought that wave wire or some other type of field observation would have been analyzed or at least readily available to determine this relationship, but surprisingly we found no such analysis in the literature. Instead we have analyzed original data from a four-wire wave-gauge array on the University of Miami’s ASIS buoy [Will Drennan, personal communication]. The work is described in detail by W. Plant.[*Plant, 2015a; b*] but we provide a brief synopsis here. The ASIS Buoy data were collected in the Deep Ocean Gas Exchange Experiment in the Atlantic Ocean on July 3, 2007 at a wind speed between 10 and 11 m/s. The wave-gauges measure surface heights at orthogonal positions 20 cm apart, so in principle any two gauges measure slope directly down to  $\sim 2$  Hz or wavelength  $\sim 0.8$  m in this case. A single gauge yields a time series of height, and with the dispersion relation, the spectrum of height can be converted to a spectrum of surface slope. The single gauge approach is complicated by the need for the dispersion relation for the short waves to be modified to account for the orbital velocities of the long waves. We have compared the two approaches and found the two-gauge approach yields results inconsistent with the known gauge spacing. However, we can account for the complications to the dispersion relation and produce consistent estimates of the short-wave slope spectra. Spectra for higher frequencies (wave numbers) than 2 Hz are extrapolated using the observed frequency<sup>-1</sup> spectral slope at 2 Hz. The MSS is obtained by integrating the spectrum out to a maximum frequency (100 Hz), above which increases in MSS are negligible.

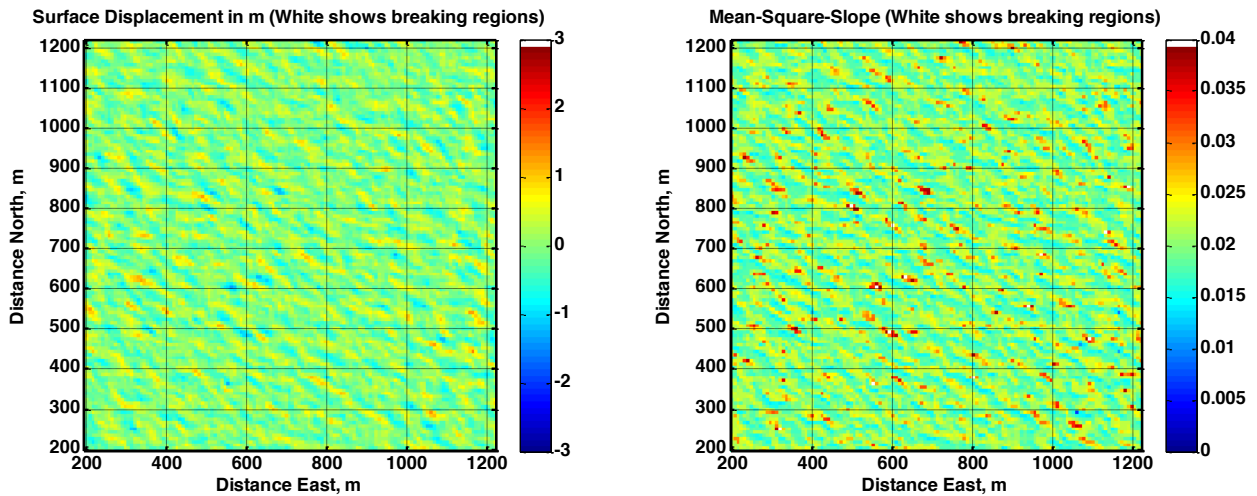


Figure 7. From *Plant* [2015b]. Left – Simulated 2D surface displacement, Right – 2D variation of short-wave mean MSS values that were calculated up to 2 Hz. Downwind direction is from upper right to lower left.

The preliminary result of this analysis has been the dependence of observed short-wave MSS on the slope and height of the long-waves (Fig. 6). MSS is greatest for high heights and negative slopes, i.e., on the upper part of the downwind face of the long-waves. The correlation maps of Figure 6 have been used as a table to specify MSS in a 10-m spot corresponding to the 2D model of long-wave slope and displacement derived from the Donelan spectrum. A realization of long wave height and slope and the corresponding 10-m spot MSS is shown in Figure 7 [*Plant*, 2015a&b].

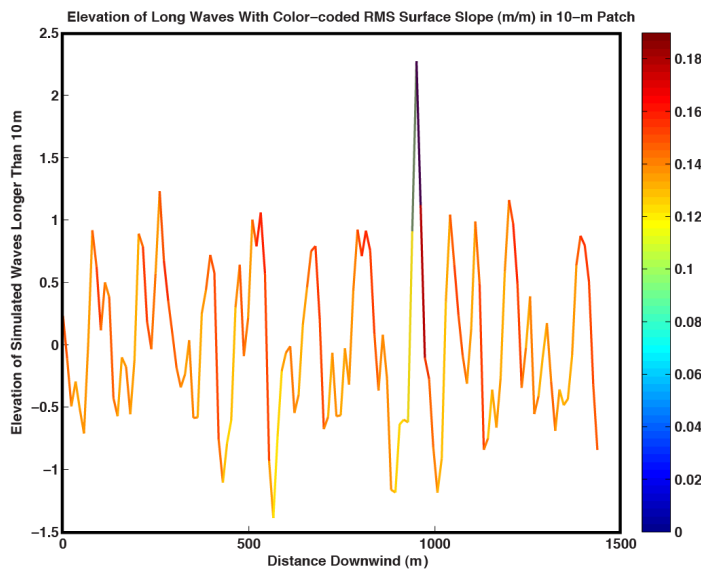


Figure 8. Height due to long-waves versus distance downstream (from upper right corner to lower left in Figure A-left) with color-coded corresponding MSS from Figure A-right.

7 illustrates how MSS slope tends to increase on the upper parts of the downwind face of waves. It also illustrates in a much-simplified way how the interplay of the short-wave MSS and long-wave amplitude and slope can affect the probability of specular reflection and

consequent sea state bias. For each point along the slice, we assume the surface is normally distributed with a mean equal to the local long-wave slope and a variance equal to the MSS corresponding (Fig. 6) to the long-wave height and slope. The probability of any one photon striking the spot finding a specular point is estimated as the integral of the idealized slope distribution between plus and minus  $10^{-5}$  radians (Fig. 9).

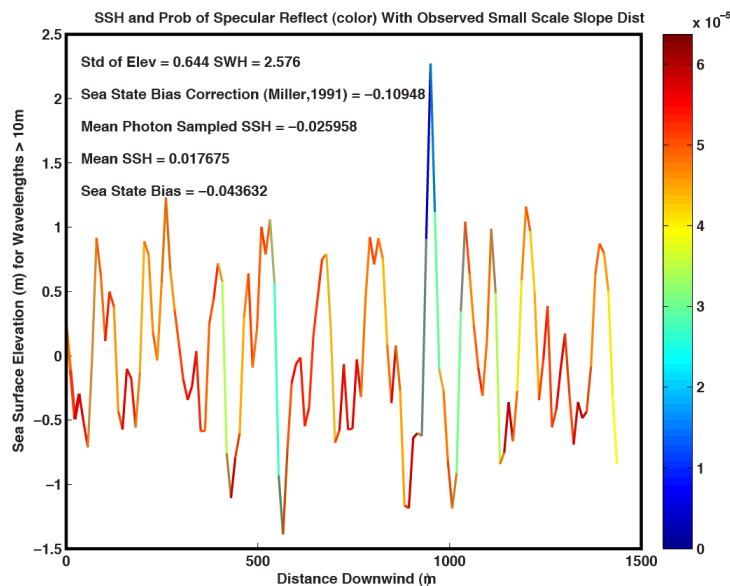


Figure 9. Height due to long-waves versus distance downstream (from upper right corner to lower left in Figure 6-left) with color-coded probability of specular reflection.

The simulation uses a linear spectrum-based representation of the long waves; there are no trochoidal long waves. When we repeat the probability weighted mean calculation assuming the MSS is uniformly equal to the cut-wise mean MSS, the mean height is only biased -0.7 cm.

There are improvements to be made to this wave analysis, including drawing the MSS values as random values from distributions conditioned on long-wave slope and height and doing the analysis for data at other wind speeds. However, this limited sample suggests that the systematic distribution of small-scale surface roughness towards the upper parts of the waves produces a negative sea state bias because the wave troughs provide more specular returns than the wave crests. This type of bias is likely compounded by shape-induced biases due to any nonlinearity in the long-waves. As a result is that the SSH observations by ICESat-2 will be non-Gaussian and exhibit sea state bias.

However, further analysis of the wave gauge data taking into account both the Doppler shifting of the small scale wave by long wave orbital velocity of the long waves and the effects of convergence by long-wave orbital velocity on short wave amplitude results in almost the opposite dependence of short wave slope on long wave height and slope and suggests a positive sea state bias. Consequently, lacking further data about the dependence

The probability of finding a specular point is highest in the troughs and at the peaks, likely because the mean slope is zero. However, the increased MSS in the upper parts of the waves tends to decrease the probability of specular points for higher heights. We know the true mean height along the slice is 1.8 cm. Weighting the samples of height by the probability of a specular point yields a photon sampled mean height of -2.6 cm, a -4.4 cm bias. Interestingly this is about twice the typical sea state bias for radar altimeters for the 10-m wind speed at the time of these ASIS Buoy observations. The bias is not due to nonlinearities

of short wave characteristics on long wave position, we have derived a method whereby the SSB can be determined from ICESat-2 data themselves.

### 2.2.3 ICESat-2 Height Statistics and Sea State Bias

Sea State Bias (SSB) is the error in average sea surface height measured by an altimeter due to the dependence of altimeter returns over different parts of waves. The SSB for radar altimeters is negative because the troughs of waves reflect more radar energy than the crests of waves. This effect is averaged over many surface waves encompassed by the typical radar footprint (e.g. 17 km for CryoSat2). Improved corrections for SSB in the TOPEX altimeters have been developed [*Chambers et al., 2003*] relating SSB to wind speed,  $U_{10}$ , and significant wave height (SWH, the trough-to-crest height of the highest third of ocean waves) measured with the radar altimeter. All these studies have measured the SSB empirically by comparing SSH measured by various means or comparing repeat measurements at the same location by a given satellite for different sea states and wind speeds [*Hausman and Zlotnicki, 2010*].

Studies using both laser and radar instruments find a fair degree of commonality [*Chapron et al., 2000; Vandemark et al., 2005*]. Urban and Schutz [*Urban and Schutz, 2005*] compare ICESat-derived SSH with TOPEX/Poseidon SSH and find a negative 10 cm bias in ICESat relative to the radar altimeters. They indicate that the bias is unknown, but that it may be related in part to sea state, and they recognize that the radar altimeter is corrected for SSB using a relation with SWH. Unfortunately, a SWH parameter was not provided with the ICESat GLAS data, a shortcoming we cannot repeat with ICESat-2.

#### ***A Priori Estimation of SSB Using Only Altimeter Data***

The small footprint of ICESat-2 (17 m for  $4\sigma$  diameter Gaussian intensity), short distance between pulse/footprint centers (0.7 m) and the essential point sampling at random positions within the footprint of the photon counting lidar, presents a unique opportunity to capture the shape of the long wave length, energy containing surface waves. This makes it possible to estimate ICESat-2 sea state bias solely on the basis of contemporaneous ICESat-2 returns without resorting to outside data or even comparison with past ICESat-2 returns. The key is evaluating the rate of surface photon returns as a function of surface height. A simple example of this considers an ocean surface with sea surface height,  $H_{SS}$ , disturbed by a long sinusoidal surface wave with amplitude  $A$ , plus random normally distributed perturbations,  $N$ :

$$Y = H_{SS} + A \sin \frac{2\pi}{L} x + N(0, \sigma) \quad 2$$

If ICESat-2 samples this surface at a constant rate,  $\bar{r}$  surface returns per meter, the surface will be uniformly sampled, and there will be no sea state bias. If there is a variation in sample rate,  $r$ , that is correlated with variations in sea surface height such that:

$$r = \bar{r} + \alpha A \sin \frac{2\pi}{L} x, \quad (3)$$

where  $\alpha$  is the covariance between  $r$  and  $y$  normalized by the variance in  $y$ :

$$\alpha = \frac{\text{cov}(ry)}{\sigma_y^2} . \quad (4)$$

The surface height estimate,  $y_e$ , over a large distance,  $X$ , is the average of the true height weighted by the sample rate:

$$\begin{aligned} y_e &= \frac{1}{X\bar{r}} \int_0^X Yr dx = \frac{1}{X\bar{r}} \int_0^X (H_{SS} + A \sin \frac{2\pi}{L} x + N)r dx \\ &= \frac{1}{X\bar{r}} \int_0^X (H_{SS} + A \sin \frac{2\pi}{L} x + N)(\bar{r} + \alpha A \sin \frac{2\pi}{L} x) dx \end{aligned} \quad (5)$$

$$\begin{aligned} &= \frac{1}{X\bar{r}} \int_0^X H_{SS}(\bar{r} + \alpha A \sin \frac{2\pi}{L} x) dx \rightarrow \frac{1}{X\bar{r}} \int_0^X H_{SS}\bar{r} dx \\ &+ \frac{1}{X\bar{r}} \int_0^X (A \sin \frac{2\pi}{L} x)(\bar{r} + \alpha A \sin \frac{2\pi}{L} x) dx \rightarrow \frac{1}{X\bar{r}} \int_0^X (A \sin \frac{2\pi}{L} x)(\alpha A \sin \frac{2\pi}{L} x) dx \\ &+ \frac{1}{X\bar{r}} \int_0^X N(\bar{r} + \alpha A \sin \frac{2\pi}{L} x) dx \rightarrow 0 \end{aligned} \quad (6)$$

For  $X$  equal to an integral number of wavelengths or very long compared to many wavelengths:

$$y_e = \frac{1}{X\bar{r}} \left[ H_{SS} X\bar{r} + \frac{X}{2} \alpha A^2 \right] = H_{SS} + \frac{\alpha A^2}{2\bar{r}} \quad (7)$$

So sea state bias,  $SSB = y_e - H_{SS}$ , is:

$$SSB = y_e - H_{SS} = \frac{\alpha A^2}{2\bar{r}} \quad (8)$$

Similarly, Arnold et al. [Arnold et al., 1995] in evaluating Ku-band SSB measured with a combination of radar altimeters and capacitive wave wires mounted on an oil platform in the Gulf of Mexico, calculate electromagnetic bias,  $\varepsilon$ , due to the variation of backscatter coefficient with surface waves as

$$\varepsilon = \frac{\sum_{i=1}^N b_i^0 \eta_i}{\sum_{i=1}^N b_i^0} \quad (9)$$

where  $\eta_i$  is the measured surfaced displacement corresponding  $A \sin(2\pi x/L)$  in our idealized example and  $\sigma_i^0$  is the measured backscatter coefficient proportional to the rate of photon returns,  $r$ . Our  $\alpha$  expressed in the terms of Arnold et al. [1995] is:

$$\alpha = \frac{\frac{1}{N} \sum_{i=1}^N b_i^0 \eta_i}{\frac{1}{N} \sum_{i=1}^N \eta_i^2}, \quad (10)$$

so their expression for electromagnetic bias is the same as the SSB for the sine wave example:

$$\varepsilon = \frac{\sum_{i=1}^N b_i^0 \eta_i}{\sum_{i=1}^N b_i^0} = \frac{\frac{\alpha}{N} \sum_{i=1}^N \eta_i^2}{\frac{1}{N} \sum_{i=1}^N b_i^0} = \frac{\alpha A^2}{2\bar{r}} = SSB \quad (11)$$

Appendix B gives a more detailed derivation of (9) in terms of rate of photon return for a photon counting lidar in place of cross-section. It also describes the corresponding EM or sea state bias in the higher moments of the surface distribution (Equation B20 in Appendix B).

### Example of SSB Determination for the Uneven Data Distribution of a Photon Detecting Pulsed Lidar Altimeter

Application of 8 is straightforward, and is accurate in cases such as that of *Arnold et al.* [1995], in which the spacing of the data is uniform and the energy of the return is measured and is the metric weighting the sampled surface height. In that application, each radar pulse was powerful and the range and footprint size were small so that every pulse returned a surface height. The energy returned with each pulse and its correlation with height could be expected to aggregate into the SSB over the much larger footprint of satellite radar altimeter.

This is not totally true in the case of the pulsed photon-counting altimeter such as MABEL or ICESat-2; the return rate of the height samples is not uniform and the average sea surface height is derived from the histogram of photon heights. The correlation between the rate of surface returns and surface height is only one of several components in the histogram skewness. Other contributors to skewness include the true distribution to surface height and subsurface returns. However, the dominant surface waves typically have long wavelengths and are nearly linear so they can be approximated as sine waves. With this in mind, we experimented with fitting multiple sine waves to the raw history of unevenly spaced photon surface heights and calculating the correlation of observed rate of surface returns with the sine wave fit to yield an estimate of SSB using equation 7. However, in testing the method on Greenland Sea MABEL data and Airborne Topographic Mapper (ATM) over the Pacific, we found the method was sensitive to finding the correct wavenumbers for the spectral decomposition of the ocean surface. A more robust method

is to average both the raw photon heights from the surface finding step and the rate of photon returns in evenly spaced bins of along track distance. The covariance of these averages is then used to evaluate equation 7 for the sea state bias. This method is easier to automate and accounts for more of the energy in the wave field than does the harmonic method.

MABEL data from the Greenland Sea in April 19, 2012 illustrates the application of equation 7. In this example, a 9-km length of MABEL track is broken into 3-km segments. Each 3-km segment is divided into 300 10-m along track bins. Once surface finding selects the surface photon heights, these are edited with two passes of a 3-standard deviation editor, and detrended with along track distance.

The rate of photon returns is computed from the along-track record of sample intervals. The record of sample intervals is given by the difference between successive surface photon along-track locations. For the MABEL data shown here, the sample spacings vary significantly but average a little over one meter. To align the data, the surface height

Aggregate SSB Determination for three 3-km MABEL Greenland Sea Segments 4/25/2012

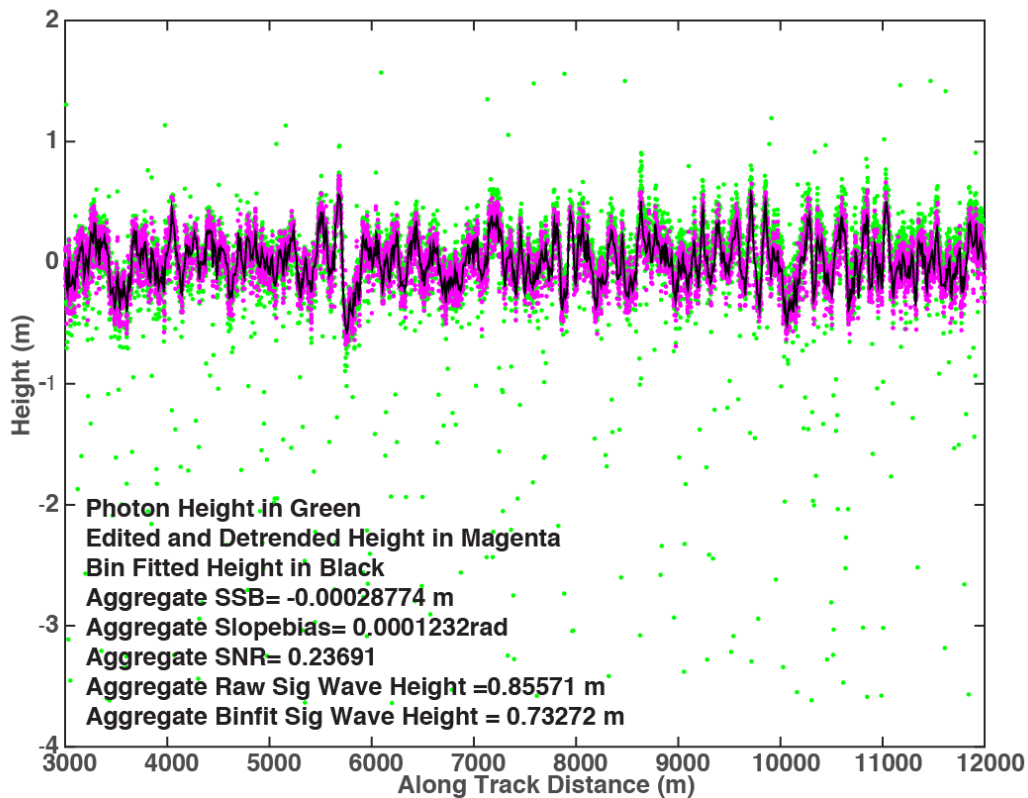


Figure 10. Surface return heights in green from MABEL transit over the Greenland Sea versus distance along track. Three-sigma edited and detrended heights are plotted in green and a 10-m bin averages are plotted in black. The bin averages and a priori SSB estimates were computed in three 3000-m segments and aggregated to yield SSB = -0.00029 m.

and sample position are interpolated to the center of the sample interval by computing the average of pairs of successive sample heights and position. The resulting records of sample rate are then accumulated in 10-m along track bins and averaged. The bin averaged sample intervals are then inverted to yield the bin averaged sample rate. Interpolating height to the center of the sample interval and bin-averaging sample interval before inverting avoids an apparent increase in average sample rate in adjacent sample intervals.

The bin averaged sample rates and heights are then used to compute the height rate covariance and the average sample rates used in X8 to determine SSB.

The method is illustrated in Figure 10 with MABEL data gathered April 25, 2012 over the Greenland Sea. Aggregated over three 3000-m intervals, the correlation of photon return rate and height is very low on average, and results in a sea state bias of 0.3 mm, a result that is not surprising given the low energy of the surface waves with a significant wave height (4 x Std of height) of less than a meter for the raw photon returns and the bin-averaged heights.

### **3.0 OPEN OCEAN PRODUCTS**

#### **3.1 Open Ocean Surface Height (ATL12/L3A)**

The ATL12 product contains sea surface heights over the ice-free oceans for each of 3 ATLAS strong beams. It provides the most basic data from ICESat-2: the sea surface height at a given point on the open ocean surface at a given time plus parameters needed to assess the quality of the surface height estimates and to interpret and aggregate the estimates over greater distances. These heights can be used in comparisons of ICESat-2 data with other geodetic data and as inputs to higher-level ICESat-2 products, particularly ATL19.

Heights over the sea surface are defined for ocean segments with variable length at variable intervals along the ground track; this is necessary to adapt to the reduced photon counts from the low but variable reflectance of the open ocean surfaces. It also is consistent with surface finding routine used for sea ice covered ocean (ATL07/L3A). Based on initial data ATLAS gets on the order of one surface reflected photon per laser pulse or 0.7 m of track, so 100 photon retrievals in the adaptive surface detection algorithm would result in segment lengths of about 70 m. Given the 17-m footprint of the ICESat-2 beams, this is equivalent to 4 independent (non-overlapping) spatial samples of the sea surface.

In future developments, heights in marginal ice zones or coastal zones may be defined for shorter variable length segments sampled at variable intervals along the ground track to adapt to the patches of water between sea ice in the first instance or near land in the second instance. These overlap regions are those that are classified as both sea ice and ocean (marginal ice zone) or land and ocean (coastal zone). The possible methods of distinguishing open ocean from sea ice and land and setting the ocean segment lengths in these mixed regions are TBD.

In purely ocean regions, only strong beams will be active, but in the marginal ice zone and coastal zone overlap regions, the three weak beams will also be active and should be processed identically to the strong beams and output in addition to the strong beam results as part of the ATL 12 ocean product. This is to facilitate a rational merging of the open ocean products (ATL12) and sea ice products (ATL07) and coastal products (ATL??) related to sea surface height.

However, the presence of ocean surface waves in the open ocean far from marginal ice zone and coastal regions, present challenges and an opportunity. The non-Gaussian character of ocean surface waves and the scattering and effective reflectance of the ICESat-2 photons likely cause a negative sea state bias (SSB). We anticipate that the higher order moments of the photon height statistics will allow us to better estimate SSB. We will estimate for each ATL12 variable segment at minimum the mean, standard deviation, skewness and kurtosis of the height distribution. These four moments can be determined from the means and standard deviations of a 2-component Gaussian mixture, which will also provide a mixing ratio for the two components. These higher moments make it possible to characterize not only the mean sea surface height, but also the sea state and likely sea state bias of the height estimate.

However, it is necessary to accumulate large number of surface reflected photons to

make meaningful estimates of the higher moments of the height distribution. Given the low number of returns from open water (e.g., 0[1 photon / pulse]), and considering that ocean waves can have wavelengths of hundreds of meters, to get meaningful statistics over open water with significant wave activity requires accumulating data over several kilometers. The atmospheric cloud flag (***layer\_flag*** in ATL03) is used in part in setting the ocean segment length required to achieve a minimum number of photons. It and other geophysical data such as the background photon rate from ATL09 and the geoid are reported every 400 pulses (25 Hz) or 14 geo-bins where a geo-bin is the ATL03 geolocation segment and amounts to about 20-m along-track distance. Consequently, over the open ocean, we will seek a minimum photon count of 8,000 photons equivalent to about 5.6 km or 280 20-m geo-bins for meaningful higher order statistics.

### 3.1.1 Height Segment Parameters (output group *gtx/ssh\_segments/heights/*)

#### 3.1.1.1 Geolocation/Time

The location is the mean location of designated signal photons used as input to the surface finding procedure (*gtx/ssh\_segments/ longitude & latitude*, see Table 6). The time (*gtx/ssh\_segments/delta\_time*) is the mean time of designated signal photons used as input to the surface finding procedure.

#### 3.1.1.2 Height

This is the mean height estimate from the surface detection algorithm (*gtx/ssh\_segments/heights/h*). The primary quality metric is the uncertainty in the average sea surface height, (*gtx/ssh\_segments/heights/h\_uncrtn*) determined as a function of height variance and length of the ocean segment divided by the height correlation length scale.

#### 3.1.1.3 Subsurface-scattering corrections

Subsurface-scattering corrections are yet to be determined. We find subsurface returns in ICESat-2 ocean photon returns. They tend to be minimal for the deep open ocean where the water is relatively clear. Our surface finding is designed to include few subsurface returns in the first place by rejecting photon heights at greater noise levels below the surface than above the surface. More recently, starting with Release 4, the surface finding, instead of being based on the distribution of photon heights, is based on the distribution of the photon height anomalies relative to a moving 11-point bin average of high-confidence photon heights. This excludes subsurface returns under the crests of surface waves obviating the immediate need for a subsurface return correction.

Subsurface scattering is more significant in near coastal regions where more scattering elements are to be expected in the water. These conditions will be most likely to be apparent as positive skewness in the return height distributions especially as correlated

with outside measures of surface color or scattering. Guided by the treatment of subsurface scattering for the Inland Water ATBD and we may be able to develop relations between photon height distribution skewness and other evidence of scattering, and if so, derive an appropriate correction for subsurface scattering where applicable and provide it as an output of ATL12.

#### 3.1.1.4 First-photon-bias corrections

Generally, given the normally low reflectance of the ocean surface first-photon-bias corrections are not needed for the ocean products. However, in looking at on-orbit data, we find rare instances of quasi-specular returns that we think occur when the sea surface is smooth but has very short wavelength ripples. For these cases photon detector saturation can occur leading to first-photon bias and the appearance of subsurface afterpulses. In the current ATL12 processing (Release 4), photons in these afterpulses are edited out by considering only photons with the index of photon height quality from ATL03 (*quality\_ph*) equal to 0. In future releases (Release 5) we will delete all photons coming from laser pulses that include any photons with a quality index indicative of saturation, or we will consider applying a TBD first-photon-bias correction if there are ocean segments for which the fraction of saturated photons is high as indicated by *full\_sat\_fract\_seg* and *near\_sat\_fract\_seg*.

#### 3.1.1.5 Height Statistics

The photon statistics describe the distribution of the population used in the surface-tracking algorithm. These parameters include the: number of photons (*gtx/ssh\_segments/stats/n\_photons*), histogram of the population (*gtx/ssh\_segments/heights/y*), and, at minimum the mean, variance, and skewness, and kurtosis (*gtx/ssh\_segments/heights/ymean, yvar, yskew, ykurt*). Note that *ymean* should be nearly zero and differs from the average sea surface height relative to the geoid by *meanoffit2* (*gtx/ssh\_segments/heights/meanoffit2*)

#### 3.1.1.6 Initial Sea State Bias Correction and Surface Wave Properties

As discussed in 2.2.3, ICESat-2 gives us a unique opportunity to make an a priori estimate of sea state bias using only the heights from the surface finding system. The approach is to use the surface photon heights to estimate the surface height (*gtx/ssh\_segments/heights/xrbin*) and the rate of photon returns (*gtx/ssh\_segments/heights/hybin*) in 10-m along-track segments (see *gtx/ssh\_segments/heights/bin, latbin, lonbin*). The correlation of height and return rate normalized by the average photon return rate is the electro magnetic (EM) sea state bias (*gtx/ssh\_segments/heights/bin\_ssbias*). This will be estimated from the surface photon height record before separation of the impulse response in the height histogram and made available as output. The standard deviation of photon heights over the whole segment will be provided as a measure of SWH (*gtx/ssh\_segments/heights/swh*) (=4xStd.) that can be compared with reanalysis products.

### 3.1.1.7 Solar Background

The solar background photon rate, *backgr\_r\_200*, is estimated as an average over 50 laser pulses in ATL03. It is based on the photons included in the altimetric histogram less the photons deemed signal (surface or cloud reflected) photons by ATL03. This is converted to a rate in photons per second by dividing by the total time window reduced by the duration of the window containing signal photons.

For ATL12 we will use the average of the estimated solar background. We will not use the predicted solar background rate based on the solar zenith angle, the solar flux in the receiver etalon's pass band, and the effective aperture of the detectors.

### 3.1.1.8 Apparent Reflectance

This is based on the comparison of expected photon counts over a sea surface with SWH estimated from photon statistics and photon counts from the actual surface (see 2.2.1.4 and Fig. 2).

### 3.1.1.9 Ocean Segment Statistics

Important statistics for each ocean segment will also be output (in the *gtx/ssh\_segments/starts/* group). These include: the number of surface photons found for the segment, *n\_photons*; the number of photons in the  $\pm 15$ -m ocean downlink band, *n\_ttl\_photon*; solar background rate from ATL03 averaged over the segment, *backgr\_seg*; the percentage of geo-segs in the ocean segment with *layer\_flag* = 1, *cloudcover\_percent\_seg*; the segment average dynamic atmospheric correction to SSH, *dac\_seg*; segment average ocean depth, *depth\_ocn\_seg*; the ocean segment average of the conversion factor added to ATL03 *geoid* to convert from the tide-free to the mean-tide system; *geoid\_free2mean\_se* and the ocean segment average of EGM2008 geoid in the mean-tide system height above the WGS - 84 reference ellipsoid, *geoid\_seg*.

## 3.1.2 Input from IS-2 Products

### 3.1.2.1 Classified photons (Level 2)

Photons classified as to whether the height is signal, noise, or extended signal. These have a confidence as to type.

### 3.1.2.2 Atmosphere (Level 3)

Relative/calibrated backscatter, background rates, cloud statistics at 25 Hz.

## 3.1.3 Corrections to height (based on external inputs)

In anticipation of higher level processing, the standard height products will include a number of corrections applied to the raw height estimates. For example to reduce aliasing problems, corrections for high frequency and fine spatial scale variations in SSH (e.g., tides and other high frequency ocean circulation changes) that may be inadequately sampled by

ICESat-2 should be applied before averaging. Estimates of these corrections will be given here. All corrections will be given in terms of height so that to apply a correction, users will add it to the height estimate, and to remove it they will subtract it. Additional corrections that some users may decide to apply will be provided with the product.

### **3.1.3.1 Geoid adjustment (Static)**

Heights are adjusted for local geoid height using mean-tide EGM2008. Prior to ATL03 Release 4, the EGM2008 was reported by ATL03 as taken from the mean-tide EGM2008 model. Starting with Release 4 ATL03 reports EGM2008 in the tide-free system and provides a conversion (*geoid\_free2mean*) that can be added to the tide-free geoid to yield the mean-tide EGM2008 for use in the ATL12 ocean product.

### **3.1.3.2 Atmospheric delay corrections**

Heights will be corrected based on an atmospheric model, giving corrections for total delay correction that accounts for wet and dry wet troposphere.

Corrections will be available for the forward-scattering bias, based on available atmospheric-scattering data and an estimate of the attenuation calculated from the apparent surface reflectance.

### **3.1.3.3 Dynamic Atmospheric Correction and the Inverse Barometer Effect (IBE, time-varying)**

Heights are corrected for the inverse barometer effect due to the direct application of atmospheric pressure to the sea surface and the dynamic changes forced by wind. ICESat-2 has adopted the utilization of global, empirical, 6-h, AVISO MOG2D,  $1/4^\circ \times 1/4^\circ$  grids to be used as a near-real time Inverted Barometer (IB) and Dynamic Atmospheric Correction (DAC)[*Carrère and Lyard, 2003*]. These grids are forced by the European Center for Medium-Range Weather Forecasting (ECMWF) model for the surface pressure and 10-m wind fields. This combined correction typically has amplitude on the order of  $\pm 50$  cm [*Markus et al., 2016*].

### **3.1.3.4 Tidal corrections (time-varying)**

The tide related geophysical corrections applied to ATL03 ellipsoidal photon heights input to ATL12 include solid earth tides (in tide free system), ocean loading, and pole tides (both ocean and solid earth):

Solid earth tides (*tide\_earth*): ATL03 photon heights input to ATL12 are relative to solid earth tides in the tide-free system derived using IERS (2010) conventions are  $\pm 30$  cm max (details in ATL03 ATBD section 6.3.3). The ATL03 solid earth tides are appropriate to all higher level products, but they are appropriate to the ocean and sea ice products only insofar as they are the reference to which ocean tides are added for a full accounting of tides in ocean surface heights.

Ocean load tides (*tide\_load*): The local displacement due to ocean loading (-6 to 0 cm) derived from ocean tide model GOT4.8. Details in ATL03 ATBD, section 6.3.1

Pole tide (*tide\_pole*): Pole tides include both solid earth and ocean pole tides. These each are computed via IERS (2010) conventions. Details are found in ATL03 ATBD sections 6.3.5 and 6.3.6, respectively.

Ocean pole tide (*tide\_oc\_pole*): Ocean Pole Tide -Loading due to centrifugal effect of polar motion on the oceans (2 mm, max), subsumed in Pole tide (*tide\_pole*)

Tidal corrections to be applied in ATL12 include short period ocean tides and longer period equilibrium tides:

Ocean tides (*tide\_ocean*): Ocean Tides including diurnal and semi-diurnal (harmonic analysis), and longer period tides (dynamic and self-consistent equilibrium) ( $\pm 4$  m) are from the GOT4.8. Details in ATL03 ATBD, section 6.3.1.

Equilibrium tides (*tide\_equilibrium*): Equilibrium long-period tide computed using a subroutine attached to GOT4.8 called LPEQMT.F by Richard Ray. It is a Fortran routine in which fifteen tidal spectral lines from the Cartwright-Tayler-Edden tables are summed. (See section 6.3.1 of the ATL03 ATBD.)

### **3.1.3.5 Wind and SWH Estimates**

Surface winds and significant wave height for forecast/reanalysis products will be taken from an appropriate source such as the ECMWF and with the ATL12 product for comparison with ICESat-2 derivations of SWH as part of the sea state bias calculation.

## **3.2 Gridded Sea Surface Height (ATL19/ L3B)**

The ATL19 product includes gridded monthly estimates of dynamic ocean topography (DOT) taken from ATL12 ocean segment data. Ocean segments range in length roughly from 3 to 7km. The ocean segment data are averaged in  $\frac{1}{4}^\circ$  or 25km grid cells. Data from all six beams (gtxr and gtxl) are used from the beginning to the end of each month, although commonly over most of the ocean only data from the strong beams will be available. The IS-2 data are averaged onto three grids, called mid-latitude, north-polar and south-polar. The ATL19 product has groups with the same names containing the gridded data for each of those regions. The grids, gridding schemes, input variables and output variables are described in detail in the ATBD for ATL19.



## **4.0 ALGORITHM THEORY**

In this section, we discuss the following topics:

1. Finding the collection of photon heights representing reflection from the sea surface.
2. Separating the surface wave generated variation in photon heights from other sources of variance.
3. Determining SWH and higher order measures of sea state
4. Formulating the best sea state bias correction

### **4.1 Introduction**

The main purpose of the algorithms developed here is the determination of Sea Surface Height (SSH). There are two main steps to determining sea surface height (SSH) from ICESat-2 photon heights (ATL-03) over the ocean. These are identifying photon heights that likely represent reflection from the sea surface, loosely termed surface finding (Sec. 4.2), and determining the correct statistics of the sea surface height distribution (Sec 4.3). Most importantly we seek the SSH equal to the mean of the height distribution. Because of the motion of the sea surface, surface finding over open water is inherently a search for a distribution of heights representative of the sea surface. Our main product will be the mean of this distribution over time, length and space scales to be determined as part of testing and analysis. In addition other properties of the distribution are useful for assessing the surface wave environment and biases in the SSH determination. Though we focus here on obtaining meaningful statistical distributions of sea surface heights, we have found it possible in tests with MABEL data to create meaningful moving 21-photon means of the heights from the photons designated signal photons by the surface finding routines. This gives a relatively high-resolution time- (or space-) series trace of the sea surface in fair agreement with the analysis using the high-resolution sea ice analysis. This may be used in experimental analyses for surface waves. Figure 11 shows the block diagram for the ATL12 processing to go from ATL03 photon data to along-track histograms and statistics of dynamic ocean topography. Figure 13 illustrates the gridding procedure to go from ATL12 products to ATL19 gridded DOT and SSH.

### **4.2 ATL12: Finding the surface-reflected photon heights in the photon cloud**

Surface finding over the open ocean rests on our limited experience with MABEL data over open water. With few surface returns per pulse and significant wave heights much less than the range of samples, the majority of the bins will contain only noise photons so that the median will equal the number of noise photons per bin. Thus, the fundamental idea for surface finding is to identify as surface height bins, those bins with counts exceeding the median number of counts. In extreme cases where ICESat-2 encounters significant wave heights approaching the 30-m downlink range of bins, we may have to adopt a slightly different threshold such as the count value equal to or exceeding 20% of the bin population.

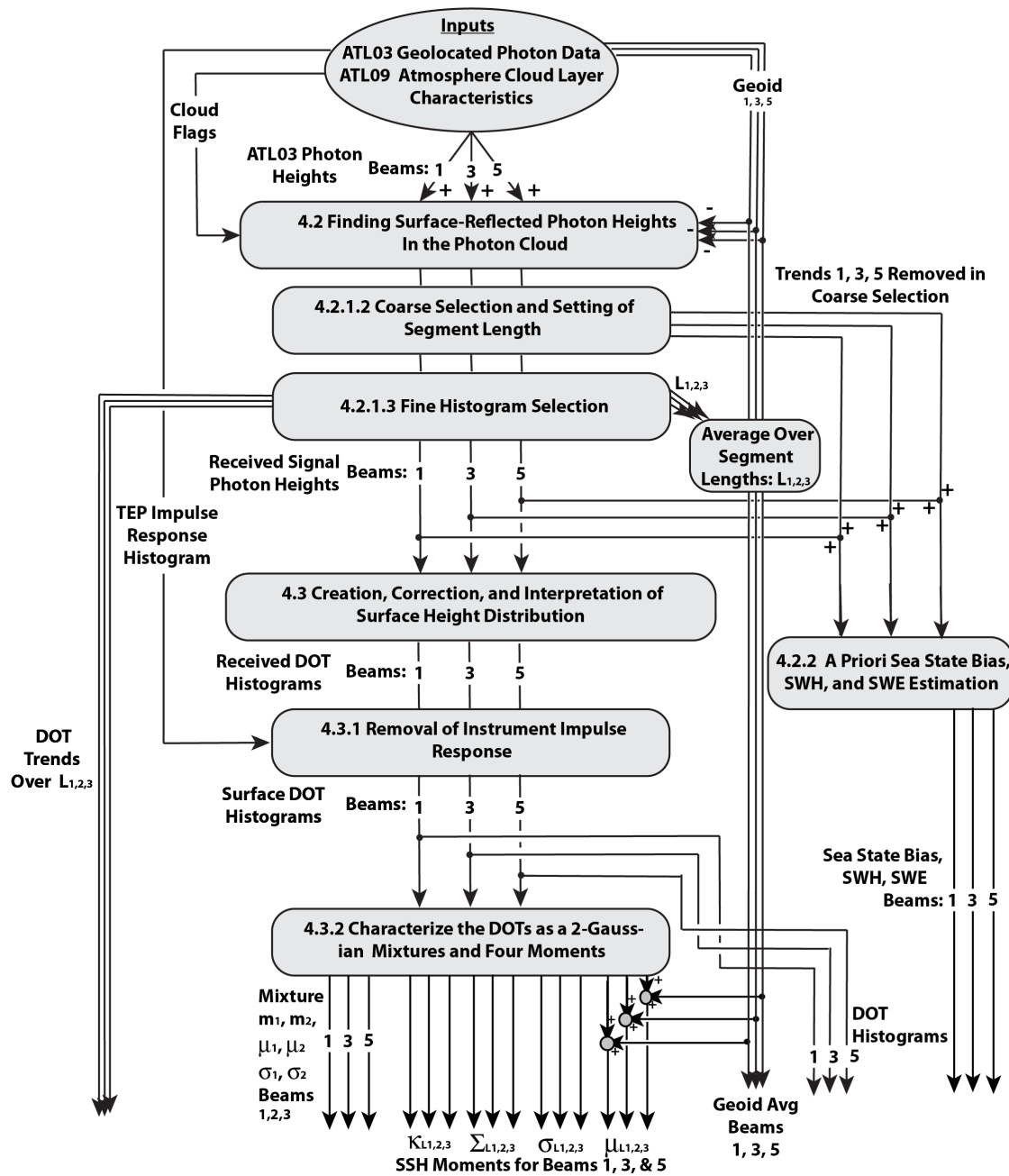


Figure 11. ATL 12 processing block diagram as discussed in Section 3 and 4.  $\mu$ ,  $\sigma$ ,  $\Sigma$ , and  $K$  denote mean, standard deviation, skewness, and kurtosis respectively.

We anticipate a large number of surface reflected photons may be needed to adequately resolve the higher moments of the sea surface height distribution. Also, fine spatial resolution is probably not required in most open ocean settings. Therefore, we will use a semi-adaptive scheme to accumulate segments long enough to capture up to 10,000 candidate surface photons. This will involve a coarse median-based selection and segment-length setting process (4.2.1.2). This will be followed by a finer scale histogram construction that includes median-based selection of surface photons, a detrending process, and repeat selection (4.2.1.3)

#### 4.2.1 Selection of Signal Photon Heights

##### 4.2.1.1 Input to Selection of Photons:

ATL12 will require ATL03 photon heights for each pulse in the ocean downlink band and associated time geolocation, geophysical corrections (geoid, tides, dynamic atmospheric correction), and confidence level information, plus the cloud flag, **layer\_flag**, every 400 pulses from ATL09.

As of Release 3, the ATL03 includes a flag for each ground track indicating the quality of the precision orbit and pointing determination: **gtx/geolocation/podppd\_flag**, and we found unrealistic values for ocean segments when this flag was non-zero indicating degraded orbit and/or pointing data. Consequently ATL12 processing for Release 4 is done with data for which **gtx/geolocation/podppd\_flag**=0.

It is important to note that non-zero values of the **podppd\_flag** have been commonly associated with ocean scans over the Western Pacific Ocean or round-the-world (RTW) scans, which in either case require ICESat-2 to execute conical scans with 5° off-pointing. In the past, **podppd\_flag** was set to zero in ATL03 throughout these maneuvers. As a consequence of the **podppd\_flag** editing, ATL12 Release 4 had a significant data gap in the Western Pacific. However, with the present processing, the science data is reasonable in most parts of ocean scans and RTW scans other than transitions into them. Consequently, the **podppd\_flag** has been refined.

As of Release 5, the **podppd\_flag** will have seven possible values: normal operations values: 0=NOMINAL; 1=POD\_DEGRADE; 2=PPD\_DEGRADE; 3=PODPPD\_DEGRADE; plus possible calibration maneuver related "CAL" values: 4=CAL\_NOMINAL; 5=CAL\_POD\_DEGRADE; 6=CAL\_PPD\_DEGRADE; 7=CAL\_PODPPD\_DEGRADE. For ATL12, we will only use data when the POP/PPD flag indicates nominal normal operations or nominal CAL maneuvers, **podppd\_flag** equal to 0 or 4. For each ocean segment processed, we will report the higher of these two **podppd\_flag** values, 0 or 4, of data used in the ocean segment.

Further, as of April 17, 2020 ICESat-2 started doing segmented RTW scans in three parts to cover a reference ground track excluding the ice sheets. More importantly, to reduce the Western Pacific data gap, on April 8, 2021, instead of two ocean scans per day ICESat-2 will only do two ocean scans on the same day as an RTW scan, and with two

(sometimes three) RTW scans per week, this will result in only four (sometimes five or six) ocean scans per week.

Based on early discussions, this ATBD and the developmental software developed from it was assumed that ICESat-2 over the ocean would downlink photon heights within  $\pm 15$  m of the EGM2008 geoid. Aside from the  $\pm 15$ -m band about the geoid, no classification as to surface/non-surface photons was to be made.

However, as configured in December 2018, the Flight Science Receiver Algorithms (FSRA) downlinks photon heights in bands about heights chosen by signal finding procedure described in text in "ATLAS Flight Science Receiver Algorithms Version 3.7c". This identifies center heights over 200-shot major frames as those where the most photon heights relative to noise are found in adjacent bins of a coarse altimetry band. When operating in local daylight and in the presence of even thin clouds, and perhaps over parts of the ocean with reduced reflectance, for example wave slopes, the most popular height bin can shift to chance concentrations of noise photons up to 200 to 300 m above or below the geoid. The resulting 30-m erroneous downlink bands of photon heights appear in 200-pulse major frames and one or two height bands supposedly bracketed by heights topping at (using the example of ground track 2 right) `gt2r/bckgrd_atlas/tlm_top_band1` and `gt2r/bckgrd_atlas/tlm_top_band2`, with heights given as `gt2r/bckgrd_atlas/tlm_height_band1` and `gt2r/bckgrd_atlas/tlm_height_band2`.

The most concerning problem is that when the downlink band is pulled away from the true surface we can arguably lose true surface reflected photons, biasing sea surface heights in some unknown direction and violating the assumptions of the ATL12 sea state bias determination. In subsequent revisions of ATL03, the photons from major frames for which the center of the downlink band is far removed from the geoid are eliminated.

In practice we have found that the erroneous downlink bands can be edited out as those containing no ATL03 high confidence photons. Therefore, we use the signal confidence product in ATL03 to edit out the erroneous downlink bands. This grades each photon height return as to likelihood that it is a surface return by examining height bins at 50-pulse rate for signal to noise ratio in the context of noise level. Early ICESat-2 ocean data suggests that photon heights with high, medium, and low (4, 3, 2) confidence levels very seldom appear in the erroneous downlink bands. Further, the confidence level software assigns a fill-in confidence level of 1 to what would be zero confidence heights in order to fill a  $\pm 15$  bin about the high confidence heights. Therefore, in practice confidence level 1 or greater essentially covers the geoid  $\pm 15$ -m band and can be used to edit out the erroneous downlink bands. In processing, ATL12 considers photons with confidence level equal to 1 or greater as the possible surface photons subject to the surface finding routine.

Because we are using this ground-based editing, in the future we will have to investigate the effect on the sea surface height and SSB calculation of missing true surface photons not downlinked in the presence of erroneous downlink bands, probably by comparing daytime and nighttime data over the same region.

#### 4.2.1.2 Coarse Selection and Setting of Segment Length

The process is basically to first establish a variable length (e.g., up to 7 km) ocean segment with enough (e.g.) photon heights to yield a histogram with reasonable moments up to 4<sup>th</sup> order.

2. Examine ocean depth and cloud parameters against control parameters to test for suitability for ocean processing.
  - If control parameter *layer\_swtch* is equal to 1, then remove the ATL03 segment ids from ocean processing that are associated with the ATL09 segment ids where *layer\_flag* is equal to 1. When *layer\_swtch* equals 0 (the default value), the software will ignore the cloud cover in accepting data during coarse surface finding.
  - Ignore data collected over land or too close to land. If ocean depth, *depth\_ocn*, is less than a depth, *depth\_shore*, specifying the effective shoreline of water for which ocean processing is appropriate, then proceed to next 14 geo-bin (400-pulse) segment. The default value for control parameter *depth\_shore* will be -10 m for depths given by GEBCO as negative elevation values.
3. Correct photon heights for short period and long period ocean tides (*gtxx/geophys\_corr/tide\_ocean and tide\_equilibrium*), the inverse barometer effect and the modeled dynamic response to the atmosphere (dynamic atmospheric correction, *gtxx/geophys\_corr/dac*),
4. Select only photon heights for which the signal confidence (*gtxx/heights/signal\_conf\_ph*) is greater than or equal to 1 and indicator for saturation *gtxx/heights/quality\_ph* is zero. This will select photons in the likely surface  $\pm 15$ -m buffer window. Also delete any photon heights outside the band defined by geoid plus or minus half the height of the ocean downlink window (presently geoid  $\pm 15$ -m, to become geoid  $\pm 20$ -m). **(Is the height of the downlink band reported in ATL03 perhaps at the geoseg rate and if so, what is the variable name? The height is listed at the major frame rate. But it would be handier if it was at the geoseg rate)**
5. Subtract the EGM2008 geoid in the mean-tide system from photon heights to reference all heights to the geoid. Note that as of Release 4, EGM2008 provided by ATL03 is in the tide-free system. However, ATL03 also provides the conversion that should be added to the tide-free geoid to yield EGM2008 in the mean-tide system.
6. Establish an initial coarse histogram array,  $H_c$ , spanning  $\pm 15$  m with bin size  $B_l$  (TBD, e.g., 0.01 m) and a data array,  $A_{coarse}$ , for up to 10,000 photon heights and associated information (index, geolocation, time) plus noise photon counts. This will be populated with data for the coarse selection of signal photons.
7. Aggregate photon heights over 14 geo-bins (400-pulses) and construct a temporary 14 geo-bin (400-pulse) height histogram spanning  $\pm 15$  m with bin size  $B_l$  (e.g., 0.01 m). This is used to estimate a running total number of signal and noise photons. We suggest a bin size of 0.01 for consistency with later steps in the processing. The 14 geo-bin (400-pulse) segment should be aligned so that the once per 14 geo-bin (400-pulse, approximately 280 m along track distance) cloudiness flag, *layer\_flag* in ATL09, represents the aggregate effect of cloudiness and background radiation derived from solar

zenith, *asr\_cloud\_probability*, *cloud\_flag\_atm*, and *bsnow\_con*, during the 280-m segment.

8. Photons in the 14 geo-bin (400-pulse) histogram bins with greater than the  $Th_{Nc\_c}$  times the median number of photons,  $N_{median}$ , are candidate signal photons and photons in the bins with the median number of samples or less are considered noise photons. We have been using  $Th_{Nc\_c} = 1$  in our tests with early ICESat-2 data. Note that with few surface returns per pulse and significant wave heights much less than 30 m, the majority of the of the bins will contain only noise photons so that the median will equal the number of noise photons per bin. In extreme cases where ICESat-2 encounters significant wave heights approaching 30 m, we may have to adopt a slightly different threshold such as the count value equal to or exceeding 20% of the bin population.
9. Add the signal and noise photons from this 14 geo-bin (400-pulse) segment to the running total of candidate signal photons and noise photons, and add all the photons to the coarse histogram,  $H_c$ .
10. If the total number of candidate signal photons is greater than or equal to a minimum number,  $Th_{Ps}$  (e.g., 8,000), of photons or  $Seg_{max}$  (e.g., 25) 14 geo-bin (400-pulse) segments have been collected this defines an ocean segment, and we go on to Fine Selection (Sec 4.2.1.3) with the populated coarse histogram,  $H_c$ ,  $\pm 15$  m with bin size  $B_1$  (TBD, e.g., 0.01 m), and the data array,  $A_{coarse}$ . If the total number of signal photons is less than  $Th_{Ps}$ , repeat steps 4.2.1.2-2 to 4.2.1.2-5 above and intake another 14 geo-bin (400-pulse) segment until the ocean segment reaches a length of 7 km maximum. If the 7-km length is reached and there are less than a threshold number of photons (e.g.  $photon\_min = 4000$ ), ignore that ocean segment and repeat 4.2.1.2-2 to 4.2.1.2-6. For photon counts above this in the 7-km segment, proceed to 4.2.1.3 and fine histogram based signal finding.

#### 4.2.1.3 Fine Histogram Selection

1. Considering the coarse histogram array,  $H_c$ , perform a  $N_{bmv} = 20$ -cm/ $B_1$  bin (e.g., 21 bins over 20-cm) moving bin arithmetic average incremented by 1 bin. Pad the ends of the smoothed histogram with  $N_{bmv}/2$  bins (equal the smoothed first and last values) to match the length of the original histogram.
2. The ASAS 5.1 finds the bin

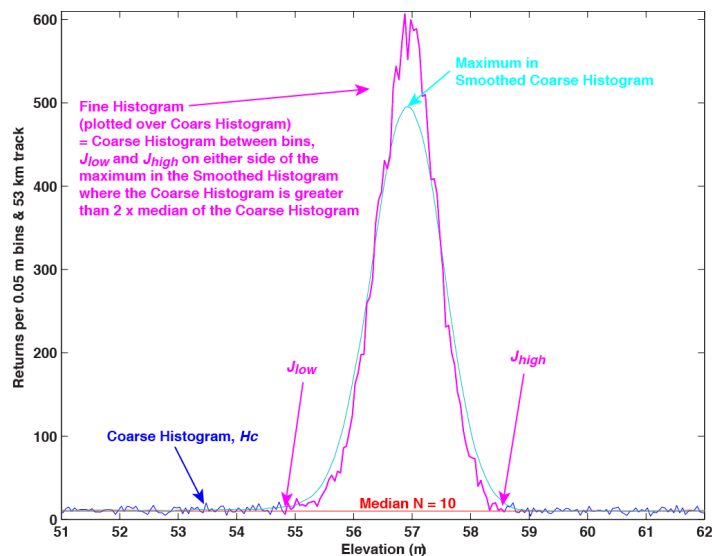


Figure 12. Illustrative coarse, smoothed, and fine histograms from steps 1 and 2 of 4.2.1.3 as applied 66 to 10 minutes of April 2012 MABEL data over Chesapeake Bay. The corresponding figure for detrended data in the second iteration (steps 4-6) are similar.

limits of the fine histogram as all the coarse histogram bins on either side of the maximum in the 20-cm smoothed histogram, from the  $J_{low}$  bin position to the  $J_{high}$  bin, where the smoothed histogram bin photon count is greater than the median of the smoothed histogram photon count. In practice with preliminary ATLAS data the median has usually been zero. Essentially, we have moved out from the middle of the histogram until the histogram levels fall to zero.

As of 6/4/2019, the developmental code finds preliminary bin limits of the fine histogram as all the coarse histogram bins on either side of the maximum in the 20-cm smoothed histogram, from the preliminary  $J_{low}$  bin position to the preliminary  $J_{high}$  bin, where the coarse bin photon count is greater than the coarse histogram median. Then the average counts in the bins above the preliminary  $J_{high}$  are calculated and set equal to  $tailnoisehigh$  and the average counts in the bins below the preliminary  $J_{low}$  are calculated and set equal to  $tailnoiselow$ . Then we find the bin limits of the fine histogram as all the coarse histogram bins on either side of the maximum in the 20-cm smoothed histogram, from the final  $J_{low}$  bin position to the final  $J_{high}$  bin, where the final  $J_{low}$  bin position is that below which the smoothed histogram bin photon count is less than  $Th\_Nc\_f$  times  $tailnoiselow$ , and the final  $J_{high}$  bin position is that above which the smoothed histogram bin photon count is less than  $Th\_Nc\_f$  times  $tailnoisehigh$ . This procedure is better able to differentially remove subsurface noise returns and above surface returns.  $Th\_Nc\_f$  is TBD, but we have used  $Th\_Nc\_f = 1.5$  in practice with Release 001 ATLAS data and this has resulted in greatly improved rejection of subsurface returns.

As of 11/5/2019 for Release 4, we modified the surface finding procedure as described in section 5.3.2. Instead of basing surface finding on the distribution of photon heights, it is now based on the distribution of the photon height anomalies relative to a moving 11-point bin average of high-confidence photon heights. This excludes subsurface returns under the crests of surface waves that otherwise fall inside the histogram of true surface heights. This further reduces any error due to subsurface returns, obviating the immediate need for a subsurface return correction.

3. Consider the time series of all the heights stored in  $A_{coarse}$  with heights anomalies that lie between anomalies corresponding the  $J_{low}$  and the  $J_{high}$  bin positions in the distribution of height anomalies. This array of heights and times represents the first iteration on surface height statistics, but the higher moments are elevated by variations of the mean with time (or distance). Therefore, calculate the least squares linear fit to these versus time (or distance). Store the constant and first order coefficients,  $P0$  and  $P1$ , of the linear fit used for detrending **as output variables for the segment** and subtract them from the data of  $A_{coarse}$  to yield array  $A_{fine}$  of detrended photon heights and associated geolocation data.
4. From the heights of  $A_{fine}$ , create the detrended coarse histogram,  $H_d$ ,  $\pm 15$  m with bin size  $B_1$  (TBD, e.g., 0.01 m). Then repeat steps 1 and 2 substituting  $H_d$  for  $H_c$  including creating the 11-point moving average of high-confidence photons the height anomalies about this moving average, and the histogram of height anomalies.
5. Considering the detrended coarse histogram array,  $H_d$ , perform a  $N_{bmv} = 20\text{-cm}/B1$  bin (e.g., 21 bins) moving bin arithmetic average incremented by 1 bin. Pad the ends

of the smoothed histogram with  $N_{bmv}/2$  bins (equal the smoothed first and last values) to match the length of the original histogram.

6. The ASAS 5.1 finds the bin limits of the fine histogram as all the coarse histogram bins on either side of the maximum in the 20-cm smoothed histogram, from the  $J_{low}$  bin position to the  $J_{high}$  bin, where the smoothed histogram bin photon count is greater than the median of the smoothed histogram photon count. In practice with preliminary ATLAS data the median has usually been zero. Essentially, we have moved out from the middle of the histogram until the histogram levels fall to zero.

As of 6/4/2019, the developmental code finds preliminary the bin limits of the fine histogram as all the coarse histogram bins on either side of the maximum in the 20-cm smoothed histogram, from the preliminary  $J_{low}$  bin position to the preliminary  $J_{high}$  bin, where the coarse bin photon count is greater than the coarse histogram median. Then the average counts in the bins above the preliminary  $J_{high}$  are calculated and set equal to *tailnoisehigh* and the average counts in the bins below the preliminary  $J_{low}$  are calculated and set equal to *tailnoiselow*. Then we find the bin limits of the fine histogram as all the coarse histogram bins on either side of the maximum in the 20-cm smoothed histogram, from the final  $J_{low}$  bin position to the final  $J_{high}$  bin, where the final  $J_{low}$  bin position is that below which the smoothed histogram bin photon count is less than  $Th\_Nc\_f$  times *tailnoiselow*, and the final  $J_{high}$  bin position is that above which the smoothed histogram bin photon count is less than  $Th\_Nc\_f$  times *tailnoisehigh*. This procedure is better able to differentially remove subsurface noise returns and above surface returns. We have used  $Th\_Nc\_f=1.5$  in practice with Release 001 ATLAS data and this has resulted in greatly improved rejection of subsurface returns.

As of 11/5/2019 for Release 4, as for the first pass, for the second pass we modified the surface finding procedure as described in section 5.3.2. Instead of basing surface finding on the distribution of photon heights, it is now based on the distribution of the photon height anomalies relative to a moving 11-point bin average of high-confidence photon heights. This excludes subsurface returns under the crests of surface waves that otherwise fall inside the histogram of true surface heights. This further reduces any error due to subsurface returns, obviating the immediate need for a subsurface return correction. Note that although surface finding is based on the height anomalies, the final product of these steps is the histogram of the actual heights of the selected surface photons,  $H_R$ .

7. The resulting  $H_R$  is the fine histogram of received surface heights to be used in further analysis. The time series of all the heights stored in  $A_{fine}$  that lie between heights corresponding the second iteration  $J_{low}$  and the  $J_{high}$  bin positions will be saved for wave and sea state bias analysis (Section 4.2.2).

#### 4.2.2 A Priori Sea State Bias Estimation and Significant Wave Height

As a side calculation, we will use the spatial record of signal photon heights derived through the process described in Sections 4.2.1.1-4.2.1.3 as an approximation to the true surface height. This height record has been detrended during surface finding and the mean

of this fit (linear fit coefficients  $P0$  and  $P1$  in 4.2.1.3) over the positions of the surface detected points must be added back to the surface heights to include all SSB in the record. With this height record, we resolve the structure of surface waves versus along track distance and the variation in photon return rate to estimate sea state bias. The inherently high spatial resolution of ICESat-2 will allow us to measure the variation in surface height over the large energy-containing surface waves that lead to sea state bias. We will also know the photon return rate along the waves. Over the ocean segments (equivalent to 8,000 candidate signal photons or 7 km whichever is less), we will determine surface height variation and photon return rate in 10-m along-track bins. To calculate the photon return rate per meter it will be necessary to sort the photon height record in ascending order of along-track distance. From the height and photon rate records we will compute the covariance of surface height and photon return rate. Combined with the average photon return rate, the covariance of height and return rate is the sea state bias according to equation (11). We can approximate the significant wave height (SWH) as four times the standard deviation of the bin-averaged heights.

### 4.3 ATL12: Correction and Interpretation of the Surface Height Distribution

There are two main issues in deriving surface statistics from the apparent heights of surface-reflected photons identified in the surface detection phase and manifest in the fine histogram,  $H_R$ , of Section 4.2. These are correcting the heights for the instrument impulse response and deriving higher order moments of the corrected surface height distribution.

#### 4.3.1 Separating the Uncertainty due to Instrument impulse response

The received heights of surface reflected photons are the sum of a true height of the surface plus an uncertainty due to the instrument impulse response. The latter is the total of all instrument uncertainty, but it is dominated by uncertainty in the time the individual photons are transmitted. The ATLAS uncertainty in height due to instrument impulse response will have a standard deviation of 15-22 cm. Because the instrument impulse response uncertainty and the true height variation are additive, the received surface photon distribution,  $H_R$ , is equal to the convolution of the instrument impulse response height error distribution,  $H_T$ , and the true height distribution,  $H_Y$ :

$$H_R = H_T * H_Y \quad (12)$$

where  $*$  denotes convolution. Consequently, if we want to know the statistics of the surface from ICESat-2 returns, we must deconvolve  $H_T$  from  $H_R$  to get  $H_Y$ .

If we know that  $H_Y$  is a Gaussian distribution, we only need concern ourselves computing the mean and standard deviation of the distribution. However, we expect received ocean surface heights to depart from a Gaussian distribution because of a combination the shape of surface waves and the non-uniform sampling due wave-induced variations of specular reflection. In addition to the mean and standard deviation, the third and second moments (skewness, and kurtosis) are also important. If we knew the true sample heights, we could

calculate these moments as sample moments, e.g., the  $n^{\text{th}}$  sample moment for  $Y_i$  from the time series of heights:

$$M_n(Y) = \frac{1}{m} \sum_{i=1}^m (Y_i - \bar{Y})^n \quad (13)$$

or as the discrete form of the integral over the probability density function,

$$\int_{-\infty}^{\infty} (Y - M_1)^n H(Y) dY, \text{ if we knew } H(Y).$$

However, the instrument impulse response delay,  $T$ , and the received height,  $R$ , are independent and additive ( $R=T+Y$ ), so in principle it is possible to calculate sample moments for  $Y$  from the sample moments of  $T$  and  $R$ :

$$M_1(Y) = M_1(R) - M_1(T) \approx \frac{1}{m} \sum_{i=1}^m R_i - \frac{1}{m} \sum_{i=1}^m T_i \quad (14)$$

$$M_2(Y) = M_2(R) - M_2(T) \approx \frac{1}{m} \sum_{i=1}^m (R_i - \bar{R})^2 - \frac{1}{m} \sum_{i=1}^m (T_i - \bar{T})^2 \quad (15)$$

$$M_3(Y) = M_3(R) - M_3(T) \approx \frac{1}{m} \sum_{i=1}^m (R_i - \bar{R})^3 - \frac{1}{m} \sum_{i=1}^m (T_i - \bar{T})^3 \quad (16)$$

$$\begin{aligned} M_4(Y) &= M_4(R) - M_4(T) - M_2(Y)M_2(T) \\ &\approx \frac{1}{m} \sum_{i=1}^m (R_i - \bar{R})^4 - \frac{1}{m} \sum_{i=1}^m (T_i - \bar{T})^4 - M_2(Y)M_2(T) \end{aligned} \quad (17)$$

These sample moments will be calculated for the ICESat-2 heights as a check on more exact methods. The uncertainty in sample moments is significant [Percival, personal communication] and this uncertainty is compounded with combinations such as (14)-(16). These problems are liable to be particularly important when looking for small variation in skewness,  $M_3/M_2^{3/2}$ , and excess kurtosis,  $M_4/M_2^2 - 3$ . Optimized approaches for determining the moments of the height distribution require that we separate the effect of instrument impulse response from the received heights to give us the distribution of surface height,  $H_Y$ . To do this we must deconvolve  $H_T$  from  $H_R$ .

Deconvolution can be done in several ways. The Inland Water ATBD (ATL-13) expresses the convolution of (12) for the received histogram as the multiplication of a matrix representing the instrument impulse response histogram times a vector representing the surface height histogram. This matrix is inverted and multiplied times the received histogram to yield the surface histogram. The technique is reportedly sensitive to proper binning to produce a matrix that can be inverted.

Deconvolution can also be done by taking the Fourier transform of (12) and noting that the Fourier transform,  $\mathcal{F}(\cdot)$ , of the convolution of two variables,  $H_R(k)=\mathcal{F}(H_R)=\mathcal{F}(H_T*H_Y)$  is equal to the product of the Fourier transform of the two variables,

$$H_R(k)=\mathcal{F}(H_R)=\mathcal{F}(H_T*H_Y)=\mathcal{F}(H_T)\mathcal{F}(H_Y) \quad (18)$$

where  $k$  is the wavenumber in units of  $m^{-1}$ , the Fourier space counterpart to height in meters, the histogram independent variable. From (18), we can compute  $H_Y$  as an inverse Fourier transform,  $\mathcal{F}^{-1}(\cdot)$  of the ratio of  $\mathcal{F}(H_R)$  and  $\mathcal{F}(H_T)$ ,

$$H_Y=\mathcal{F}^{-1}(\mathcal{F}(H_R)/\mathcal{F}(H_T)) \quad (19)$$

The problem with this approach is that there is invariably noise in the received signal histogram,  $H_R$ , that produces significant values in  $\mathcal{F}(H_R)$  at wavenumbers where  $\mathcal{F}(H_T)$  has small values or zeros. This may have something in common with problem of conditioning of the matrix in the matrix inversion technique. In any event, these unrealistic combinations make the inverse Fourier transform unstable. To account for the noise in  $H_R$ , we consider Wiener deconvolution, in which it is assumed the received histogram is contaminated with noise,  $N$ , and (12) and (18) become

$$H_R = H_T * H_Y + N \quad (20)$$

and where  $H_T(k)=\mathcal{F}(H_T)$ ,  $H_Y(k)=\mathcal{F}(H_Y)$ ,  $H_R(k)=\mathcal{F}(H_R)$ , and  $N(k)=\mathcal{F}(N)$ ,

$$H_R(k) = H_T(k)H_Y(k) + N(k) \quad (21)$$

An estimate  $H_Y(k)$  for  $H_{Yest}(k)$  of the form

$$H_{Yest}(k)=W(k)H_R(k)/H_T(k) \quad (22)$$

is sought such the expected value of  $(H_Y(k)-H_{Yest}(k))^2$  is a minimum. This is found for

$$W(k)=\mathcal{F}(H_T)^2/[\mathcal{F}(H_T)^2+\mathcal{F}(Noise)^2/\mathcal{F}(H_Y)^2] \sim \mathcal{F}(H_T)^2/[\mathcal{F}(H_T)^2+\mathcal{F}(Noise)^2/\mathcal{F}(H_R)^2] \quad (23)$$

and

$$H_{Yest}=\mathcal{F}^{-1}(H_{Yest}(k))=\mathcal{F}^{-1}(W(k)\mathcal{F}(H_R)/\mathcal{F}(H_T)) \quad (24)$$

For wave numbers where the inverse signal to noise ratio,  $\mathcal{F}(Noise)^2/\mathcal{F}(H_R)^2$ , is low relative to  $H_T(k)$ ,  $W(k)$  goes to one and equation (24) reverts to (19). Where the inverse signal to noise ratio is high (high noise),  $W(k)$  goes to zero and the noise is filtered out of the resulting  $H_{Yest}(k)$ .

#### 4.3.2 Characterizing the Random Sea Surface

The best method for determining sample moments is the method of expectation maximization (ML). For a distribution of known type  $f(x \setminus \mu_{1,2,3,4})$ , the optimum choice of

parameters,  $\mu_{1,2,3,4}$ , for data values  $x_1, x_2, x_3, \dots, x_m$ , are those which maximize the likelihood,  $L$ ,

$$L(\mu_{1,2,3,4} \setminus x_1, x_2, x_3, \dots, x_m) = \prod_{i=1}^m f(x_i \setminus \mu_{1,2,3,4}) \quad (25)$$

For ICESat-2 sea surface height, we are not sure of the form of the probability density function but commonly the ocean surface has been characterized by the Gram-Charlier distribution for which the first 4 moments are important. Such a distribution can be represented it by mixture of two Gaussian distributions,  $N_a$  and  $N_b$

$$\begin{aligned} f(x_i \setminus \mu_{1,2,3,4}) &= m_a N_a(x_i \setminus \mu_{a1,2}) + m_b N_b(x_i \setminus \mu_{b1,2}) \\ m_a + m_b &= 1 \end{aligned} \quad (26)$$

and the two moments of each distribution plus the mixing ratio,  $m_a/m_b$ . Given the surface height histogram, the parameters of the two normal distributions and the mixing ratio can be determined by expectation maximization.

The aggregate moments of the Gaussian mixture  $X$  with  $n$  component Gaussian distributions are functions of the component means,  $\mu_i$ , and variances,  $\sigma_i^2$ , and the mixing ratio,  $m_i$ ,

$$E[(X - \mu_{mix})^j] = \sum_{i=1}^n \sum_{k=0}^j \frac{j!}{k!(j-k)!} (\mu_i - \mu_{mix})^{j-k} m_i E[(X_i - \mu_i)^k] \quad (27)$$

For example, the aggregate mixture mean is:

$$\mu_{mix} = m_1 \mu_1 + m_2 \mu_2 \quad (28)$$

and the aggregate variance is:

$$\sigma_{mix}^2 = m_1 \left( (\mu_1 - \mu_{mix})^2 + \sigma_1^2 \right) + m_2 \left( (\mu_2 - \mu_{mix})^2 + \sigma_2^2 \right) \quad (29)$$



owing to the presence of long large waves, successive photon heights are far from independent. The fact that the underlying wave signal is periodic makes the estimate of the effective degrees of freedom in terms of correlation length scale more problematic. As a worst case if we set  $N_{df}$  equal to the number of wave periods in the ocean segment, 15 in the case of long waves crossed at an acute angle, the uncertainty,  $\sigma_L$ , in the estimate of the mean equals 0.16 m, close to the mean SSH we see over many similar ocean segments. This problem is not instrumental; it is just made apparent by the ability of ICESat-2 to resolve waves. To lower this uncertainty, we are exploring using harmonic analysis of surface height over each ocean segment and use of the zero wave-number amplitude to represent SSH (D. Percival, personal communication, 2019) as a way of removing large periodic variations in height as a cause of uncertainty. A further advantage of this approach will be that it will add a measure of wave spectral properties to ATL 12. In any event, we will have to derive measures of the effective number of degrees of freedom as an ATL12 output for each ocean segment in order to properly account for uncertainties in the gridded SSH product.

#### **4.5 ATL19: Gridding the DOT and SSH**

This product, based on Product ATL12/L3A, contains gridded monthly estimates of sea surface height from all IS-2 tracks from the beginning to the end of each month. Below 60°N and above 60°S, the data are mapped on the curvilinear grid of the TOPEX/Poseidon with spacing equivalent to 0.25° of longitude. Above 60°N and below 60°S the grid data are mapped onto a planimetric grid using the SSM/I Polar Stereographic Projection equations at a grid spacing of about 24 km.. ATL12 provides the histograms and first four moments of dynamic ocean topography over ocean segments ~ 3-7-km long (means of DOT are converted to mean sea surface heights by adding ocean segment mean geoid height, which is also output by ATL12). It also provides the number of photon heights,  $n_{photons}$ , going into the moments and an effective degrees-of-freedom,  $NP_{effect}$ , based on the correlation length scale of surface heights. Using these, ATL19 will produce monthly aggregate histograms of surface heights and averages of the ocean segment moments weighted by both  $n_{photons}$  and  $NP_{effect}$  (Fig. 13). See the ATL19 ATBD for a complete description.

## 5.0 ALGORITHM IMPLEMENTATION

This section describes the specific implementation of the algorithm for program development.

### 5.1 Outline of Procedure

- 1) Finding the surface-reflected photon heights in the photon cloud
  - a) Coarse Selection and Setting of Segment Length:  
Use a median-based selection criterion to accumulate a large number of surface-reflected photons.
  - b) Fine Histogram Selection:  
Use a median-based selection criterion to derive a preliminary surface height histogram, compute the mean and trend in surface height, remove this trend from all heights, and repeat the median-based selection criterion to derive a final surface height histogram
- 2) Using the along track signal photon heights from the fine histogram selection step and signal photon return rate to estimate sea state bias and surface wave properties.
- 3) Correction and Interpretation of the Surface Height Distribution
  - a) Separating the Uncertainty due to Instrument impulse response  
Use Wiener deconvolution to derive the surface height histogram with the uncertainty due to the instrument impulse response removed.
  - b) Characterizing the Random Sea Surface  
Characterize the surface height histogram as a mixture of two normal distributions and calculate up to 4<sup>th</sup> moment of the mixture.
  - c) Compute the mean, variance, skewness, and kurtosis for the aggregate Gaussian mixture using Equation 17; the final determination of SSH for ATL12 is the mean of the aggregate mixture distribution computed using (28) and the SSH variance is given by (29).

### 5.2 Input Parameters

#### 5.2.1 Parameters Required from ICESat-2 Data

See Tables 2 and 3. For ATL12, the primary inputs will be photon heights in the downlink band and associated time, geolocation, the geoid (*geoid*), ocean tides (*tide\_ocean*, *tide\_equilibrium*), and dynamic atmospheric correction (*dac*) information from ATL03, plus the cloud flag (*layer\_flag* in ATL09) every 400 laser pulses from ATL09 and ocean depth, *depth\_ocn*, from interpolated from GEBCO-2014 gridded ocean bathymetry. Normally over the open ocean (or sea ice) regions not overlapping with terrestrial or ice sheet regions, the downlink band will be  $\pm 15$  m centered about the signal area identified by the ATLAS on-board flight software. In the ocean regions overlapping with land and ice sheet regions, the downlink band will expand to match the band for those regions. Also for ATLAS special operations such as ocean scans and Transmitter Echo Pulse

data collection the telemetry band is expanded. For the purposes of ATL12, the EGM2008 geoid supplied with ATL03 (*gtx/geophys\_corr/geoid* posted at the 20m along-track rate for each beam in ATL\_03) will be used to establish the narrower  $\pm 15$ -m band within the expanded downlink band of the overlap and special operations regions. In addition to the  $\pm 15$ -m band about the geoid, we use several classifications and flags from ATL03 to edit photon heights.

The photon quality flag, *quality\_ph*, detects various conditions such as saturated laser pulses for which we want to discard photon height, so we only process heights with this flag equal to 0.

We have also found unrealistic values for ocean segments when ATL03 *gtx/geolocation/podppd\_flag* is non-zero indicating degraded orbit and/or pointing data. Per Section 4.2.1, for Release 5 with seven possible values of *podppd\_flag*, ATL12 processing should only be done with data for which *gtx/geolocation/podppd\_flag*=0 indicating nominal operations or *gtx/geolocation/podppd\_flag*=4 indicating nominal calibration maneuvers.

Perhaps most importantly, we use the ATL03 confidence that the photon is surface reflected, *signal\_conf\_ph* at high levels (3 or 4) to determine if we have a viable surface in a downlink band, and we use only photons with *signal\_conf\_ph* greater than or equal to 1 in our surface finding procedure

Also, the surface finding now (as of Release 4) uses the distribution of the anomaly of photon heights relative to a 11-point moving average of photons with *signal\_conf\_ph* greater than or equal to 2 to segregate surface photons from noise photons. This method is more sensitive than editing the height histogram and shows better rejection of subsurface returns under ocean waves.

The 14 geo-bin (400-pulse) ocean segment are aligned so that the once per 14 geo-bin (400-pulse) cloud flag (*layer\_flag* in ATL09) represents the cloud conditions during the ocean segment. We have found that we can get good surface heights even when the *layer\_flag* indicates the presence of waves, but we do compute the average ocean segment cloud cover as the fraction of *layer\_flag* =1 over the ocean segment.

Table 2 Input parameters (Source: ATL03)

| Label                 | Description                                       | Symbol              |
|-----------------------|---|---------------------|
| <i>delta_time</i>     | Elapsed seconds since first data point in granule | <i>time_initial</i> |
| <i>lat_ph</i>         | latitude of each received photon                  | <i>lat_initial</i>  |
| <i>lon_ph</i>         | longitude of each received photon                 | <i>lon_initial</i>  |
| <i>h_ph</i>           | height of each received photon                    | <i>ht_initial</i>   |
| <i>dist_ph_along</i>  | Along track distance                              |                     |
| <i>sigma_along</i>    | Uncertainty in along-track distance               |                     |
| <i>dist_ph_across</i> | Across-track distance                             |                     |
| <i>sigma_across</i>   | Uncertainty in across-track distance              |                     |
| <i>segment_id</i>     | Along-track segment ID number                     | <i>segment_id</i>   |

|                           |  |                                  |
|---------------------------|--|----------------------------------|
| <i>signal_conf_ph</i>     | Confidence level associated with each photon event selected as signal. Zero equals noise. One means added to allow for $\pm 15$ -m buffer around high confidence, but algorithm classifies as background. Two equals low confidence. Three equals medium. Four equals high. With release 4 <b><i>signal_conf_ph</i></b> equal = -2 indicates possible TEP photon | <b><i>signal_conf_ph</i></b>     |
| <i>quality_ph</i>         | Photon quality as to saturation and after-pulse <ul style="list-style-type: none"> <li>• 0 = nominal, no saturation</li> <li>• 1 = possible after-pulse</li> <li>• 2 = possible long-tail impulse response</li> <li>• 3 = possible TEP (also indicated by <i>signal_conf_ph</i> = -2)</li> </ul>   | <b><i>quality_ph</i></b>         |
| <i>ref_azimuth</i>        | The direction, eastwards from north, of the laser beam vector as seen by an observer at the laser ground spot viewing toward the spacecraft (i.e., the vector from the ground to the spacecraft). When the spacecraft is precisely at the geodetic zenith, the value will be 99999 degrees. 40 Hz.   |                                  |
| <i>ref_elev</i>           | Co-elevation (CE) is direction from vertical of the laser beam as seen by an observer located at the laser ground spot.  |                                  |
| <i>solar_azimuth</i>      | The direction, eastwards from north, of the sun vector as seen by an observer at the laser ground spot.  |                                  |
| <i>solar_elevation</i>    | Solar Angle above or below the plane tangent to the ellipsoid surface at the laser spot. Positive values mean the sun is above the horizon, while negative values mean it is below the horizon. The effect of atmospheric refraction is not included. This is a low precision value.   |                                  |
| <i>bckgrd_rate</i>        | Background count rate ( <i>bckgrd_atlas/bckgrd_rate</i> ), simply averaged over the segment  |                                  |
| <i>fpb_parm(n)</i>        | Parameter needed to compute first-photon bias correction to a mean height. This is not used as of Release 4. See Section 3.1.1.4.  | TBD                              |
| <i>dac</i>                | Dynamic atmospheric correction (DAC) includes inverted barometer (IB) effect ( $\pm 20$ cm)  |                                  |
| <i>tide_earth</i>         | Solid Earth Tides in the tide-free system ( $\pm 30$ cm, max)  |                                  |
| <i>tide_equilibrium</i>   | Equilibrium long-period tide   |                                  |
| <i>tide_load</i>          | Load Tide - Local displacement due to Ocean Loading (-6 to 0 cm)   |                                  |
| <i>tide_oc_pole</i>       | Ocean Pole Tide -Loading due to centrifugal effect of polar motion on the oceans ( 2 mm, max)  |                                  |
| <i>tide_ocean</i>         | Ocean Tides including diurnal and semi-diurnal (harmonic analysis), and longer period tides (dynamic and self-consistent equilibrium) ( $\pm 4$ m)   |                                  |
| <i>tide_pole</i>          | Pole Tide -Rotational deformation due to polar motion (-1.5 to 1.5 cm)   |                                  |
| <i>neutat_delay_total</i> | Total neutral atmospheric delay correction   | <b><i>neutat_delay_total</i></b> |
| <i>surf_type</i>          | Five-element array in the geolocation group indicating the surface masks that apply to that segment  |                                  |
| <i>geoid</i>              | Geoid height, EGM2008 in the tide-free system (mean-tide in Rel. 3 and earlier)  | <b>5.2.1</b>                     |
| <i>geoid_free2mea</i>     | Conversion factor to be added to <i>geoid</i> to convert to a mean-tide system   |                                  |

|                    |   |       |
|--------------------|---|-------|
| <i>n</i>           |   |       |
| <i>podppd_flag</i> | 5.2.2 Indication of degraded pointing or orbit determination. Possible values are: : 0=NOMINAL; 1=POD_DEGRADE; 2=PPD_DEGRADE; 3=PODPPD_DEGRADE; possible CAL values are: 4=CAL_NOMINAL; 5=CAL_POD_DEGRADE; 6=CAL_PPD_DEGRADE; 7=CAL_PODPPD_DEGRADE. | 5.2.2 |

**Table 3 Input parameters (Source: ATL09)**

| Label                        | Description   | Symbol |
|------------------------------|---|--------|
| <i>delta_time</i>            | Elapsed GPS seconds since start of the granule. Use the metadata attribute granule_start_seconds to compute full gpstime. |        |
| <i>latitude</i>              | Latitude, WGS84, North=+, Lat of segment center   |        |
| <i>longitude</i>             | Longitude, WGS84, East=+, Lon of segment center   |        |
| <i>asr_cloud_probability</i> | Cloud probability based on Apparent Surface Reflectivity $p=(1-asr/t)*100$  |        |
| <i>apparent_surf_reflec</i>  | Apparent Surface Reflectivity (25Hz)  |        |
| <i>Layer_flag</i>            | Represents presence (1) or absence (0) of significant cloud layers.   |        |

### 5.2.3 Parameters Required from Other Sources

**Bathymetry** – Because the ocean mask extends into non-ocean areas we need a way to determine which parts of the ocean data are over water for which our analysis procedure is appropriate. For this we will take the ocean depth, ***depth\_oce***, from the General Bathymetric Chart of the Oceans (GEBCO) 2014 gridded data set ([https://www.gebco.net/data\\_and\\_products/gridded\\_bathymetry\\_data/](https://www.gebco.net/data_and_products/gridded_bathymetry_data/)) evaluated at the geo-segment ***latitude*** and ***longitude***.

**Ice Concentration** – Because the ocean mask extends into sea ice covered oceans (the province of ATL07 and ATL10), in gridding and other analysis we seek ways of reconciling ATL12 ocean surface heights with DOT with ATL10 freeboard and ocean surface heights as measured in open water regions amongst the sea ice. To do this we need to output ice concentration, ***ice\_conc***, in ATL12 at the average latitude and longitude of each ocean segment. These values of ice concentration are to be from the same source used in the derivation of the ATL07 and ATL10 products found as daily values of ice concentration from the National Snow and Ice Data Center: Near-Real-Time NOAA/NSIDC Climate Data Record of Passive Microwave Sea Ice Concentration, Version 1, available at <https://nsidc.org/data/g10016>. Ocean segment mean latitude and longitude,

*gtx/ssh\_segments/latitude* and *longitude*, should be converted to the NSIDC Northern and Southern Hemisphere polar stereographic grids and these grid locations used to interpolate the ice concentration, *gtx/ssh\_segments/stats/ice\_conc*.

### 5.2.4 Control Parameters for ATL12 Processing

Bathymetry – The coarse surface finding described in 5.3.1 will ignore data collected in ocean waters with a depth, *depth\_ocn*, less than a depth, *depth\_shore*, defining the effective shoreline of water for which our analysis procedure is appropriate. The default value for *depth\_shore*, will be 10 m.

Cloud cover – In the coarse surface finding described in 5.3.1 we may need to ignore data collected in ocean waters where and when the cloud cover is heavy as indicated by *layer\_flag*, equal to 1. The control parameter *layer\_swatc* will specify if the cloudiness test is to be applied. If control parameter *layer\_swatc* is equal to 1 and *layer\_flag* is equal to 1, photon heights will not be included in the ATL12 processing. When *layer\_swatc* equals the default value, 0, the software will ignore the cloud cover in accepting data during coarse surface finding.

These control parameters are output in *ancillary\_data/ocean* for each granule/file ATL12.

## 5.3 Processing Procedure

### 5.3.1 Coarse Surface Finding and Setting of Segment Length

The process is basically to first establish a variable length (e.g., up to 7 km) ocean segment with enough (e.g.) photon heights that will yield a histogram with reasonable moments up to 4<sup>th</sup> order. We start with 14 geo-bin (400-pulse) segments of ATL03 photon heights (see 5.2.1)

Table 4 Control parameters – Coarse surface finding

| Parameter                | Description  | Value         |
|--------------------------|--|---------------|
| <i>B<sub>c</sub></i>     | Bin size of coarse histogram   | 5 cm          |
| <i>Th<sub>Nc_c</sub></i> | Number of photons times median required to classify as surface bin   | 1 typical     |
| <i>Th<sub>Ps</sub></i>   | Minimum number of candidate surface photons per segment  | 8,000         |
| <i>Segmax</i>            | Max number of 400-pulse segments in a surface finding segment  | 25            |
| <i>layer_swatc</i>       | Flag determining if <i>layer_flag</i> will ( <i>layer_swatc</i> =1) or won't ( <i>layer_swatc</i> =0) be editing photon heights. | Default = 0   |
| <i>depth_shore</i>       | Prescribed depth defining ( <i>depth_ocn</i> > <i>depth_shore</i> ) boundary of ocean processing                                 | Default= 10 m |

(A) Ocean Data Selection and Basic Geophysical Corrections

- 
- 1) Stepping through 14-geobin segments, examine ocean depth and cloud parameters against control parameters to test for suitability for ocean processing. If ocean depth, *depth\_ocn*, is less than a depth, *depth\_shore*, specifying the effective shoreline of water for which ocean processing is appropriate, then proceed to next 14 geo-bin (400-pulse) segment. The default value for control parameter *depth\_shore* will be 10 m.

Similarly, if control parameter *layer\_swth* is equal to 1 and *layer\_flag* is equal to 1, then proceed to next 14 geo-bin (400-pulse) segment. When *layer\_swth* equals the default value, 0, the software will ignore the cloud cover in accepting data during coarse surface finding.

- 2) Correct for photon heights for short period and long period ocean tides (*gtxx/geophys\_corr/tide\_ocean* and *tide\_equilibrium*), the inverse barometer effect and the modeled dynamic response to the atmosphere (dynamic atmospheric correction, *gtxx/geophys\_corr/dac*),
- 3) Select only photon heights for which the signal confidence (*gtx/heights/signal\_conf\_ph*) is greater than or equal to 1 and photon quality (*gtxx/heights/quality\_ph*) is equal to zero. This will select photons in the likely surface  $\pm 15$ -m buffer window. Also delete any photon heights outside the band defined by geoid plus or minus half the height of the ocean downlink window (presently geoid  $\pm 15$ -m, to become geoid  $\pm 20$ -m). **(Is the height of the downlink band reported in ATL03 and if so, what is the variable name?)**
- 4) To narrow the range of variability, subtract the EGM2008 geoid height (*gtxx/geophys\_corr/geoid*), varying over meters to tens of meters, from the photon heights so that we are dealing dynamic ocean topography varying over centimeters to 10s of centimeters. from photon heights to reference all heights to the geoid. Note that as of Release 4, EGM2008 provided by ATL03 is in the tide-free system, but ATL03 also includes a correction mean-tide system, which should be added to the tide-free EGM2008 to obtain the mean-tide EGM2008.

(B) Establish a Working Histogram Array

-----

Establish an initial coarse histogram array,  $H_c$ , spanning  $\pm 15$  m with bin size  $B_1$  equal to 0.01 m with center bin centered at zero and bin centers at whole centimeters. Also establish a data array,  $A_{coarse}$ , for up to 10,000 photon heights and associated information (index, geolocation, time) plus noise photon counts. This will be populated with data as we step through 14-geobin segments searching for an adequate number of surface photon candidates.

(C) Step Through 14-Geo-bin Segments

-----

Aggregate photon heights over 14 geo-bins (400-pulses) and construct a temporary 14 geo-bin (400-pulse) height histogram spanning  $\pm 15$  m with bin size  $B_1$  (e.g., 0.01 m). This is

used to estimate a running total number of signal and noise photons. We suggest a bin size of 0.01 for consistency with later steps in the processing. The 14 geo-bin (400-pulse) segment should be aligned so that the once per 14 geo-bin (400-pulse, approximately 280 m along track distance) cloudiness flag, **layer\_flag** in ATL09, represents the aggregate effect of cloudiness and background radiation derived from solar zenith, **asr\_cloud\_probability**, **cloud\_flag\_atm**, and **bsnow\_con**, during the 280-m segment.

(D) Test for Surface Photons

Photons in the 14 geo-bin (400-pulse) histogram bins with greater than the **Th\_Nc\_c** times the median number of photons,  $N_{median}$ , are candidate signal photons and photons in the bins with the median number of samples or less are considered noise photons. **Th\_Nc\_c** is

Table 5 Control parameters – Fine surface finding and analysis

|             |   |                                |
|-------------|---|--------------------------------|
| $B_f$       | Bin size of fine histogram  | 5 cm, MABEL<br>1 cm, ICESat-2  |
| $Th\_Nc\_f$ | Surface qualified= smooth hist > $Th\_Nc\_f$ * tail noise                         | 1.5, ICESat-2                  |
| $pts2bin$   | Bins in boxcar smoother   | 21, ICESat-2                   |
| $conf\_lim$ | Minimum confidence level to be included in moving average                         | Typically, 3 or 4 for ICESat-2 |
| $nphoton$   | Number of photons either side of central photon to consider averaging             | 5 for an 11 point average      |
| $nharms$    | Number of harmonics to fit to selected surface photons                            | 32 default                     |
| $gaplimit$  | Gap between photons above which gaps are filled with white noise for harmonic fit | 3.2 m default                  |

TBD, but we have been using **Th\_Nc\_c** = 1 in our tests with early ICESat-2 data. Note that with few surface returns per pulse and significant wave heights much less than 30 m, the majority of the of the bins will contain only noise photons so that the median will equal the number of noise photons per bin. In extreme cases where ICESat-2 encounters significant wave heights approaching 30 m, we may have to adopt a slightly different threshold such as the count value equal to or exceeding 20% of the bin population.

(E) Increase the Count of Surface Photons

Add the number of surface reflected photons to  $N_{good}$ , the running total of candidate surface photons and noise photons.

(F) Add All Photons to Data Array

-----  
 Add the all the photons, signal and noise, and their associated geolocation, time, and confidence level information from this 14 geo-bin (400-pulse) segment to the data array **HTin**.

(G) Test Counter for Sufficient Surface Photons

-----  
 If the total number of candidate signal photons is greater than or equal to a **minimum number, Th\_Ps** (8,000), of photons or if the number, **Nseg400**, of 14 geo-bin (400-pulse) segments collected reaches **Segmax** (e.g., 25 equivalent to ~7 km)), go on to 5.3.2 Processing Procedure for Classifying Ocean Surface Photons, Detrending, and Generating a Refined Histogram of Sea Surface Heights with the data array, **HTin**. The total number of pulses for the segment, **n\_pls\_seg**, equals 400 x **Nseg400**. If the total number of candidate surface reflected photons is less than **Th\_Ps**, intake another 14 geo-bin (400-pulse) segment and repeat steps 5.3.1 A-G above.

**5.3.2 Processing Procedure for Classifying Ocean Surface Photons, Detrending, and Generating a Refined Histogram of Sea Surface Heights**

The procedure based on development of Matlab Program:  
 ATBDdraftMABEL\_reader\_PhotonClassifyX2Channel6B\_noprint.m.

We start with the array of photon height data in **HTin** from 5.2.4. These are candidate heights accumulated over a segment of sufficient length to provide an adequate number of signal photons. In view of the low reflectance of the ocean surface this may require as many as 10,000 laser pulses. Break **HTin** into a vector of initial photon heights, **ht\_initial**, a vector of initial times, **time\_initial**, and vectors of initial location, **lat\_initial**, **lon\_initial**, a vector of along track distance, **trackdist\_initial**, and the vector of confidence level, **conf\_initial**, for each photon height.

(A) Establish or Summon the Bin Edge Vector

-----  
 Set up for the surface finding histogram, **N**, by establishing the vector, **Edges**, (with a length one greater than **N**) of histogram bin edges with bins **Bf** wide between -15 m to +15 m in steps of 1cm. Also establish the vector, **Ctrprt**, of bin center points with length equal to **N**. In practice **Bf** equals 1 cm, **Ctrprt** values are whole centimeters, and **Edges** are at half centimeter values. Also establish a vector array, **BinB**, as long as **ht\_initial** for bin assignments.

(B) Compute Moving Average of High Confidence Surface Photon Heights

-----  
 Here we want a moving average of high confidence surface heights, **mvng\_avg**, with a value corresponding to each photon raw photon height in **ht\_initial**. For the value of **mvng\_avg**,

compute the average of the photon heights in *ht\_initial* within *nphoton* either side of the central photon, including in the average only heights with *conf\_initial* greater than or equal to *conf\_lim*. For the first *nphoton* photons, pad *mvng\_avg* with the average for the *nphoton* + 1 photon in the sequence. For the last *nphoton* photons, pad the running average with the average for the last photon minus *nphoton*. For example, in testing we used *nphotons* = 5 and *conf\_lim* = 3 to make an 11-point running average centered on each photon height, and included in each average, only heights with confidence level 3 and 4.

C) Compute the Anomaly in Height About the Moving Average

-----

For each height in *ht\_initial*, compute *anom\_initial* equal to *ht\_initial* minus *mvng\_avg*.

(D) Compute Initial Histogram and Keep Track of Bin Assignment for Each Photon Height

-----

Populate the histogram array *N* such that each element equals the number of values from *anom\_initial* that are in the corresponding bin boundaries of *Edges*. Also, for each value in *anom\_initial*, populate the vector *BinB* with the bin number to which *anom\_initial* is assigned from one to the length, *LN*, of *N* (in Matlab, `[N,BinB]=histcounts(anom_initial,Edges)`).

(E) Find Median of Initial Histogram

-----

Find the median, *medianN*, of *N*.

(F) Smooth Initial Histogram with Boxcar Smoother

-----

- Create a smoothed version, *smoothN*, of the histogram, *N*, with a boxcar smoother incremented in one-bin steps over *pts2bin* where *pts2bin* is a control parameter in Table 5. It should equal *nbin* + 1 where *nbin* is an even number. We have chosen *nbins*=20 and *pts2bin* set at 21 based on success with the developmental code. In this ATBD with 1-cm bin size, we refer to this nominally as the “20-cm smoother” although it actually smooths over 21 bins. (In the ASAS 5.1 code used for ICESat-2 Rel. 001, *nbin* equals 100 corresponding to *pts2bin* = 101 and a 100-cm smoother).

- If needed, pad the ends of the smoothed histogram to match length of *N*. For example, a smoother that starts *nbin*/2+1 points in from the beginning of the original array and stops at an equal number of points before the end, will be *nbin* points shorter than the original array. In this case add *nbin*/2 points equal to the first smoothed value to the beginning of the array and add *nbin*/2 points equal to the last smoothed value to the end of the array.

(G) Find Limits of Valid Histogram

-----

The ASAS 5.1 finds the limits of the histogram above (**jlow**) and below (**jhigh**) for which, searching from the index of the maximum in the 20-cm smoothed histogram **smoothN**, the value in **smoothN** is greater than median of **smoothN**.

- First find the index, **imax**, where **smoothN(imax)** equals the maximum in **smoothN**.
- Increment the index, **i**, downward from **imax** until **smoothN(i)** is less than the median of **smoothN**. At this point **jlow = i+1**.
- Increment the index, **i**, upward from **imax** until **smoothN(i)** is greater than the median of **smoothN**. At this point **jhigh = i-1**.

As of 6/4/2019, the developmental code finds the limits of the histogram above a preliminary **jlow** and below a preliminary **jhigh** for which, searching from the index of the maximum in the 20-cm smoothed histogram **smoothN**, the value in **N** is greater than **Th\_Nc\_f**\*median of **N**.

- First find the index, **imax**, where **smoothN(imax)** equals the maximum in **smoothN**.
- Increment the index, **i**, downward from **imax** until **N(i)** is less than the median of **N**. At this point preliminary **jlow = i+1**.
- Increment the index, **i**, upward from **imax** until **N(i)** is greater than the median of **N**. At this point preliminary **jhigh = i-1**.
- Then the average counts in all the bins above the preliminary **Jhigh** are calculated and set equal to **tailnoiseshigh** and
- The average counts in all the bins below the preliminary **Jlow** are calculated and set equal to **tailnoiselow**.
- Increment the index, **i**, downward from **imax** until **smoothN(i)** is less than the **Th\_Nc\_f** \* **tailnoiselow**. At this point **jlow = i+1**.
- Increment the index, **i**, upward from **imax** until **smoothN(i)** is greater than **Th\_Nc\_f** \* **tailnoiseshigh**. At this point **jhigh = i-1**.

#### (H) Choose First Cut Signal Photons

-----  
 The first-cut signal or surface photons are those in the bins of histogram **N** between **jlow** and **jhigh**. The noise photons are those from bins below the **jlow** bin and above the **jhigh** bin. The vector **BinB** lists the bin assignment for each photon elevation. Therefore, the indices **ii** for which **BinB(ii)** is less than or equal to **jhigh** and greater than or equal to **jlow**, are the indices of the surface reflected photon heights in **ht\_initial**.

- Populate the vector of surface photon heights, **ht\_initial\_surf**, with the heights at indices **ii** in **ht\_initial** (in Matlab these surface heights would be **ht\_initial\_surf=ht\_initial(ii)**; where **ii** is the vector of surface photon indices).
- Identify the corresponding track distances, **trackdist\_initial\_surf**, in **trackdist\_initial** at the indices in **ii**.

(I) Do a Linear Fit of Height Versus Track Distance

-----

We need to do a linear fit to surface heights versus track distance because the trend in surface height contributes substantial variance to the histogram, which can cloud the surface finding algorithm. Therefore, perform a least squares linear fit of the form  $P1 \times trackdist\_initial\_surf + P0$  to  $ht\_initial\_surf$ .

(J) Subtract Surface Trend

-----

We make a new vector array of detrended heights,  $ht\_initial2$ , by subtracting the linear surface trend derived above at step 5.2.4 (G) from  $ht\_initial$ ,  
 i.e.,  $ht\_initial2 = ht\_initial - P1 \times trackdist\_initial + P0$ .

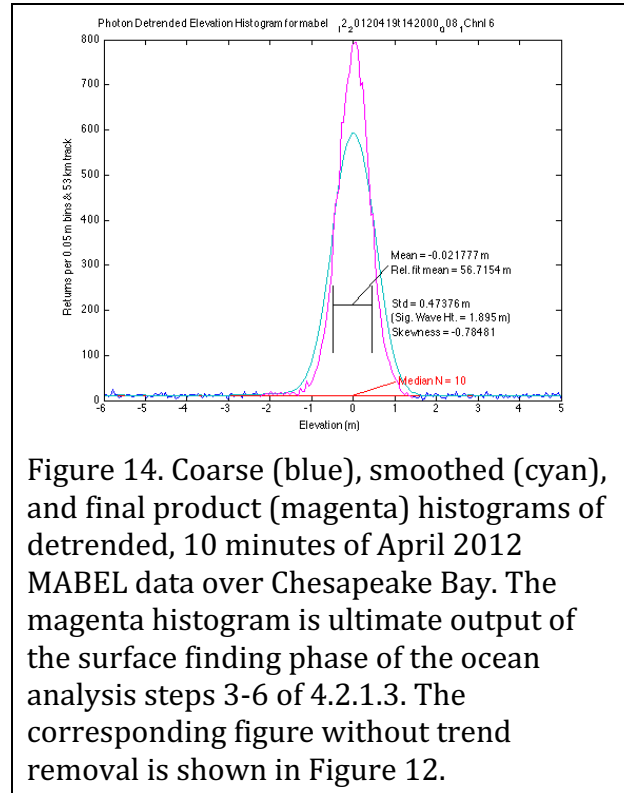


Figure 14. Coarse (blue), smoothed (cyan), and final product (magenta) histograms of detrended, 10 minutes of April 2012 MABEL data over Chesapeake Bay. The magenta histogram is ultimate output of the surface finding phase of the ocean analysis steps 3-6 of 4.2.1.3. The corresponding figure without trend removal is shown in Figure 12.

-----

REPEAT SURFACE FINDING AFTER REMOVING TREND

-----

In steps (K) through (P) below we repeat Steps (B) Through (H) Acting on the Detrended Elevations Starting With: Compute Moving Average of High Confidence Surface Photon Heights

(K) Compute Moving Average of High Confidence Detrended Surface Photon Heights

-----

Here we want a moving average of high confidence surface heights,  $mvng\_avg2$ , with a value corresponding to each photon raw photon height in  $ht\_initial2$ . For the value of  $mvng\_avg2$ , compute the average of the photon heights in  $ht\_initial2$  within  $nphoton$  either side of the central photon, including in the average only heights with  $conf\_initial$  greater than or equal to  $conf\_lim$ . For the first  $nphoton$  photons, pad  $mvng\_avg2$  with the average for the  $nphoton + 1$  photon in the sequence. For the last  $nphoton$  photons, pad the running average with the average for the last photon minus  $nphoton$ . For example, in testing we used  $nphotons = 5$  and  $conf\_lim = 4$ , to make an 11-point running average centered on each photon height, but included in each average, only heights with confidence level 4.

L) Compute the Anomaly in Detrended Height About the Moving Average of Detrended Height

-----  
 For each height in **ht\_initial2**, compute **anom\_initial2** equal to **ht\_initial2** minus **mvng\_avg2**.

Populate the histogram array **N** such that each element equals the number of values from **anom\_initial2** that are in the corresponding bin boundaries of **Edges**. Also, for each value in **anom\_initial2**, populate the vector BinB with the bin number to which **anom\_initial2** is assigned from one to the length, **LN**, of **N** [in Matlab, [N,BinB]=histcounts(anom\_initial2,Edges)].

(M) Find Median of Initial Histogram

-----  
 Find the median, **medianN**, of **N**.

(N) Smooth the Initial Histogram with Boxcar Smoother

-----  
 - Create a smoothed version, **smoothN**, of the histogram, **N**, with a boxcar smoother incremented in one-bin steps over **pts2bin** where **pts2bin** is a control parameter in Table 5. It should equal **nbin** + 1 where **nbin** is an even number. We have chosen **nbins**=20 and **pts2bin** set at 21 based on success with the developmental code. In this ATBD with 1-cm bin size, we refer to this nominally as the “20-cm smoother” although it actually smooths over 21 bins. (In the ASAS 5.1 code used for ICESat-2 Rel. 001, **nbin** equals 100 corresponding to **pts2bin** = 101 and a 100-cm smoother).

- If needed, pad the ends of the smoothed histogram to match length of **N**. For example, a smoother that starts **nbin/2+1** points in from the beginning of the original array and stops at an equal number of points before the end, will be **nbin** points shorter than the original array. In this case add **nbin/2** points equal to the first smoothed value to the beginning of the array and add **nbin/2** points equal to the last smoothed value to the end of the array.

(O) Find Limits of Valid Histogram

-----  
 The ASAS 5.1 finds the limits of the histogram above (**jlow**) and below (**jhigh**) for which, searching from the index of the maximum in the 20-cm smoothed histogram **smoothN**, the value in **smoothN** is greater than median of **smoothN**.

- First find the index, **imax**, where **smoothN(imax)** equals the maximum in **smoothN**.
- Increment the index, **i**, downward from **imax** until **smoothN(i)** is less than the median of **smoothN**. At this point **jlow** = **i+1**.
- Increment the index, **i**, upward from **imax** until **smoothN(i)** is greater than the median of **smoothN**. At this point **jhigh** = **i-1**.

As of 6/4/2019, the developmental code finds the limits of the histogram above a preliminary **jlow** and below a preliminary **jhigh** for which, searching from the index of the maximum in the 20-cm smoothed histogram **smoothN**, the value in **N** is greater than median of **N**.

- First find the index, **imax**, where **smoothN(imax)** equals the maximum in **smoothN**.
- Increment the index, **i**, downward from **imax** until **N(i)** is less than the median of **N**. At this point preliminary **jlow = i+1**.
- Increment the index, **i**, upward from **imax** until **N(i)** is greater than the median of **N**. At this point preliminary **jhigh = i-1**.
- Then the average counts in all the bins above the preliminary **Jhigh** are calculated and set equal to **tailnoisehigh** and
- The average counts in all the bins below the preliminary **Jlow** are calculated and set equal to **tailnoiselow**.
- Increment the index, **i**, downward from **imax** until **smoothN(i)** is less than the **Th\_Nc\_f \* tailnoiselow**. At this point **jlow = i+1**.
- Increment the index, **i**, upward from **imax** until **smoothN(i)** is less than **Th\_Nc\_f \* tailnoisehigh**. At this point **jhigh = i-1**.

(P) Choose Second-Cut Signal Photons

-----  
 The second-cut signal or surface photons are those in the bins of histogram **N** between **jlow** and **jhigh**. The noise photons are those from bins below the **jlow** bin and above the **jhigh** bin. The vector **BinB** lists the bin assignment for each photon elevation. Therefore, the indices **ii** for which **BinB(ii)** is less than or equal to **jhigh** and greater than or equal to **jlow**, are the indices of the surface reflected photon heights in **ht\_initial2**.

- Populate the vector of surface photon heights, **ht\_initial2\_surf**, with the heights at indices **ii** in **ht\_initial2** (in Matlab these surface heights would be **ht\_initial2\_surf=ht\_initial2(ii)**; where **ii** is the vector of surface photon indices).
- Identify the corresponding track distances, **trackdist\_initial2\_surf**, in **trackdist2\_initial** at the indices in **ii**, [i.e., in Matlab code **trackdist\_initial2\_surf = trackdist2\_initial(ii)**].

**ht\_initial2\_surf** is the main product of the surface finding routine. In addition, the second-pass surface indices in **ii** are the indices for the time, geolocation, track distance and all other data corresponding to **ht\_initial2\_surf**. The received histogram, **Nrs**, is then the histogram of **ht\_initial2\_surf** only including from the lowest height with count>0 to the highest height with count>0.

An example of the second pass and the histogram of surface heights for MABEL data are shown in Figure 14.

(Q) Calculate Number of Photons, Mean Time, and Geolocation for Segment

-----

The number of surface reflected photons in the ocean segment,  $n\_photons$ , is the length of the index vector  $ii$ . The time, geolocation, and track distance of the surface reflected photons are equal to the values in the vectors  $time\_initial$ ,  $lat\_initial$ ,  $lon\_initial$ , and  $trackdist\_initial$  at the index positions given by  $ii$  (e.g.,  $time\_initial(ii)$ ). Compute the segment time,  $t\_seg$ , as the mean of  $time\_initial(ii)$ , and the duration of the segment,  $delt\_seg$ , as the last value of  $time\_initial$  - the first value of  $time\_initial$ . Compute the segment latitude,  $lat\_seg$ , and segment longitude,  $lon\_seg$ , as the means of  $lat\_initial(ii)$  and  $lon\_initial(ii)$ , and the segment length,  $length\_seg$ , as the maximum value of  $trackdist\_initial2(ii)$  - the minimum value of  $trackdist\_initial2(ii)$ .

The total number of photons,  $n\_ttl\_photon$ , equals the length of  $time\_initial$ , and as above, the number of photons reflected from the surface equals  $n\_photons$  equal to the length of  $ii$ . The surface reflected photon rate per meter,  $photon\_rate = r_{surf}$ , is equal to  $n\_photons$  divided by  $length\_seg$ , and the noise photon rate per meter,  $photon\_noise\_rate = r_{noise}$ , is equal to the difference of  $n\_ttl\_photon$  minus  $n\_photons$  divided by  $length\_seg$ .

### 5.3.3 Processing to Characterize Long Wavelength Waves, Dependence of Sample Rate on Long Wave Displacement, and A Priori Sea State Bias Estimate

#### 5.3.3.1 Processing Steps to Estimate Sea State Bias

In this part we compute the Sea State Bias proportional to the covariance of photo return rate and surface height in 10-m along-track bins. This constitutes what is commonly referred to as the Electro-Magnetic or EM bias that is expected to dominate ICESat-2 SSB. The steps are:

5. Add  $meanoffit2$  to  $ht\_initial2\_surf$ .
6. Convert  $trackdist\_initial2\_surf$  to meters if necessary and subtract the minimum of  $trackdist\_initial2\_surf$  to obtain distance from start of the ocean segment.
7. Sort height data in ascending order of along-track distance,  $trackdist\_initial2\_surf$ , to allow calculation of photon return rate per meter
8. Define  $x$  as the sorted  $trackdist\_initial2\_surf$  and define  $hty$  the associated heights from  $ht\_initial2\_surf$ .
9. Do the following analysis for each 10-m bin in the ocean segment. In practice 710 bins to cover the max 7-km ocean segment length. For bins with no photon returns, the bin-averaged variables ( $xbind$ ,  $htybin$ ,  $xrbin$ ,  $slopebinfit$ ,  $latbind$ ,  $lonbind$ ) will be set to NaNs (not a number)
  - a) Set  $xbin$  to middle of 10-m bin.
  - b) Set  $xbind$  to the mean of  $x$  in each 10-m bin.
  - c) Set  $latbind$  to the mean of photon latitude in each 10-m bin.
  - d) Set  $lonbind$  to the mean of photon longitude in each 10-m bin
  - e) Set  $htybin$  to mean of  $hty$  in each 10-m bin.
  - f) Compute the photon data rate per meter,  $xrbin$ , by dividing the number of photons in each 10-m,  $nbind$ , bin by 10.
  - g) Establish  $slopebinfit$ :

- I. = NaN if only one photon in a 10-m bin
  - II. = change in *hty* over change in *x* if only two photons in a 10-m bin
  - III. = linear fit if three or more photons in a 10-m bin
10. Compute covariance of bin averaged height and data rate, *binCOVHtXr*, as the average over all 10-m bins of the product of the detrended binned heights, *htybin*, and the detrended binned data rate, *xrbin*.
  11. Compute, *binAVG\_Xr*, the average of binned data rate, *xrbin*, over the 10-m bins with photons.
  12. Compute the sea state bias, *binSSBias*, as *binCOVHtXr* divided by *binAVG\_Xr*.
  13. If there are more than one 10-m bin in an ocean segment with a valid *slopebinfit*:
    - a) Compute *slopeXreturn* as the product of the detrended slope, *slopebinfit*, and the detrended binned data rate, *xrbin*.
    - b) Compute the covariance of the photon rate and the slope, *binCOVslope\_Xr*, as the sum of the *slopeXreturn* divided by the number of 10-m bins with a valid *slopebinfit*.
    - c) Compute the sea state slope bias, *binSlopeBias*, as the covariance of the data rate and the slope, *binCOVslope\_Xr*, divided by the mean of the data rate.
  14. Save vector arrays *xbin*, *xbind*, *htybin*, and *xrbin* for segment output.

Since the rationale for some of these steps may not be obvious, we provide the following explanations for the steps:

To determine the SSB using Eq. 11 requires that we know the covariance of the surface return rate and the height anomaly associated with the dominant surface waves. To do this we must establish the height variations and photon return rate in evenly spaced 10-m bins along each ocean segment found during the coarse signal finding step. Section 5.3.1.

#### Estimating sea state bias over ocean segments

At this point, if not earlier, because we want to estimate the properties of waves typically hundreds of meters long, it will be necessary to aggregate *ht\_initial2\_surf* and *trackdist\_initial2\_surf* along each ocean segment found during the coarse signal finding step. Section 5.3.1

#### Add mean from detrending used after first cut surface finding

The means from the first cut of surface finding are computed from photon heights over surface waves and are therefore contaminated by the correlation of photon return rate with height of the surface over surface waves. If these are not added back into the height record, that contamination by SSB will be lost. Therefore, we add *meanoffit2*, the mean of  $P0 + P1 \times trackdist\_initial2\_surf$  (the along-track position of 2<sup>nd</sup> iteration surface photons), back into the photon height record,  $hty = ht\_initial2\_surf + meanoffit2$

#### Calculate the Photon Return Rate

After experimenting with more complicated schemes using photon spacing to determine photon return rate, we have concluded the return rate that most directly represents the EM sea state bias is to simply divide the number of photon returns in each 10-m bin by 10 to

yield the photon return rate per meter in each bin.

Quantify surface height and slope and return rate in 10-m along-track bins.

Establish a vector ***xbin***, the middle of 10-m bins along a length of 7,100 m, i.e., 5:10:7095, where 7,100m is the understood maximum of our ocean segments. Assign each sample interval (*ii*) in the, ***x<sub>i</sub>***, and ***hty<sub>i</sub>***, to one of these bins with a bin index ***ibin*** where ***ibin(ii)***=round-up (***x(ii)***-min(***x***))/10) and cumulatively add the ***hty(ii)*** to ***htybin(ibin(ii))*** and increment a bin counter, ***nbinc(ibin(ii))***, by one for each added sample.

Find averages, photon return rate and straight-line fits in each 10-m bin

For ***ibin*** equal to 1 through ***Nbin10***, the number of photons in each bin, ***nbind(ibin)*** = ***nbinc(ibin)***. Compute bin averages of surface height, ***htybin***, and data rate, ***xrbin***, as:

Compute the bin averages of height and data spacing:

***htybin(ibin)***= ***htybin(ibin)***/ ***nbinc(ibin)*** = ***htybin(ibin)***/ ***nbind(ibin)*** and

***xrbin(ibin)***= ***nbind(ibin)*** / 10.

Set ***xbind*** to the mean of the along-track positions in each 10-m bin = ***x(ibin)***/ ***nbind(ibin)***.

Also compute fits of surface height slope, ***slopebinfit***, in each bin

- In the cases with only 1 point in a bin, ***slopebinfit*** will be set to NaN (not a number).

- In the case of two points in a bin, ***slopebinfit*** will be equal to the change in ***hty*** over change in ***x***

- If the number of points in a bin is greater than or equal to 3, ***slopebinfit*** will equal the slope of a linear fit with distance over the points.

Compute Sea State Bias using all viable bins.

Compute covariance of bin averaged height and data rate, ***binCOVHtXr***, as the average over all 10-m bins of the product of the detrended binned heights, ***htybin***, and the detrended binned data rate, ***xrbin***, i.e., the sum over viable bins (bins with nonzero ***nbind***), ***iii***, from 1 to ***Nbin10*** of (detrended(***htybin (iii)***) \*detrended(***xrbin(iii)***))/***Nbin10***.

Similarly, compute ***binAVG\_Xr***, the average of binned data rate, ***xrbin*** , i.e, the average of ***xrbin(iii)*** from ***iii***=1 to ***Nbin10***.

Compute the bin average sea state bias estimate according to Equation X7:

***binSSBias*** equals ***binCOVHtXr*** divided by ***binAVG\_Xr***.

Compute Significant Wave Height, SWH

Compute significant wave height (***SWH***) equal to four times the standard deviation of the bin-averaged surface heights in all the 10-m along-track bins in the segment.

Compute photon rate slope correlation.

The bin average slope bias estimate is an experimental parameter that indicates if photons are being preferentially returned from the backsides or front faces of waves.

If there are more than one 10-m bin in an ocean segment with a valid **slopebinfit**, compute **slopeXreturn** as the product of the detrended slope, **slopebinfit**, and the detrended binned data rate, **xrbin**.

Then compute the covariance of the photon rate and the slope, **binCOVslope\_Xr**, as the sum of the **slopeXreturn** divided by the number of 10-m bins with a valid **slopebinfit**.

Save vector arrays **xbin**, **xbind**, **htybin**, and **xrbin** for segment output.

### 5.3.3.2 Harmonic Analysis of Along-track Heights With Requisite Gap Determination and Filling

Starting with the **n\_photons** points in the along track sorted **trackdist\_initial2\_surf**, and corresponding ocean heights in **ht\_initial2\_surf** with **meanoffit2** added back in, our aim is to compute the harmonic coefficients for **nharm** harmonics plus the zero-frequency coefficient best representing the sea surface.

The Vaníček method to be used is a least squared error technique that is not dependent on evenly space data. However, we have found that significant gaps in the data can result in wide and unrealistic variations in the resulting harmonic coefficients. This is because under the technique, the coefficients can vary unrestrained to fit the existing data, while producing wildly unrealistic Fourier series in the gaps where unconstrained by data. The solution to this problem is to find and fill the data gaps with white noise from a Gaussian distribution with mean equal to **meanoffit2** and standard deviation equal to that of the existing data. The first step is identifying significant data gaps in an ocean segment.

- 1) Letting  $X(j)$  be each value of **trackdist\_initial2\_surf(j)**, if we take the difference, **DX(1 to N-1)** between  $X(2\text{to}N)$  and  $X(1\text{ to }N-1)$ , it will be the vector of spaces between points, and we will know that there is no data for **DX(j)** meters after  $X(j)$ . We can think of the **DX** as a random variable so compute the sample median, mode, mean ( $\text{DXbar} = \text{Sum } DX \text{ from } 1 \text{ to } N-1 \text{ divided by } N-1$ ), sample variance ( $\text{DXvar} = \text{Sum } (DX - \text{DXbar})^2 \text{ from } 1 \text{ to } N-1 \text{ divided by } N-2$ ), and sample skewness ( $\text{DXskew} = \text{Sum } (DX - \text{DXbar})^3 / \text{DXvar}^{3/2} \text{ from } 1 \text{ to } N-1 \text{ divided by } N-2$ ). If there are no major gaps, the mean will be 0.4 to 0.7 m. If there are many small gaps, the variance and skewness will increase but the mean, mode, and median will probably stay close to 1 m. If there is one big gap, the skewness should become large. It will be helpful on many fronts to compute these statistics for ocean segments as indications of gaps in the ocean segment data. For example, in our tests with one ocean granule, we found unreasonable harmonic coefficients came from the Vaníček method only when  $\text{DXskew} > 10$ . The user could ignore ocean segment harmonic coefficients and/or ocean heights altogether if these indicators suggested there were many gaps in the data.
- 2) Alternatively, for the purposes of computing harmonic coefficients we will fill any gaps greater than **gaplimit** (e.g., **gaplimit** = 3.2 m) with random numbers every 0.7 m drawn from a Gaussian distribution with mean equal to **meanoffit2** and standard deviation equal to the standard deviation of **ht\_initial2\_surf**. To do this:

- 3) Identify the  $DX(l) > \text{gaplimit}$  and for each create gap-filling vectors of corresponding distances vectors,  $\mathbf{xgap}$ , every 0.7 m from  $X(l)$  to  $X(l)+DX(l)/0.7$  and of heights,  $\mathbf{hgap}$ , chosen as random numbers from a Gaussian distribution with mean equal to  $\text{meanoffit2}$  and standard deviation equal to the standard deviation of  $\text{ht\_initial2\_surf}$ . For each the  $DX(l) > \text{gaplimit}$  concatenate the  $\mathbf{xgap}$  and  $\mathbf{hgap}$  onto the previous  $\mathbf{xgap}$  and  $\mathbf{hgap}$  vectors until the final  $DX(l) > \text{gaplimit}$  is reached.
- 4) When the final  $DX(l) > \text{gaplimit}$  is reached, concatenate  $\mathbf{xgap}$  onto the end of  $\text{trackdist\_initial2\_surf}$  to make  $\mathbf{xtemp}$  and  $\mathbf{hgap}$  onto the end of  $\text{ht\_initial2\_surf}$  to make  $\mathbf{htemp}$ . Sort both  $\mathbf{xtemp}$  and  $\mathbf{htemp}$  on ascending order in  $\mathbf{xtemp}$  to insert the filled gaps in their proper order versus along-track distance. Set  $\mathbf{x}=\mathbf{xtemp}$  and  $\mathbf{y}=\mathbf{htemp}$ , and the resulting gap-filled records will be the  $\mathbf{x}$  and  $\mathbf{y}$  in the harmonic coefficient determination below. The length of the gap-filled  $\mathbf{x}$  is called  $n\_photontemp$ . Reference  $\mathbf{x}$  to the start by subtracting  $\mathbf{x}(1)$  from each  $\mathbf{x}$  value. Note that the gap-filled  $\mathbf{x}$  and  $\mathbf{y}$  will only be used for computing harmonics and will not be used for the other calculations of 10-m bin averages and sea surface height statistics.
- 5) For  $n\text{harm}$  harmonics, compute the wavelengths starting with the fundamental wavelength equal to the maximum of  $\mathbf{x}$  minus the minimum of  $\mathbf{x}$ . The vector of harmonic wavelengths,  $\mathbf{lwave}$ , is given by  $\mathbf{lwave}(i) = \text{length\_seg} / i$ ,  $i = 1$  to  $n\text{harms}$ , and the vector of harmonic wavenumbers is given by inverse of the wavelengths  $\mathbf{wn}(i) = 1/\mathbf{lwave}(i)$ ,  $i = 1$  to  $n\text{harms}$ .
- 6) Create matrix  $\mathbf{F}$  with  $n\_photontemp$  rows and  $1+2 * n\text{harms}$  columns. Populate  $\mathbf{F}$  as follows:

$$\mathbf{F}(j=1 \text{ to } n\_photontemp, i=1) = 1$$

$$\mathbf{F}(j, 2*i) = \sin(2*\pi*\mathbf{wn}(i)*\mathbf{x}(j)) \text{ for } j=1 \text{ to } n\_photontemp \text{ and } i=1 \text{ to } n\text{harms}$$

$$\mathbf{F}(j, 2*i+1) = \cos(2*\pi*\mathbf{wn}(i)*\mathbf{x}(j)) \text{ for } j=1 \text{ to } n\_photontemp \text{ and } i=1 \text{ to } n\text{harms},$$

And where  $\mathbf{x}(j)$  is each value of gap-filled  $\text{trackdist\_initial2\_surf}(j)$ .

- 7) Form left pseudo inverse and compute coefficients. For  $\mathbf{x}$  = the gap-filled  $\text{trackdist\_initial2\_surf}$ , a  $n\_photontemp$  x 1 column vector,  $\mathbf{F}$  is a  $n\_photontemp$  rows by  $m = 1 + 2*n\text{harms}$  columns matrix. The transpose of  $\mathbf{F}$ , here called  $\mathbf{F}'$ , is a  $m$  by  $n\_photontemp$  matrix. The matrix product,  $\mathbf{F}'\mathbf{F}$  is  $m$  by  $m$ . The product of  $\mathbf{F}'$  and  $\mathbf{x}$  = the gap-filled  $\text{trackdist\_initial2\_surf}$ , is a  $m$  by 1 vector.
- 8) For  $\mathbf{y}$  equal to the column vector of gap-filled  $\text{ht\_initial2\_surf}$  with  $\text{meanoffit2}$  added to it, versus  $\mathbf{x}$ , the gap-filled along track distance, compute the vector of harmonic coefficients,  $\mathbf{a}$ , by the Vaníček least squared error or left pseudo inverse method, where

$$\mathbf{a} = \mathbf{F}'\mathbf{F} \setminus \mathbf{F}'\mathbf{y}.$$

The  $m$  x 1 vector of harmonic coefficients,  $\mathbf{a}$ , for the optimum harmonic fit of  $\mathbf{y}$  to  $\mathbf{x}$ :

$$\mathbf{yfit} = \mathbf{a}(1) +$$

$$\mathbf{a}(2) * \sin(\mathbf{wn}(1) * 2 * \pi * \mathbf{x}) + \mathbf{a}(3) * \cos(\mathbf{wn}(1) * 2 * \pi * \mathbf{x}) +$$



5.2.5 (Characterizing the Random Sea Surface) breaks the processed histogram into a Gaussian Mixture and computes the aggregate distribution statistics for ATL12 using equation 17.

### 5.3.4.1 Separating the Uncertainty due to Instrument impulse response

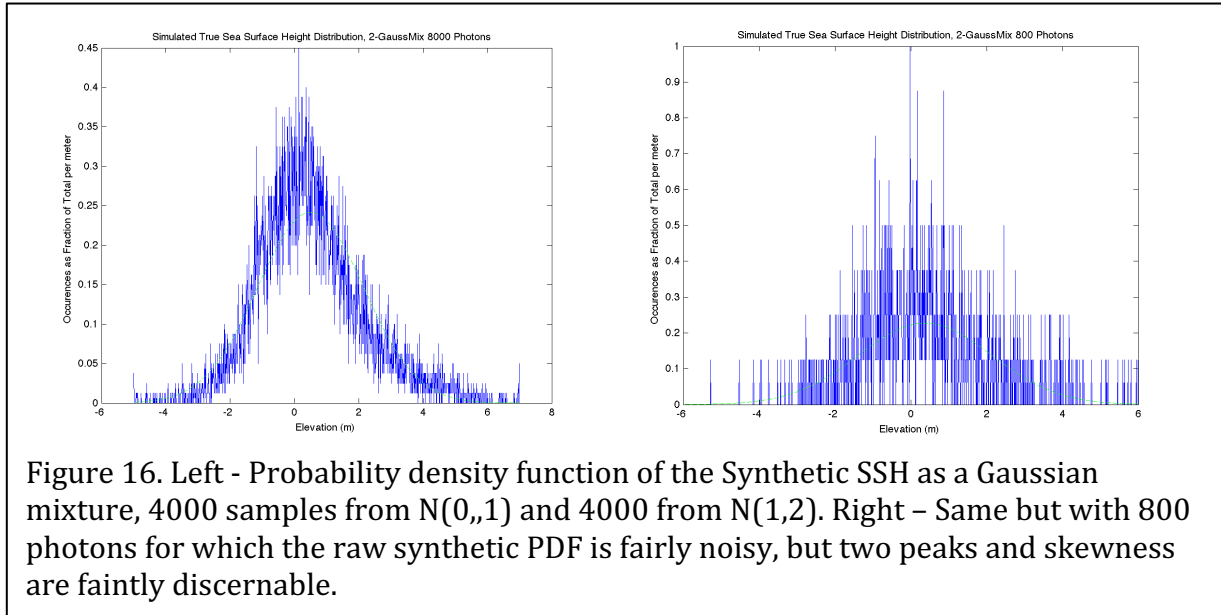
Parts

- (A) Starting with histogram of received photon heights from the previous section, compute a constant signal to noise ratio (SNRc)
- (B) Impulse Response Distribution
- (C) Fourier transform of the received histogram
- (D) Fourier transform of the instrument impulse response histogram
- (E) Compute the Wiener filter
- (F) Apply Wiener Deconvolution to Yield the Fourier Transform of the Surface Distribution
- (G) Compute the Surface Height Distribution

#### Code Steps

(A) Noise Ratio Determination

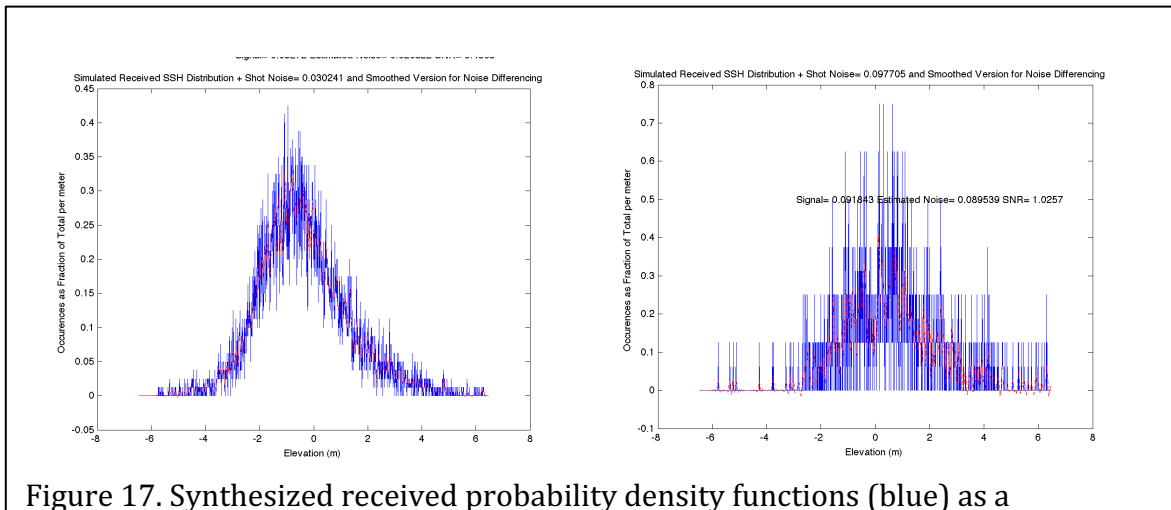
- 
- Start with the histogram of surface reflected photons heights, *Nrs*, from section (5.3.2 (P)) versus the sea surface height vector, *sshx*, with height bin size equal to *Bf* (e.g., *Bf*= 0.01 m). Convert the histogram to a vector array of probability density function (pdf) values, *rechist*. The dimensions of *rechist* and *sshx* are the same.
  - Smooth the received pdf with a 12<sup>th</sup> order, low-pass Butterworth filter with cutoff wavenumber corresponding to  $0.1/binsize$ . Run the filter forward and backward over *rechist* to yield the smoothed histogram, *smoothrechist*. Figure 17 shows *rechist* in blue and *smoothrechist* in red for an 8000 photon sample (left) and 800 photon sample (right)
  - Compute a signal to noise ratio (*SNRc*) equal to the standard deviation (std) of *smoothrechist* divided by the standard deviation of the difference between the received histogram and the smoothed histogram,  $SNRc = \text{std}(\text{smoothrechist}) / \text{std}(\text{rechist} - \text{smoothrechist})$ .



(B) Impulse Response Distribution

Obtain the current best estimate for the instrument response distribution, *XmitHist000*, a vector array of probability density function values for the impulse response.

The instrument impulse response distribution is calculated from the most recent transmit echo pulse (TEP) passed from ATL03 in */atlas\_impulse\_response/pce1\_spot1* or */pce2\_spot3*.



### *The Transmit Echo Pulse*

The TEP are derived from photons detected via the transmitter echo path (TEP, see Section 7.2.2 of the ATL03 ATBD). These photons are picked off from the transmitted laser pulse, and routed into the ATLAS receiver, for ATLAS strong beams 1 and 3. These data monitor the internal timing bias of ATLAS, as well as the instrument impulse response for the beam. We will assign TEP 1 or TEP 3 to each beam we process, mainly 1, 3, and 5, according to the recommendations in *tep\_valid\_spot*, a 6x1 array indicating which TEP to use for each spot. Order of the array is by ground track (gt1l; gt1r; gt2l; gt2r; gt3l; gt3r), from ATL03. (Note also, that when the spacecraft is flying forward beam 1 with a TEP is covering spot gt1r and beam 3 with a TEP is covering spot gt2r. When the spacecraft is flying backward beam 1 with a TEP is covering spot gt3l and beam 3 with a TEP is covering spot gt2l.) According to ATL03, the parameters are generated as often as sufficient TEP data exists in the granule, typically about every five granules (granules each span about 1/14<sup>th</sup> of an orbit.). Otherwise data from the prior granule is retained in the current granule. The TEP photon event arrival times are provided in a histogram, *tep\_hist\_times*.

The TEP photon events are downlinked when the TEP photon events happen to occur within the telemetry band approximately twice per orbit, for about three hundred seconds. The number of TEP photons per shot for a particular beam varies. However, the ratio of the number of TEP photons between beams 1 and 3 appears stable with a value of 0.7, with beam 1 being the stronger of the two. Averaging across a range of instrument configurations, beam 1 generates approximately 0.09 TEP photons per laser pulse, and beam 3 generates approximately 0.07 TEP photons per laser pulse. Assuming one TEP photon event per twenty pulses as the lower limit for the TEP strength, downlinking TEP photons for approximately three hundred seconds should yield about 150,000 TEP photons. TEP photon events are captured any time there are more than thirty seconds of contiguous possible TEP photon events identified in ATL02 (e.g., 15,000 TEP photons), and there are at least 2000 possible TEP photons in the set. All available TEP photons within a given set are used; there is no upper limit on the duration or number of TEP photons. The set is ended when the TEP photons are no longer present in the telemetry band, or five seconds have passed with no additional TEP photons. With a sufficient number of possible TEP photon events identified, these will either be background photon events, misclassified signal photon events, or TEP photon events. The time of day of the start of the TEP data used in subsequent analyses is reported on ATL03 as *tep\_tod*, while the duration of TEP data is reported as *tep\_duration*.

The histogram of these possible TEP photon events is formed using 50 picoseconds bin widths. There is more than a single mean arrival time of TEP photons; with two bands with the primary band being at ~ 20 nanoseconds and the secondary band being at 46 nanoseconds. The actual time band limits for each TEP will be indicated by the ATL03 variable *tep\_range\_prim*. Additional noise photons are also present. The mean background photon rate is determined by excluding the bins between 17 and 24 ns (the region of the primary return) and the region between 43 and 50 ns (the region of the secondary return) and calculating the mean of the remaining bins. This value is reported on the ATL03 output product as *tep\_bckgrd*, and is subtracted from all bin counts. The number of counts in the

remaining histogram is reported as **tep\_hist\_sum**. The number of counts in each bin is normalized by **tep\_hist\_sum** and reported for each bin as **tep\_hist**. Time is measured relative to the centroid transmit pulse, and on average for the TEP represents the travel time back and forth through the ATLAS optical path. The time of the histogram bin centers (the mean of the times of the leading and trailing edges of the bins) is recorded as **tep\_hist\_time**. The parameter **tep\_tod** indicates when the TEP data on a given ATL03 granule was generated. The parameters derived from TEP data are part of the ATL03 data product in the groups /atlas\_impulse\_response/pce1\_spot1/ and /atlas\_impulse\_response/pce2\_spot3/.

#### *Turning the TEP histogram into the Instrument Impulse Response*

We convert from **tep\_hist** expressed as normalized counts in **tepbinsize**=50 picosecond wide bins to an impulse response expressed as the probability density function with **binsize** wide bins of surface height. For the purpose of calculating the length of the derived surface distribution it is conceptually useful to interpolate to values in **XmitHist000** so that there are an odd number of bins with the origin bin at zero delay (or elevation) and the same bin size (**binsize**) as is used for the received elevation histogram. The process of deriving this impulse response from a TEP first requires identifying the appropriate TEP to use for a particular beam specified by **tep\_valid\_spot**, isolating the primary band of times specified by **tep\_range\_prim**, trimming the TEP to primary histogram levels above the background noise rate, converting from travel time to surface photon height offset, converting to **binsize** wide bins starting from negative offsets, and normalizing to a probability density function by dividing by the sum of the histogram levels multiplied by **binsize**. For the purpose of calculating the length of the derived surface distribution it is conceptually useful to interpolate values in **XmitHist000** so that there are an odd number of bins with the origin bin at zero delay (or elevation) and the same bin size (**binsize**) as is used for the received elevation histogram.

In part this pseudo code comes from the Matlab program BinconvertWF\_JM3.m.

- The appropriate TEP histogram, **tep\_hist**, as specified by **tep\_valid\_spot** for a particular beam includes both the primary and secondary arrivals. Choose the primary TEP arrivals in bins between **tep\_range\_prim**(1) and **tep\_range\_prim**(2) (typically around 17 and 24 ns) for use in ATL12 processing. e.g., (iprimary=find(tepT>= **tep\_range\_prim**(1) & tepT<= **tep\_range\_prim**(2); tepT=tepT(jprimary); tepP=tepP(jprimary);
- Because **tep\_bckgrd** is subtracted from the TEP histogram, the tails of the TEP will include bins with negative values. We trim off these tails where negative values appear indicating the TEP is below the noise floor. Working from time of TEP maximum out, set the TEP value to zero at the first bins where TEP is less than zero, and delete all bins beyond those points.
- Convert from travel time to surface height coordinate for the histogram by multiplying it times minus half the speed of light.
- Reverse the order of the histogram and its distance axis so that the array starts at negative height offsets.
- Center the TEP histogram so that it has height offset equals zero at the centroid of the distribution.

- Confirm the TEP bin size, ***bin\_TEP***, as the distance between bin centers 50 picoseconds/ (2 x speed of light).
- Convert TEP bin centers to bin boundaries in meters
- Establish an array of impulse response histogram bin boundaries with an odd number of bins, a bin size equal to ***binsize***, interior bin centered on zero, and all within the range of the TEP bin boundaries.
- Compute the cumulative histogram of the TEP versus the TEP bin boundaries and interpolate to the impulse response histogram bin boundaries.
- Differentiate the resulting cumulative impulse response histogram and form a corresponding array of bin centers to produce the instrument impulse response histogram.
- Divide the impulse response histogram by the product of ***binsize*** and the sum of values in the histogram to yield the impulse response probability density function.

At this point, we have described the averaged pulse shape characteristics from the threshold crossing times posted at the nominal ~20 meters along-track segment rate. We also have described the TEP photon events and have formed a histogram and related parameters based on TEP events. Since the times of these respective groups are known, it is possible to examine how the SPD-based statistics vary during the period spanned by the TEP data. However, combining these two groups quantitatively is complicated by two aspects. First, the SPD-based data and the TEP-based data have unique paths through the instrument and so the reported times of these data will be substantially different. While these differences are characterized with pre-launch data, we have little insight into how the temporal bias between these data will evolve through time. Secondly, the SPD-based data is derived from the reported times when a filtered version of the transmitted laser pulse crosses a particular amplitude threshold (measured in volts). The TEP-based data on the other hand is a histogram of counts of a massively attenuated version of the transmitted laser pulse. As such a quantitative correspondence between voltages and counts is problematic. A relationship could possibly be made between the standard deviation of the threshold crossing times and the apparent width of the TEP-based histogram at several points along the profile. This may allow a user to better predict how the transmitted pulse is changing between realizations of the TEP.

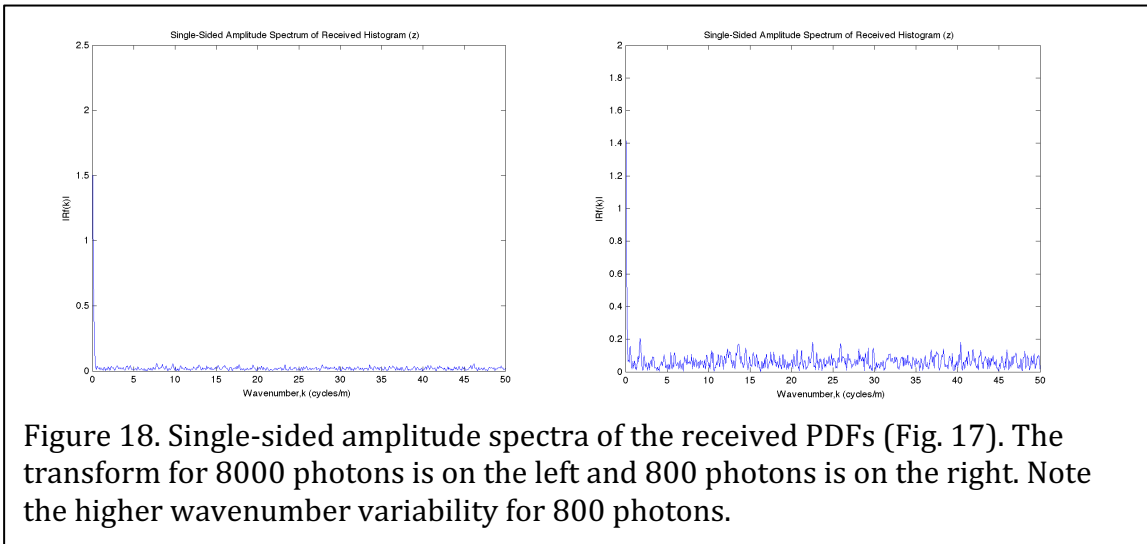


Figure 18. Single-sided amplitude spectra of the received PDFs (Fig. 17). The transform for 8000 photons is on the left and 800 photons is on the right. Note the higher wavenumber variability for 800 photons.

(C) Fourier Transform of Received Height Distribution

- Find length of record ( $NFFT$ ) equal to the next power of two greater than the length of  $rcvhist$ . This should cover the longest of the impulse response distribution,  $XmitHist000$ , and  $rcvhist$ .
- Pad the end of  $rcvhist$  with zeros to extend it to length  $NFFT$
- Compute the fast Fourier transform,  $Rf$ , of the received height distribution,  $rcvhist$

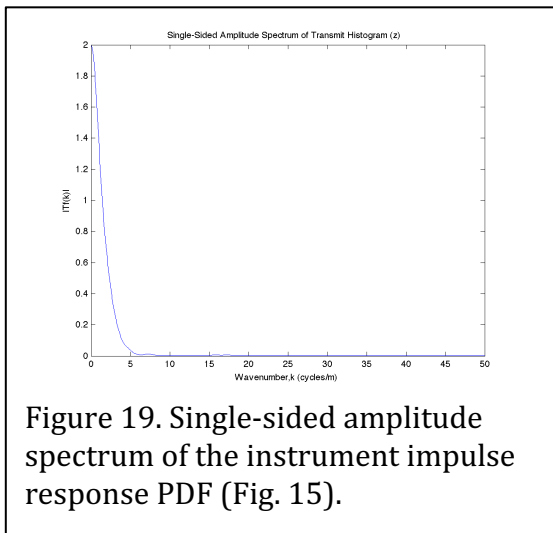


Figure 19. Single-sided amplitude spectrum of the instrument impulse response PDF (Fig. 15).

- Ensure consistent scaling so that energy is preserved (e.g., with Matlab FFT, we multiply the result by the binsize to reflect integration in the space domain
- The highest wavenumber (cycles per meter) is the Nyquist wavenumber equal to half the sampling wavenumber,  $wvns$ , which equals the inverse of  $binsize$  ( $wvns=1/binsize$ ). Using this, we compute the wavenumber vector ( $wvn$ ) corresponding to the Fourier transform of the received histogram. Examples of  $Rf$  plotted versus  $wvn$  are shown in Figure 18.

(D) Fourier Transform of Instrument Impulse Response

- Pad the end of  $XmitHist000$  with zeros to extend it to the length  $NFFT$
- Compute the fast Fourier transform,  $Tf$ , of the impulse response distribution,  $XmitHist000$
- Ensure consistent scaling so that energy is preserved (e.g., with Matlab FFT, we multiply the result by the  $binsize$  to reflect integration in the space domain
- Examples of  $Tf$  plotted versus  $wvn$  are shown in Figure 19.

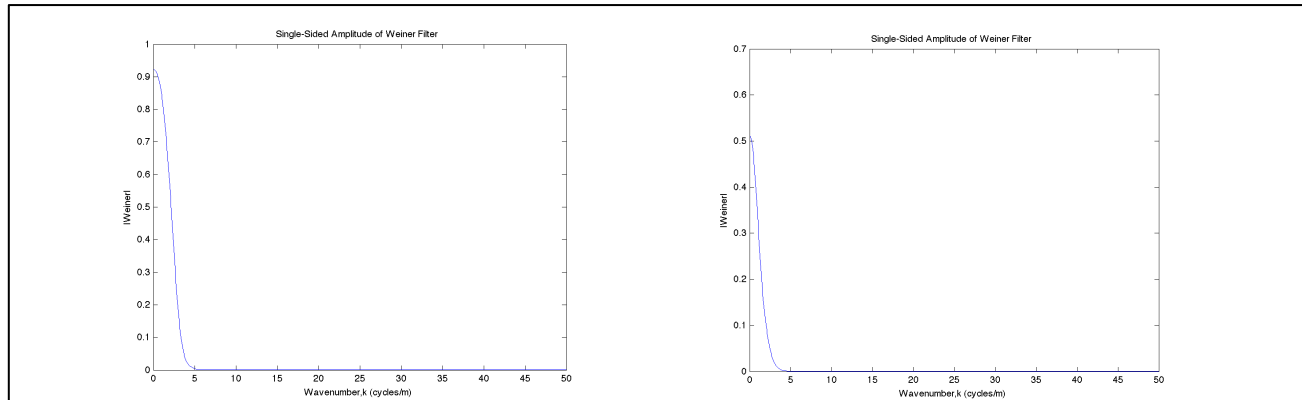


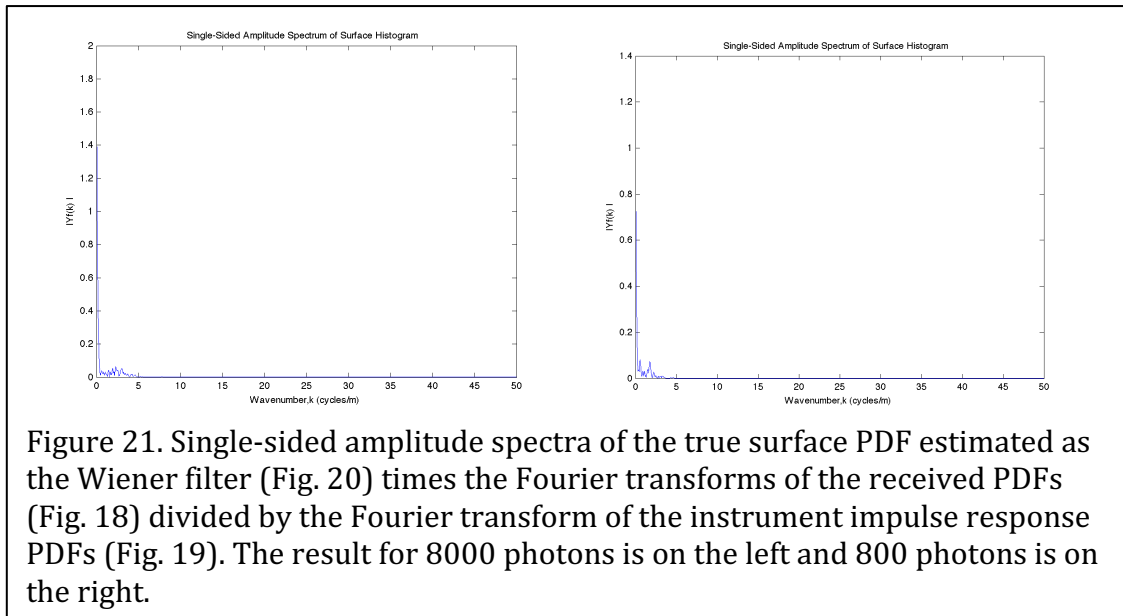
Figure 20. Single-sided amplitude spectra of the Wiener filters computed from the Fourier transform of the instrument impulse response PDFs (Fig. 19) and the signal to noise ratio estimated from the received height PDFs and smoothed versions of them (Fig. 17). Owing to a lower signal to noise ratio, the Wiener filter for 800 photons (right) has a narrower low frequency pass band than the 8000 photon filter (left).

(E) Compute the Wiener Filter

- Compute the Wiener filter, **WienerF**, equal to  $Tf \times Tf_{cc} / (Tf \times Tf_{cc} + SNRc^2)$ , where subscript cc denotes complex conjugate.
- Note that ultimately, we may compute the Wiener filter with a signal to noise variation, **SNRf**, that varies with wavenumber wavenumber, e.g., **SNRf** equal the absolute value of the Fourier transform of the received distribution (**Rf**) divided by the perceived noise (**NoiseRec**), but tests so far using the constant **SNRc** have worked well.
- Examples of **WienerF** plotted versus **wvn** are shown in Figure 20.

(F) Apply Wiener Deconvolution to Yield the Fourier Transform of the Surface Distribution

- Compute the Fourier transform of the surface distribution, **Yf**, as the Wiener deconvolution of the instrument impulse response distribution and the received height distribution. In Fourier (wavenumber) space this is the Wiener filter, **WienerF**, multiplied times the ratio of the transform of the received distribution, **Rf**, and the transform of the impulse response, **Tf**, i.e.,  $Yf = WienerF \times Rf / Tf$ .
- Examples of **Yf** plotted versus **wvn** are shown in Figure 21.



### G) Compute the Surface Height Distribution

The surface histogram should be the same length and have the same horizontal (height) axis as the received histogram, *rechist*. In this part, we compute the distribution of surface height as a probability density function (PDF), *Y*, starting with the Fourier transform of that PDF output by the Weiner deconvolution. The steps are:

8. Compute *Yfi*, as the inverse Fourier Transform of *Yf* divided by *binsize*. *Yfi* as it comes from the inverse Fourier transform is *NFFT* points long with the first half appearing displaced to the end of the array. We reorder this by first putting the last *NFFT/2* points ahead of the first *NFFT/2* points. To establish the surface height probability density function, *Y*, we then remove the first (*rzbin-1*) points where *rzbin* is the index of the centroid (height equals zero) index of the received histogram. We keep as *Y* the remaining points equal to the length of the *rechist*. In the case of the ASAS FORTRAN code, which pads each end of *rechist* to reach heights of  $\pm 15$  m, *rzbin* is the center bin of *rechist*.
9. Set the x-axis of *Y*, *derivedsshx* equal to the x-axis, *xrechist*, of the received histogram *rechist*.
10. Normalize *Y*, by dividing *Y* by the sum of the product of *Yfi* and *binsize*.
11. Compute the mean or centroid of *Y*, *meanY*, by summing the product of *Y* and *derivedsshx* and dividing that sum by the sum of *Y*.
12. Compute the standard deviation of *Y*, *stdY*:
  - a) square *derivedsshx* minus *meanY*
  - b) Multiply a) by *Y*
  - c) Take sum of b)
  - d) Divide c) by sum of *Y*
  - e) Take square root of d)

13. Compute the skewness of  $Y$ , **skewnessY**:
  - a) Cube **derivedsshx** minus **meanY**
  - b) Multiply a) by  $Y$
  - c) Take sum of b)
  - d) Divide c) by sum of  $Y$
  - e) Divide d) by the cube **stdY**.
14. Compute the kurtosis of  $Y$ :
  - a) Compute **derivedsshx** minus **meanY** to the fourth power
  - b) Multiply a) by  $Y$
  - c) Take sum of b)
  - d) Divide c) by sum of  $Y$
  - e) Divide d) by the **stdY** to the fourth power
  - f) Subtract three from e)

Since the rationale for some of these steps may not be obvious, and the steps may have to be modified depending on the differences between the Matlab (used in the developmental code) and Fortran (used in the ASAS code), we provide the following explanations for the steps:

- Compute **Yfi**, equal to the inverse Fourier transform of the output of the Wiener filtering process, **Yf**. Ensure that the result is normalized to conserve energy and dimensional consistency. For example, the output of the Matlab inverse Fourier transform (`ifft.m`) must be divided by **binsize** for dimensional consistency.

Compute x-axis derived from **xrechist** and characteristics of instrument impulse response. Convolution of one finite series of length  $N$  with another of length  $M$  results in a series of length  $N+M-1$ . We know further that if the instrument impulse response histogram has zero mean with the zero bin at index position **zbin** this will dictate where the points are added to the true height histogram to lengthen the received height histogram. If the impulse response distribution were symmetric, equal points would be added to each end, but this is not generally true. In fact, assuming length the length of the impulse response histogram is **lxmithist**, and the zero point is at index, **zbin**, **zbin-1** points will be added to the beginning of the true surface height histogram and **lxmithist-zbin** points will be added to the end of the surface height histogram to produce the convolved received histogram.

- In processing, we reverse this to trim the length of the vector x-axis of the received height histogram, **xrechist**, to the appropriate x-axis for the underlying surface height histogram, by deleting the first **zbin-1** points and the last **lxmithist-zbin** points from **xrechist** to yield the vector of x-axis of the surface histogram, **derivedsshx**, with length, **derivedlsshist** equal to  $\text{length}(\text{xrechist}) - (\text{lxmithist} - 1)$ .

Trimming the vector of surface histogram values is complicated by the necessity of padding received histogram with zeros to a length equal to a power of two for computation of its fast Fourier transform. As a result, at least in the prototype Matlab code, the inverse Fourier transform of the output of the Wiener deconvolution process, **Yfi**, also has a length equal to this same power of two and should be truncated to the appropriate length.

- Consequently, truncate  $Y_{fi}$  keeping only the first number of points in the original received histogram less  $(l_{xmithist}-1)$ , i.e., set  $derivedlsshx$  equal to  $length(xrechist)-(l_{xmithist}-1)$ . This yields the surface histogram,  $Y$ , defined over  $derivedsshx$ , that will have the number of points consistent with deconvolving the impulse response from the received histogram.
- To give the surface height probability density function,  $Y$ , normalize the  $Y_{fi}$  to make up for energy lost in the Wiener filter application. The integral of  $Y$  should equal unity, so take  $Y$  equal to  $Y_{fi}$  divided by the integral of  $Y_{fi}$ , i.e.,  $Y = Y_{fi} / (\text{sum of } Y_{fi} \times \text{binsize})$ .
- As a check on the deconvolution computation, the centroid of  $rechist$  and  $Y$  should both be near zero on account of the detrending of the surface heights and the assumed zero mean of the instrument impulse response computation
- Examples of  $Y$  and the difference between  $Y$  and the synthetic surface examples that we started

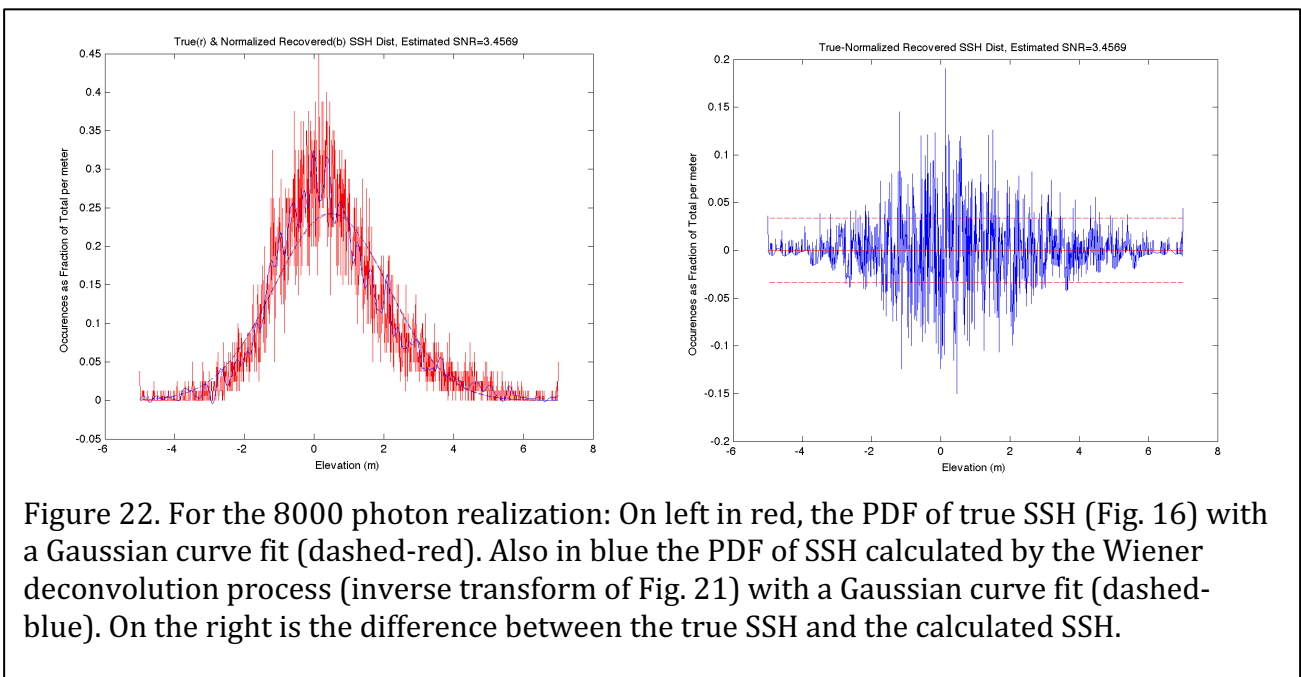


Figure 22. For the 8000 photon realization: On left in red, the PDF of true SSH (Fig. 16) with a Gaussian curve fit (dashed-red). Also in blue the PDF of SSH calculated by the Wiener deconvolution process (inverse transform of Fig. 21) with a Gaussian curve fit (dashed-blue). On the right is the difference between the true SSH and the calculated SSH.

with are given in Figure 22 for 8000 photons and Figure 23 for 800 photons.

- For subsequent use in the derivation of the ATL19 gridded product, the surface pdf,  $Y$ , will also be output for each segment along with the total number of surface photons,  $N$ , and bin size,  $binsize$ .
- $Y$  is defined over a vector of bin centers,  $sshx$ , but for  $binsize = 1$  cm  $Y$  will be output as a 3001-element vector from -15 m to +15 m for every segment with the 1,501<sup>st</sup> center bin being for height zero. Values will be zero for bins outside the range of  $sshx$ . Owing to noise and the effect of the FFT-deconvolution-inverse-FFT process, small negative values occur in  $Y$  within the range of  $sshx$ . These will be set to zero in the output  $Y$  vector.
- As a simple check on the optimum Gaussian Mixture determination of the higher moment of the sea surface distribution we will compute and output the mean, variance, skewness, and excess kurtosis ( $Y_{mean}$ ,  $Y_{var}$ ,  $Y_{skew}$ ,  $Y_{kurt}$ ) related to the higher moments of  $Y$  directly.

$$Y_{mean} = \mu_Y = \left( \sum_{Y_i > 0} X_i Y_i \right) / \left( \sum_{Y_i > 0} Y_i \right) \quad (30)$$

$$Y_{var} = \left( \sum_{Y_i > 0} (X_i - \mu_Y)^2 Y_i \right) / \left( \sum_{Y_i > 0} Y_i \right) \quad (31)$$

$$Y_{skew} = \left[ \left( \sum_{Y_i > 0} (X_i - \mu_Y)^3 Y_i \right) / \left( \sum_{Y_i > 0} Y_i \right) \right] / Y_{var}^{3/2} \quad (32)$$

$$Y_{kurt} = \left[ \left( \sum_{Y_i > 0} (X_i - \mu_Y)^4 Y_i \right) / \left( \sum_{Y_i > 0} Y_i \right) \right] / Y_{var}^2 - 3 \quad (33)$$

### 5.3.4.2 Characterizing the Random Sea Surface

This part goes through the analysis process described in part 4.3.2 to determine the true surface distribution, namely: Expectation Maximization analysis to determine the means, variance, and mixing ratio of the two parent normal distributions.

(H) Compute the 2-component Gaussian mixture Equivalent of the Surface Distribution

- 
- At this point we have the probability density function,  $Y$ , of detrended DOT over height bins with centers at  $sshx$ . The detrending process used in surface finding removed an average, **meanoffit2**, from the original heights. Once we have determined the mean and higher moments of  $Y$ , we could add **meanoffit2** to the mean of  $Y$  to learn the mean DOT over the ocean segment. However, preliminary analysis suggests if we add **meanoffit2** back into the distribution before the optimal Gaussian Mixture determination, the resulting higher moments are less noisy over many ocean segments. This can be done by shifting  $sshx$  by adding **meanoffit2** to each value in  $sshx$ . Then the true average DOT will be a derived as the aggregate mean of the optimally derived Gaussian mixture. For the developmental Matlab code a slightly different but equivalent approach was used.
  - The Matlab development code used `gmdistribution.fit`, an expectation maximization approach, to compute the 2-component Gaussian mixture corresponding to the observed surface height distribution,  $Y$ . The ASAS Fortran code uses the expectation maximization routine from ATBD ATL07 Appendix E.
  - To apply the expectation maximization approach, we first derive a sea surface height spatial series from the height distribution  $Y$ , which is defined over a range of heights the same as the received height histogram (i.e., **jlow** to **jhigh** from surface finding). This is accomplished by first multiplying  $Y$  by 10,000, rounding and deleting any values less than or equal to zero (a few unrealistic weakly negative values to occur in  $Y$  associated with the Weiner deconvolution process) to produce an integer distribution,  $YI$ . A series,  $XY$ , is assembled by concatenating for each value of  $YI(i)$  for index  $i$  corresponding to height  $sshx(i)$ ,  $YI(i)$  values equal to  $sshx(i)$ . The shift to heights including

*meanoffit2* was accomplished in developmental code by adding *meanoffit2* to each value in *XY*. (ASAS FORTRAN code does not add *meanoffit2* at this point but after the Gaussian Mixture calculation.) Although it is not strictly necessary, the values of *XY* are randomly permuted to produce a realistic distribution of heights with the probability density function *Y* on heights given in

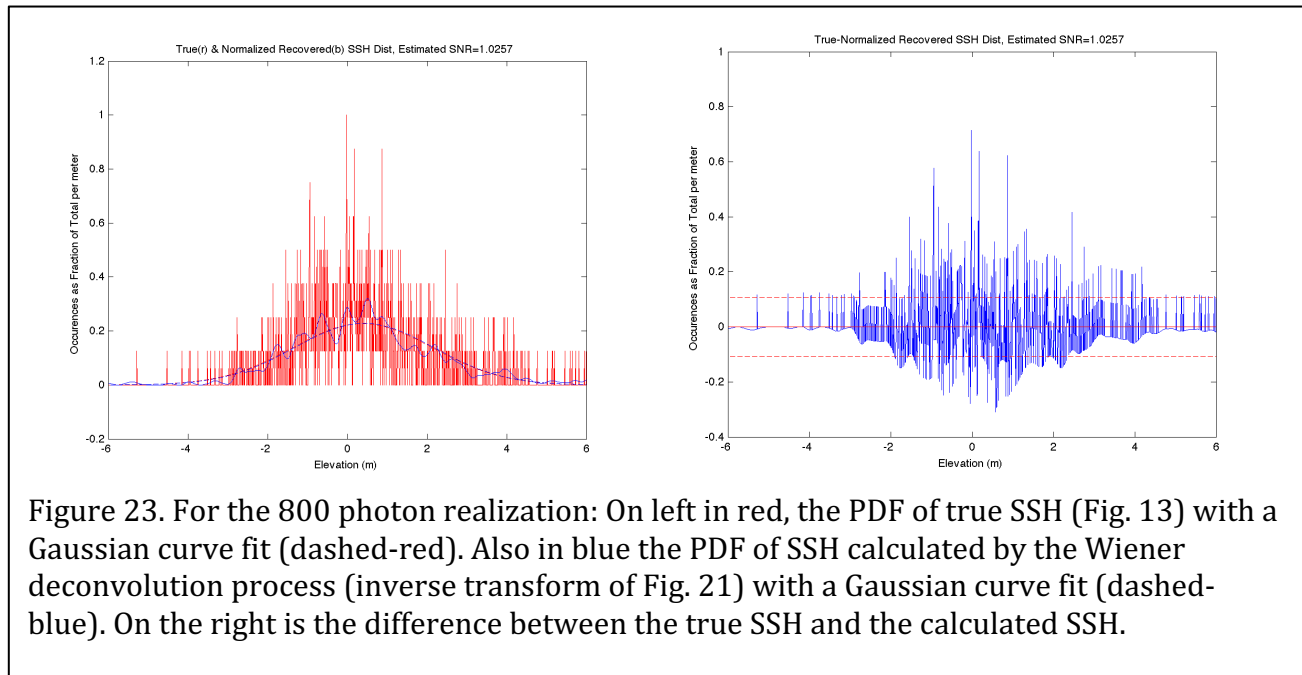


Figure 23. For the 800 photon realization: On left in red, the PDF of true SSH (Fig. 13) with a Gaussian curve fit (dashed-red). Also in blue the PDF of SSH calculated by the Wiener deconvolution process (inverse transform of Fig. 21) with a Gaussian curve fit (dashed-blue). On the right is the difference between the true SSH and the calculated SSH.

*sshx* shifted by adding *meanoffit2*.

- We then compute the 2-component Gaussian mixture variables, of the two-Gaussian mixture using expectation maximization, Matlab GMfit=gmfitdistribution.fit (*XY'*,2).
- The result is Gaussian mixture distribution with 2 components:

- With example output for 8000 photons

Gaussian mixture distribution with 2 components in 1 dimensions

Component 1:

Mixing proportion, ***m1*** = 0.457026

Mean, ***mu1*** = 1.0488

Standard Deviation, ***Sig1*** = 2.0062

Component 2:

Mixing proportion, ***m2*** = 0.542974

Mean, ***mu2*** = 0.0081

Standard Deviation, ***Sig2*** = 1.0533

- For the 800 photon case the results are:

Gaussian mixture distribution with 2 components in 1 dimensions

Component 1:

Mixing proportion, ***m1*** = 0.533033

Mean, ***mu1*** = 0.8430

Standard Deviation, ***Sig1*** = 2.0559

Component 2:

Mixing proportion, **m2** = 0.466967

Mean, **mu2** = -0.0553

Standard Deviation, **Sig2** = 1.0533

(I) Compute the Aggregate Mean, Variance, Skewness and Kurtosis of Sea Surface Height

-----

– Use the five parameters of the 2-Gaussian mixture to compute the aggregate moments, first through fourth of the aggregate mixture. From (27), for a mixture of two Gaussians with a fraction **m1** ( $m_1$ ) from the first Gaussian with mean **mu1** ( $\mu_1$ ) and standard deviation **sig1** ( $\sigma_1$ ) and a fraction **m2** ( $m_2$ ) (note:  $m_1+m_2=1$ ) from the second Gaussian with mean **mu2** ( $\mu_2$ ) and standard deviation **sig2** ( $\sigma_2$ ) the  $j^{\text{th}}$  moment of the mixture is calculated according to:

$$E\left[(X - \mu_{mix})^j\right] = \sum_{i=1}^2 \sum_{k=0}^j \frac{j!}{k!(j-k)!} (\mu_i - \mu_{mix})^{j-k} m_i E\left[(X_i - \mu_i)^k\right] \quad (34)$$

$$E\left[(X - \mu_{mix})^j\right] = \sum_{i=1}^L \sum_{k=0}^j \frac{j!}{k!(j-k)!} (\mu_i - \mu_{mix})^{j-k} m_i E\left[(X_i - \mu_i)^k\right]$$

Note that in computing the moments (34), the histogram data the expectation operation ( $E[ ]$ ) is not actual executed, because obviously we do not have the sample populations of the mixture components. The expectation operator appears in (34) to indicate the mixture moments and the mixture component moments coming from Section 5.2.5.2 (H) above. These are applied sequentially using only first and second moments of the mixture components and the mixing proportions to get up to the fourth moment of the mixture.

- The first moment or mean of the mixture,  $\mu_{mix} = m_1\mu_1 + m_2\mu_2$  (28) is the mean of the detrended surface photon heights relative to the geoid with the mean of the detrending process, **meanoffit2** (equal to the mean of **P0+P1\*trackdist\_initial2\_surf**), added back in prior to the Gaussian mixture determination. Thus, it represents the mean DOT uncorrected for sea state bias, along the ocean segment. Therefore, the mean sea surface height, **SSH**, for the segment to be output in ATL12 is equal to the mean of the mixture,  $\mu_{mix}$ , plus **meangdht** equal to the mean of geoid height, **geoid**, over the segment:

$$SSH = \mu_{mix} + meangdht = m_1\mu_1 + m_2\mu_2 + meangdht \quad (35)$$

- The second moment of the mixture is the sea surface height variance, **SSHvar**, for the segment to be output in ATL12 and used to estimate significant wave height. Here we don't include the variance due to the segment trend in sea surface height due to underlying trends in the DOT or geoid height. From (29), the second moment, or squared standard deviation,  $\sigma_{mix}^2$ , of the mixture is:

$$SSHvar = \sigma_{mix}^2 = m_1 \left( (\mu_1 - \mu_{mix})^2 + \sigma_1^2 \right) + m_2 \left( (\mu_2 - \mu_{mix})^2 + \sigma_2^2 \right) \quad (36)$$

- Using (34), compute third and fourth moments, we obtain the sea surface height skewness, *SSHskew*, and excess kurtosis *SSHkurt*,

$$SSHskew = E \left[ (Y - \mu_{mix})^3 \right] / \sigma_{mix}^3 \quad (37)$$

$$SSHkurt = E \left[ (Y - \mu_{mix})^4 \right] / \sigma_{mix}^4 - 3 \quad (38)$$

and output these as part of ATL12 to better characterize the sea surface. Here we don't include the skewness and kurtosis due to the segment trend in surface height.

### 5.3.4.3 Conclusions for Section 5.3.4:

Our synthetic true SSH distribution was assumed to be an even mix of heights drawn from two Gaussian distributions, one with a mean of zero and a standard deviation of 1 m, and the other with a mean of 1 m and a standard deviation of 2 m.

The result of the Wiener deconvolution of the synthesized received distribution, made by convolving the true SSH distribution with the instrument impulse response distribution and adding noise, produced what is essentially a smoothed version of the true SSH distribution (Fig. 22 left for 8000 photons and Fig. 23 left for 800 photons). The Gaussian fits to the true and calculated distributions means and standard deviations are virtually identical, but of course, both miss the slight bi-modality and skewness of the true and calculated SSH distributions.

Using the Matlab `gmdistribution.fit` function on the calculated SSH distribution and assuming mixture distribution with 2 Gaussian components in 1 dimension yields for 8000 photons means of 0.0081 m and 1.0488 m versus the true values of 0 m and 1 m. The Expectation Maximization (EM) of `gmdistribution.fit` yields standard deviations for the two Gaussian components of 1.1481 m and 2.0062 m versus the true values of 1 m and 2 m. The `gmdistribution.fit` value mixture ratios are 0.5430 and 0.4570 versus the true values of 0.50 and 0.50.

For 800 photons the EM process yields means of -0.0553 m and 0.8430 m versus the true values of 0 m and 1 m. The Expectation Maximization of `gmdistribution.fit` yields standard deviations for the two Gaussian components of 1.0533 m and 2.0559 m versus the true values of 1 m and 2 m. The `gmdistribution,fit` value mixture ratios are 0.4670 and 0.5330 versus the true values of 0.50 and 0.50.

These results with Wiener convolution and analysis by fitting a 2-component Gaussian Mixtures are promising. Clearly 8000 photons produces much better fidelity than 800 photons. This modeling approach gives us confidence that the analysis procedure is capable of an accurate estimate of surface statistics. Further testing with synthetic data, MABEL data and ATLAS simulator data will be needed fully understand the capabilities of

these tools. For example, a more precise test of capability might be to use an idealized synthetic surface histogram that was more nearly perfect, having been derived analytically or drawn as we have here, but from a very large number of samples (e.g., 800,000). Pulse noise would then be added corresponding to various sample sizes. Wiener deconvolution results could then be compared to the perfectly idealized surface histogram and errors attributed solely to the processing procedure, with no error associated with the initial synthesized surface.

In running the Matlab Wiener deconvolution prototype scheme, we found it to be stable over a wide range of imposed noise values and several Gaussian mixtures. For very high assumed signal to noise ratios, it more closely reproduces the true SSH PDF (e.g., Figs. 22 and 23) seemingly accepting as signal what looks to us like noise due to low sample counts. For low signal to noise ratios, the Wiener deconvolution scheme produced a smoothed version of the synthetic SSH distribution, throwing out the noise due to low sample counts. While we think the method of signal to noise estimation used here is reasonable, it must be tested with real data. In whatever way we estimate the signal to noise ratio, the Wiener deconvolution scheme appears to be a robust way of handling it. It does an excellent job of reproducing the overall mean and variance of the true SSH PDF (Figs. 22 and 23).

Fitting a Gaussian mixture model to the data also appears to work well but we should experiment with larger numbers of synthetic photon counts to see what improvements can be made to the accuracy of the component means and variances. We also need to see how the mixture means and higher moments (Eqn. 17) improve with higher photon counts. Because we have treated the Matlab routine `gmdistribution.fit` as a black box, we also need to learn more about how the EM method works and would be applied in a standalone code. The scheme can be compared to the minimum squared error approach used for GLAS and we can see if that existing routine can be used for ATLAS to derive Gaussian mixtures representing the ocean surface height distribution.

### **5.3.5 Applying *a priori* SSB Estimate**

The *a priori* SSB estimate of Section 5.3.3 can be applied to the mean SSH and DOT (=SSH-EGM2008 Geoid) for comparison to in situ cal/val or other altimeters. The impact of this SSB on the other moments is TBD.

### **5.3.6 Expected Uncertainties in Means of Sea Surface Height**

The ocean products of ATL12 are the distributions of sea surface height over ocean segments typically 5 to 7 km long and including about 8,000 candidate surface reflected photons. The height distributions are characterized up through their 4<sup>th</sup> moments (mean, standard deviation, skewness, and kurtosis) using the 2-Gaussian mixture approach. In this subsection, we examine the magnitude of the expected uncertainties in the mean of the surface height distribution. For the open ocean, we consider uncertainty in the mean height due to:

1. Signal-to-noise considerations in a distribution of photon heights.
2. Uncertainties in the mean impulse response.

### 3. Subsurface scattering.

These are borrowed from and consistent with the ATL07 Sea Ice ATBD except due the low rate of photon returns (about 1 photon per pulse) over the ocean surface, for the most part we exclude first-photon bias (See Section 3.1.1.4). We also do not consider sea state bias discussed in previous chapters because we are calculating SSB directly and the errors in this calculation will have to be determined during the ICESat-2 cal/val process.

#### 5.3.6.1 Signal-to-noise considerations and the dominant effect of surface wave roughness

We expect the largest contributions to uncertainty in the mean sea surface height to be due to surface roughness, and at least over short averaging lengths in daytime, background noise. The total number of photons

( $NP_{tot}$ ) in a height window,  $W$ , is the sum of the number of signal photons, the background rate ( $B_s$ ) and the number of pulses ( $N_{pulses}$ ) within that window:

$$NP_{tot} = NP_{signal} + NP_{bkg}$$

Background photons are uniformly distributed within the height window and thus the standard deviation,  $\sigma_{bkg}$ , can be written as,

$$\sigma_{bkg} = W (12)^{-1/2} = 0.2887 W,$$

where the factor .2887 is the standard deviation of a uniform random variable on a unit interval. The number of background photons ( $NP_{bkg}$ ) in the window ( $W$ ) is a Poisson variable with a mean value given by:

$$NP_{bkg} = 2 N_{pulses} B_s (W/c)$$

If the distribution of the received signal photons is approximately Gaussian, the variance depends on the transmit-pulse width ( $\sigma_{pulse}$ ) and the surface roughness ( $\sigma_{rough}$ ):

$$\sigma_{signal}^2 = \sigma_{rough}^2 + \sigma_{pulse}^2$$

The expected composite variance of surface height can then be written as:

$$\sigma_{surf}^2 = \frac{NP_{signal} \sigma_{signal}^2 + NP_{bkg} \sigma_{bkg}^2}{NP_{signal} + NP_{bkg}}$$

Except for the roughness, all of the quantities in this equation can be estimated from the data: the background and signal photon counts can be estimated from the total number of photons and the background rate. For a relatively smooth flat surface, the expected variance in the estimation of surface height in a window of  $N_{pulses}$  can be calculated using:

$$\hat{\sigma}_{surf}^2 = \frac{\sigma_{surf}^2}{NP_{total}}$$

Ultimately ICESat-2 ocean data will likely extend into the marginal ice zone (MIZ) for where the data will be analyzed for short along-track distances and smooth water. From the ATBD

for Sea Ice (ATL07), over a flat lead with mean returns of  $\sim 1$  photon per pulse for 100 pulses (70-m of smooth open water) with a nominal reflectance of 0.2 and no background noise, the expected uncertainty is 1.0 cm due entirely to uncertainty due to pulse width. With a 3 MHz background rate the uncertainty increases to 1.1 cm. Even at short distances, the contribution of background noise is small.

In true open ocean conditions the dominant source of uncertainty in the mean height of the sea surface over each ocean segment will be the roughness of the surface due to waves.

$$\hat{\sigma}_{surf} = \frac{\sigma_{surf}}{\sqrt{NP_{total}}} \approx \frac{\sigma_{waves}}{\sqrt{NP_{total}}} \quad (39)$$

For a typical situation with a significant wave height (SWH= $4 \sigma_{waves}$ ) equal to 2 m,  $\sigma_{waves}$  equals 0.5 m, and over a typical ocean segment with 8,000 photons, the uncertainty in the ocean segment mean sea surface height,  $\hat{\sigma}_{surf}$ , would be 0.56 cm if the heights were uncorrelated, and over 8,000 pulses,  $\hat{\sigma}_{surf}$  associated with surface roughness would remain less than 1 cm for SWH less than 3.6 m. Unfortunately, analysis of initial ICESat-2 data suggests that for large waves, the ocean segment to segment average heights vary much more than this. This is because successive height measurements are correlated due to the harmonic character of the surface. In fact, the uncertainty,  $\hat{\sigma}_f$ , of (39) appears to more

applicable to the ICESat-2 segment-to-segment height variability if we take the degrees of freedom,  $NP_{total}$ , equal to the number of wavelengths of the dominant waves in the ocean segment. For long waves, especially at an angle to the ground track, this number can easily be 15 so that the uncertainty can be in the 20 to 30 cm range. This is not a characteristic of ICESat-2, but rather a characteristic of the ever-changing ocean surface.

To address this natural uncertainty, we will calculate the approximate degrees of freedom from the autocorrelation of 10-m bin averaged heights (5.3.3)

From Brockwell and Davis [Brockwell and Davis, 2016], considering  $n$  discrete samples of  $h$ , the mean squared error of the sample mean,  $\mu_h$ , from the true mean,  $\bar{H}$ , is

$$E(\mu_h - \bar{H})^2 = n^{-1} \sum_{i=-n}^n \left(1 - \frac{|i|}{n}\right) \gamma(i)$$

where  $\gamma(i)$  is the autocovariance of  $h$  at lag  $i$ . In terms of distance, for a distance increment,  $\delta_x$ , the length of record,  $L$ , equals  $n\delta_x$  and taking  $\lambda = i\delta_x$

$$\begin{aligned} E(\mu_h - \bar{H})^2 &= (n\delta_x)^{-1} \sum_{i\delta_x = -n\delta_x}^{n\delta_x} \left(1 - \frac{|i\delta_x|}{n\delta_x}\right) \gamma(i\delta_x) \\ &= L^{-1} \sum_{\lambda=-L}^L \left(1 - \frac{|\lambda|}{L}\right) \gamma(\lambda) \end{aligned}$$

The autocovariance is symmetric with lag,  $\lambda$ , and is equal to the autocorrelation of  $h$  times the variance in  $h$ . Therefore

$$E(\mu_h - \bar{H})^2 = 2L^{-1} \sum_{\lambda=0}^L \left(1 - \frac{|\lambda|}{L}\right) \gamma(\lambda) = \sigma_h^2 2L^{-1} \sum_{\lambda=0}^L \left(1 - \frac{|\lambda|}{L}\right) R(\lambda)$$

This corresponds to (39) for:

$$\hat{\sigma}_{surf} = \frac{\sigma_{waves}}{\sqrt{NP_{effect}}} = \frac{\sigma_{waves}}{\sqrt{\frac{L}{2 \sum_{\lambda=0}^L \left(1 - \frac{|\lambda|}{L}\right) R(\lambda)}}} \quad (40)$$

So the correlation length scale,  $L_{scale}$ , and effective degrees of freedom  $NP_{effect}$  become:

$$L_{scale} = \sum_{\lambda=0}^L \left(1 - \frac{|\lambda|}{L}\right) R(\lambda) \quad \& \quad NP_{effect} = \frac{L}{2L_{scale}} = \frac{L}{2 \sum_{\lambda=0}^L \left(1 - \frac{|\lambda|}{L}\right) R(\lambda)} . \quad (41) \& (42)$$

Equations (41) and (42) for  $L_{scale}$  and  $NP_{effect}$  are written in terms of a record length,  $L$ . We can think of this a length  $L$  in meters. It is equivalent and more convenient to think of the record length in terms of the number of 10-m bins in the ocean segment,  $N=N_{bin10}$ , for which (41) and (42) become:

$$L_{scale} = \sum_{\lambda=0}^N \left(1 - \frac{|\lambda|}{N}\right) R(\lambda) \quad \& \quad NP_{effect} = \frac{L}{2L_{scale}} = \frac{L}{2 \sum_{\lambda=0}^N \left(1 - \frac{|\lambda|}{N}\right) R(\lambda)} . \quad (43) \& (44)$$

#### Pseudo Code for Determining $NP_{effect}$ and $h_{uncrtn}$

First, estimate the degrees of freedom using an approach inspired by the Matlab function `degrees_freedom.m` by Kathy Kelly (personal communication, 2020).

a) Compute as function of lag,  $l$ , the lagged autocorrelation vector  $R_L(l)$  of  $h_{tybin}$ , which is defined for 10-m bins with centers  $xbin$ . Lags will be increments of 10-m bin indices and

extend from  $l=0$  to  $l$  equal the number of bins in the ocean segment,  $N_{bin10} = L/10m$ . (Note: To consider lags up to the length of the record, it may be advisable to double the length of **htybin** by zero padding each end  $N_{bin10}/2$ . This would not usually be necessary because we should only need to use the covariance over the first 10 to 20 lags, but in cases where the ocean surface is not dominated by long waves, the autocorrelation may never be less than zero and it may be necessary to perform the integration of (41) out to a lag equal to the record length). Lagged covariance  $COV_L$  at lag  $l$  will be the sum over all  $i= 1$  to length,  $N_{bin10}$ , of the product  $htybin(i) * htybin(i+l)$ . Where either  $htybin(i)$  or  $htybin(i+l)$  does not exist, no addition is made to the sum. The autocorrelation,  $R_L$  as a function of lag,  $l$ , equals  $COV_L(l)$  divided by the covariance,  $COV_L$ , at zero lag so the  $R_L$  at zero lag,  $l = 0$ , is equal to 1,  $R_L(0) = 1$ .

b) Integrate  $(1-l/L) * R_L$  from zero lag to the first zero crossing to get decorrelation scale, **Lscale**.

Start with **Lscale** = 0 and at  $i = 1$  where the corresponding lag,  $l$ , is zero, and  $R_L(i)=1$ . Increment  $i$  and the corresponding  $l$  by 1 and keep adding to **Lscale** while  $R_L(i+1)$  is greater than zero, i.e.,

$$Lscale = Lscale + ((1-l/N_{bin10}) * R_L(i) + (1-(l+1)/N_{bin10}) * R_L(i+1)) / 2$$

When  $R_L(i+1)$  becomes less than zero, terminate the integration by essentially assuming  $R_L(i+1)$  is zero, i.e.,

$$Lscale = Lscale + (1-l/N_{bin10}) * R_L(i) / 2$$

c) Degrees of freedom, **NP\_effect**, equals length of the ocean segment,  $N_{bin10}$ , divided by two times the **Lscale**. Note that Matlab code from Kathy Kelly (personal communication, 2020) that has informed this code development deletes the division by 2 and the  $(1-l/N_{bin10})$  term in the integration and will give larger degrees of freedom than this routine. This code is more conservative.

d)  $h_{uncrtn}$  equals the standard deviation of sea surface height divided by the square root of **NP\_effect**.

### 5.3.6.2 Uncertainties in the mean impulse response

In our processing we, account for the impact of the instrument impulse response (IIP) on the distributions of surface heights by deconvolving from the received height distributions the impulse response estimated from the transmit echo pulse (TEP). To the extent that the TEP represents the impulse response this should eliminate uncertainty due to the IIP. Uncertainties due to a mismatch between the TEP and true IIP will have to be inferred by examination of the TEP in the on-orbit data, which remains to be done.

### 5.3.6.3 Uncertainties due to subsurface scattering.

Because the blue-green laser of ATLAS penetrates water, true subsurface returns have always been a concern, and the higher subsurface density of photons may be due in part to true subsurface scattering in the ocean. However, we see similarly enhanced subsurface densities over, clear deep ocean waters and even over land where penetration and backscatter shouldn't occur. Consequently present thinking expressed in the ATL03 Known Issues is that the subsurface noise level is due to forward scattering delays in the atmosphere of surface reflected photons.

Whatever their cause, some subsurface photon heights are being included in the surface height histogram, creating what we think may be an order 1-3 cm bias in average SSH. To reduce the sensitivity to subsurface returns, the processing code first makes a simple estimate of the high and low histogram limits and then uses these to determine separate above surface and subsurface noise levels, *tailnoisephigh* and *tailnoiselow*. The ultimate high limit is then chosen where the smoothed histogram falls below a factor *Th\_Nc\_f* (e.g., *Th\_Nc\_f* = 1.5) times *tailnoisephigh* and low limit is chosen where the smoothed histogram falls below the same factor times *tailnoiselow*. Also, for Release 4, the surface finding, instead of being based on the distribution of photon heights, is based on the distribution of the photon height anomalies relative to a moving 11-point bin average of high-confidence photon heights. This excludes subsurface returns under the crests of surface waves obviating the immediate need for a subsurface return correction dependent on sea state..

## 5.4 Ancillary Information

### 5.4.1 Solar Background Photon Rate and Apparent Surface Reflectance (ASR)

See section 3.1.1.5. The solar background rate is taken from ATL03 (*backgrd\_atlas/bckgrd\_rate*) and simply averaged over the length of the height segment to produce *backgr\_seg*.

The apparent surface reflectance should be taken from ATL09 (*/profile\_x/high\_rate/apparent\_surf\_reflec*) at the 25 Hz rate and simply averaged over the length of the height segment to produce *asr\_seg*.

### 5.4.2 Additional Ancillary Data

Variables from the ATL03 *geolocation/* and *geophys\_corr/* groups will also simply be averaged over each ocean segment and saved. Segment averages of the following variables, corresponding to the heights stored in *A<sub>fine</sub>* will be returned in ATL12. Those variables are locted in */gtx/stats* group and include

*neutat\_delay\_total*  
*ref\_azimuth*  
*ref\_elev*

*seg\_dist\_x*  
*solar\_azimuth*  
*solar\_elevation*  
*geoid*  
*geoid\_free2mean*  
*dac*  
*tide\_earth*  
*tide\_earth\_free2mean*  
*tide\_load*  
*tide\_oc\_pole*  
*tide\_ocean*  
*tide\_equilibrium*  
*tide\_pole*  
*full\_sat\_fract*  
*near\_sat\_fract*

Also, the first and last of the geosegment ids (*segment\_id*) for each ocean segment will be returned in ATL12 as *first\_geoseg* and *last\_geoseg*.

The percentages of each *surf\_type* of the photons from Fine Select in the ocean segment will also be returned as *surf\_type\_prcnt*. This will be a 5-element variable for each ocean segment with each element corresponding to the percentage of photons from each of the 5 surface types.

For each ocean segment, we output *layer\_flag\_seg* as equal to 1 for ocean segments with more than 50% of geosegs having *layer\_flag* = 1, indicating significant cloud layers were present. In addition, we compute *cloudcover\_percent\_seg* for each ocean segment as the percentage of geosegs in the ocean segment with *layer\_flag* = 1, i.e.,  
$$\text{cloudcover\_percent\_seg} = 100 * (\text{total number of geosegs used with } \text{layer\_flag}=1) / (\text{total number of geosegs used}).$$

### 5.5 Output Parameters

Table 6 ATL12 Output (See Appendix A for full product specifications)

| Product Label            | Units   | Description  | Symbol                |
|--------------------------|---------|--|-----------------------|
| <b>ancillary_data/</b>   |         |  |                       |
| <i>ds_a</i>              |         | Dimension scale (1:65) for the harmonic coefficients ( <i>a</i> ) in the <i>gtx/ssh_segments/heights</i> group. <i>a</i> (1) is the coefficient for wavenumber equal zero (constant part), Above <i>a</i> (1), <i>a</i> (even index <i>i</i> ) is the sine coefficient for <i>wn</i> ( <i>i</i> /2), and <i>a</i> (odd index <i>i</i> ) is the cosine coefficient for <i>wn</i> (( <i>i</i> -1)/2) | <b><i>a</i></b>       |
| <i>ds_surf_type</i>      |         | land (1), ocean (2), seaice (3), landice (4), inland water (5)   |                       |
| <i>ds_wn</i>             |         | Dimension scale (1:32) for the wavenumbers ( <i>wn</i> ) in the <i>gtx/ssh_segments/heights</i> group.   | <b><i>wn</i></b>      |
| <i>ds_xbin</i>           | m       | Center of 1 x 710 element array of 10-m bins. Note this may be included as a data description or other static array equal to [5, 15, 25, 35 ..... 7095 m]  | <b><i>xbin</i></b>    |
| <i>ds_y_bincenters</i>   | m       | -15 to +15, by 1cm bins  |                       |
| <b>ancillary/ocean/</b>  |         |  |                       |
| <i>Hist_bin_size</i>     | m       | Bin size for Y and sshx  | <b><i>binsize</i></b> |
| <b>gtx/</b>              |         |  |                       |
| <b>gtx/ssh_segments/</b> |         |  |                       |
| <i>delt_seg</i>          | seconds | Time duration segment  |                       |
| <i>delta_time</i>        | seconds | Mean time of surface photons in segment  | <b><i>t_seg</i></b>   |
| <i>latitude</i>          | °N      | Mean latitude of surface photons in segment  | <b><i>lat_seg</i></b> |
| <i>longitude</i>         | °E      | Mean longitude of surface photons in segment   | <b><i>lon_seg</i></b> |

| <b><i>gtx/ssh_segments/heights</i></b> |                |  |                          |
|--|----------------|--|--------------------------|
| <i>a</i>                               | m              | Vector of 2 x <i>nharms</i> + 1 coefficients for each harmonic component in harmonic analysis of heights (5.3.3.2). <i>a</i> (1) is the coefficient for wavenumber equal zero (constant part), Above <i>a</i> (1), <i>a</i> (even index <i>i</i> ) is the sine coefficient for <i>wn</i> ( <i>i</i> /2), and <i>a</i> (odd index <i>i</i> ) is the cosine coefficient for <i>wn</i> (( <i>i</i> -1)/2) | <b><i>a</i></b>          |
| <i>bin_ssbias</i>                      | m              | Sea state bias estimated from the correlation of photon return rate with along track 10-m bin averaged surface height (4.3.1)  | <b><i>binSSBias</i></b>  |
| <i>dxbar</i>                           | m              | Mean distance between surface reflected photons  | <b><i>DXbar</i></b>      |
| <i>dxskew</i>                          |                | Skewness of the distribution of distance between surface reflected photons   | <b><i>DXskew</i></b>     |
| <i>dxvar</i>                           | m <sup>2</sup> | Variance of the distribution of distance between surface reflected photons   | <b><i>DXvar</i></b>      |
| <i>h</i>                               | m              | Mean sea surface height relative to the WGS84 ellipsoid  | <b><i>SSH</i></b>        |
| <i>h_kurtosis</i>                      |                | Excess kurtosis of sea surface height histogram  | <b><i>SSHkurt</i></b>    |
| <i>h_skewness</i>                      |                | Skewness of photon sea surface height histogram  | <b><i>SSHskew</i></b>    |
| <i>h_uncrtn</i>                        | m              | Uncertainty in the mean sea surface height over an ocean segment   | <b><i>h_uncrtn</i></b>   |
| <i>h_var</i>                           | m <sup>2</sup> | Variance of best fit probability density function (meters <sup>2</sup> )   | <b><i>SSHvar</i></b>     |
| <i>htybin</i>                          | m              | 1 x 710 element array of 10-m bin average heights from SSB calculation   | <b><i>htybin</i></b>     |
| <i>l_scale</i>                         | decimeters     | Correlation length scale expressed in units of number of 10-m bins (may be fractional, i.e., decimeters)   | <b><i>Lscale</i></b>     |
| <i>latbind</i>                         | °N             | 1 x 710 element array of 10-m bin averages of latitude   | <b><i>latbind</i></b>    |
| <i>length_seg</i>                      | m              | Length of segment (m)  | <b><i>length_seg</i></b> |
| <i>lonbind</i>                         | °E             | 1 x 710 element array of 10-m bin averages of longitude  | <b><i>lonbind</i></b>    |

|                    |                 |   |                          |
|--------------------|-----------------|---|--------------------------|
| <i>meanoffit2</i>  | m               | Mean of linear fit removed from surface photon height   | <b><i>meanoffit2</i></b> |
| <i>mix_m1</i>      |                 | Fraction of component 1 in 2-component Gaussian mixture   | <b><i>m1</i></b>         |
| <i>mix_m2</i>      |                 | Fraction of component 1 in 2-component Gaussian mixture   | <b><i>m2</i></b>         |
| <i>mix_mu1</i>     | m               | Mean of component 1 in 2-component Gaussian mixture   | <b><i>mu1</i></b>        |
| <i>mix_mu2</i>     | m               | Mean of component 1 in 2-component Gaussian mixture   | <b><i>mu2</i></b>        |
| <i>mix_sig1</i>    | m               | Standard deviation of component 1 in 2-component Gaussian mixture   | <b><i>Sig1</i></b>       |
| <i>mix_sig2</i>    | m               | Standard deviation of component 1 in 2-component Gaussian mixture   | <b><i>Sig2</i></b>       |
| <i>n_pulse_seg</i> | counts          | Number of laser pulses in segment   | <b><i>n_pls_seg</i></b>  |
| <i>nbin10</i>      | counts          | Number of 10-m bins in an ocean segment   | <b><i>Nbin10</i></b>     |
| <i>np_effect</i>   |                 | Effective degrees of freedom of the average sea surface height for the ocean segment  | <b><i>NP_effect</i></b>  |
| <i>p0</i>          | m               | Constant of linear fit versus along-track distance to surface photon height over the ocean segment  | <b><i>PO</i></b>         |
| <i>p1</i>          |                 | Slope of linear fit versus along-track distance to surface photon height over the ocean segment   | <b><i>P1</i></b>         |
| <i>snr_harm</i>    |                 | Signal to noise ratio of harmonic fit with coefficients in a to the surface reflected photons including <b><i>meanoffit2</i></b> and with data gaps greater than <b><i>gaplimit</i></b> filled with Gaussian white noise about <b><i>meanoffit2</i></b> | <b><i>SNR_harm</i></b>   |
| <i>swh</i>         | m               | Significant wave height estimated as 4 times the standard deviation of along track 10-m bin averaged surface height   | <b><i>SWH</i></b>        |
| <i>wn</i>          | m <sup>-1</sup> | <b><i>nharms</i></b> (= 32) wavenumbers equal to the inverse of wavelengths for each harmonic component in harmonic analysis of heights (5.3.3.2)   | <b><i>wn</i></b>         |
| <i>xbind</i>       | m               | 1 x 710 element array of 10-m bin averages of along-track   | <b><i>xbind</i></b>      |

|                               |                           |   |                                      |
|-------------------------------|---------------------------|---|--------------------------------------|
|                               |                           | distance  |                                      |
| <i>xrbin</i>                  | Photon<br>m <sup>-1</sup> | 1 x 710 element array of 10-m bin average photon rate from SSB calculation                            | <b><i>xrbin</i></b>                  |
| <i>y</i>                      | m <sup>-1</sup>           | Probability density function of photon surface height   | <b><i>Y</i></b>                      |
| <i>ykurt</i>                  |                           | Excess Kurtosis = (fourth moment of <i>Y</i> ) / <i>Yvar</i> <sup>2</sup> - 3                         | <b><i>Ykurt</i></b>                  |
| <i>ymean</i>                  | m                         | Mean=first moment of <i>Y</i> , should be ~0 = <i>h</i> - meanoffit2                                  | <b><i>Ymean</i></b>                  |
| <i>yskew</i>                  |                           | Skewness = (third moment of <i>Y</i> ) / <i>Yvar</i> <sup>3/2</sup>                                   | <b><i>Yskew</i></b>                  |
| <i>yvar</i>                   | m <sup>2</sup>            | Variance = second moment (m <sup>2</sup> ) of <i>Y</i>  | <b><i>Yvar</i></b>                   |
| <b>gtx/ssh_segments/stats</b> |                           |   |                                      |
| <i>backgr_seg</i>             | m <sup>-1</sup>           | <i>backgrd_atlas/bckgrd_rate</i> from ATL03 averaged over the segment                                 | <b><i>backgr_seg</i></b>             |
| <i>cloudcover_percent_seg</i> | %                         | The percentage of geosegs in the ocean segment with <b><i>layer_flag</i></b> = 1.                     | <b><i>cloudcover_percent_seg</i></b> |
| <i>dac_seg</i>                | m                         | Ocean segment average of dynamic atmospheric correction (DAC) includes inverted barometer (IB) affect | <b><i>dac_seg</i></b>                |
| <i>depth_ocn_seg</i>          | m                         | The average of depth ocean of geo-segments used in the ocean segment.                                 | <b><i>depth_ocn_seg</i></b>          |
| <i>first_geoseg</i>           | counts                    | The first of the geosegment ids ( <b><i>segment_id</i></b> ) for each ocean segment                   | <b><i>first_geoseg</i></b>           |
| <i>first_pce_mframe_cnt</i>   | counts                    | First Major Frame ID in the SSH segment   | <b><i>first_pce_mframe_cnt</i></b>   |
| <i>first_tx_pulse</i>         | counts                    | First Transmit pulse in along-track segment   | <b><i>first_tx_pulse</i></b>         |
| <i>fpb_corr</i>               | m                         | Estimated first-photon bias correction to mean segment height currently set to INVALID. See 3.1.1.4.  | <b><i>fpb_corr</i></b>               |
| <i>fpb_corr_stdev</i>         | m                         | Estimated error in <i>fpb_corr</i> currently set to INVALID. See 3.1.1.4.                             | <b><i>fpb_corr_stdev</i></b>         |
| <i>full_sat_fract_seg</i>     |                           | fraction of all pulses in all geosegs used that were fully saturated                                  | <b><i>full_sat_fract_seg</i></b>     |
| <i>geoid_free2mean_seg</i>    | m                         | Ocean segment average of the conversion factor added to   | <b><i>geoid_free2mean_seg</i></b>    |

|                               |                 |  |                                      |
|-------------------------------|-----------------|--|--------------------------------------|
|                               |                 | ATL03 <i>geoid</i> to convert from the tide-free to the mean-tide system   |                                      |
| <i>geoid_seg</i>              | m               | Ocean segment average of geoid in the mean-tide system height above the WGS - 84 reference ellipsoid (range -107 to 86 m)  | <b><i>geoid_seg</i></b>              |
| <i>Ice_conc</i>               | %               | The percent ice concentration at the average ocean segment position from NSIDC passive microwave data used for ATL07   | <b><i>last_geoseg</i></b>            |
| <i>last_geoseg</i>            | counts          | The last of the geosegment ids ( <b><i>segment_id</i></b> ) for each ocean segment   | <b><i>last_geoseg</i></b>            |
| <i>last_pce_mframe_cnt</i>    | counts          | Last Major Frame ID in the SSH segment   | <b><i>Last_pce_mframe_cnt</i></b>    |
| <i>last_tx_pulse</i>          | counts          | Last Transmit pulse in along-track segment   | <b><i>last_tx_pulse</i></b>          |
| <i>layer_flag_seg</i>         |                 | The layer flag from ATL09 that is in effect over 50% of the ocean segment, 0 indicating absence of clouds and forward scattering, and 1 indicating possibility of forward scattering as in ATL09 | <b><i>layer_flag_seg</i></b>         |
| <i>n_photons</i>              | counts          | Number of surface photons found for the segment  | <b><i>n_photon</i></b>               |
| <i>n_ttl_photon</i>           | counts          | Number of photons in the ±15-m ocean downlink band   | <b><i>n_ttl_photon</i></b>           |
| <i>near_sat_fract_seg</i>     | counts          | fraction of all pulses in all geosegs used that were nearly saturated  | <b><i>near_sat_fract_seg</i></b>     |
| <i>neutat_delay_total_seg</i> | m               | Ocean segment average of total neutral atmosphere delay correction (wet + dry)   | <b><i>neutat_delay_total_seg</i></b> |
| <i>orbit_number</i>           | counts          | Unique identifying number for each planned ICESat-2 orbit  | <b><i>orbit_number</i></b>           |
| <i>photon_noise_rate</i>      | m <sup>-1</sup> | Noise photon count rate, averaged over the segment   | <b><i>r<sub>noise</sub></i></b>      |
| <i>photon_rate</i>            | m <sup>-1</sup> | Photon count rate, averaged over the segment   | <b><i>r<sub>surf</sub></i></b>       |
| <i>podppd_flag_seg</i>        |                 | Higher, 0 or 4, of ATL03 <b><i>gtx/geolocation/podppd_flag</i></b> of data used in the ocean segment   | <b><i>podppd_flag</i></b>            |
| <i>ref_azimuth_seg</i>        | radians         | Ocean segment average of azimuth of the unit pointing vector for the reference photon in the local ENU frame   | <b><i>ref_azimuth_seg</i></b>        |

|                            |                |   |                                   |
|----------------------------|----------------|---|-----------------------------------|
|                            |                | in radians. The angle is measured from North and positive towards East  |                                   |
| <i>ref_elev_seg</i>        | radians        | Ocean segment average of elevation of the unit pointing vector for the reference photon in the local ENU frame in radians. The angle is measured from the East-North plane and positive towards Up  | <b><i>ref_elev_seg</i></b>        |
| <i>seg_dist_x_seg</i>      | m              | Ocean segment average of the along-track distance from the equator crossing to the start of the 20-m geolocation segments included in the ocean segment   | <b><i>seg_dist_x_seg</i></b>      |
| <i>solar_azimuth_seg</i>   | degrees        | Ocean segment average of the azimuth of the sun position vector from the reference photon bounce point position in the local ENU frame. The angle is measured from North and is positive towards East. The average is provided in degrees.                | <b><i>solar_azimuth_seg</i></b>   |
| <i>solar_elevation_seg</i> | degrees        | Ocean segment average of the elevation of the sun position vector from the reference photon bounce point position in the local ENU frame. The angle is measured from the East-North plane and is positive towards Up. The average is provided in degrees. | <b><i>solar_elevation_seg</i></b> |
| <i>ss_corr</i>             | m              | Subsurface scattering correction, placeholder = INVALID pending further findings to the contrary  | <b><i>ss_corr</i></b>             |
| <i>ss_corr_stdev</i>       | m <sup>2</sup> | Estimated error of subsurface scattering correction, placeholder = INVALID pending further findings to the contrary   | <b><i>ss_corr_stdev</i></b>       |
| <i>surf_type_prcnt</i>     |                | The percentages of each <b><i>surf_type</i></b> of the photons in the ocean segment as a 5-element variable with each element corresponding to the percentage of photons from each of the 5 surface types   | <b><i>surf_type_prcnt</i></b>     |

|                                 |   |   |                                    |
|---------------------------------|---|---|------------------------------------|
| <i>tide_earth_free2mean_seg</i> | m | Ocean segment average of the factor that needs to be added to <i>tide_earth_seg</i> to convert from the tide-free to the mean-tide system. This is not used in ATL12. | <i>tide_earth_free2mean_seg</i>    |
| <i>tide_earth_seg</i>           | m | Ocean segment average of solid earth tides in the tide-free systems   | <b><i>tide_earth_seg</i></b>       |
| <i>tide_equilibrium_seg</i>     | m | Long period equilibrium tides   | <b><i>tide_equilibrium_seg</i></b> |
| <i>tide_load_seg</i>            | m | Ocean segment average of local displacement due to ocean loading (-6 to 0 cm)   | <b><i>tide_load_seg</i></b>        |
| <i>tide_oc_pole_seg</i>         | m | Ocean segment average of oceanic surface rotational deformation due to polar motion (-2 to +2 mm)   | <b><i>tide_oc_pole_seg</i></b>     |
| <i>tide_ocean_seg</i>           | m | Ocean segment average of ocean tides including diurnal and semi-diurnal (harmonic analysis)   | <b><i>tide_ocean_seg</i></b>       |
| <i>tide_pole_seg</i>            | m | Ocean segment average of solid pole tide - Rotational deformation due to polar motion (-1.5 to 1.5 cm)  | <b><i>tide_pole_seg</i></b>        |

## 5.6 Gridding DOT for ATL19.

The ATL19 product includes gridded monthly estimates of dynamic ocean topography (DOT) taken from ATL12 ocean segment data. Ocean segments range in length roughly from 3 to 7km. The ocean segment data are averaged in  $\frac{1}{4}^\circ$  or 25km grid cells. Data from all six beams (gtxr and gtxl) are used from the beginning to the end of each month, although commonly over most of the ocean only data from the strong beams will be available. The IS-2 data are averaged onto three grids, called mid-latitude, north-polar and south-polar. The ATL19 product has groups with the same names containing the gridded data for each of those regions. The grids, gridding schemes, input variables and output variables are described in detail in the ATBD for ATL19.

## 5.7 Synthetic Test Data

The first task in the creation of the developmental software has been the creation of a synthetic data set. This is not part of ATLAS processing per se, but is a good tool for algorithm testing and development.

The procedure is imbedded in a developmental Matlab code (WienerTest\_GaussMixandNoise2.m). Here, the percent sign indicates a plane text description of the procedural step and is a non-executable comment in the Matlab code. Matlab executable lines are highlighted in yellow. The program begins with parts (A) through (E) which establish an artificial surface height histogram

consisting of a mixture of 2 normal distributions convolved with a real impulse response distribution taken from MABEL data by Ron Kwok. A representative amount of noise is then added to this to synthesize a received surface height with a known underlying true surface distribution.

(A) Establish the instrument impulse response distribution from MABEL data (XmitHist000)

(B) Make a Gaussian mixture representing the ssh distribution (sshhist)

(C) Compute noise (Noise) as the rRMSdifference from the analytic Gaussian mixture and sshist in the tails (+-2sig to +-3 sig)

(D) Convolve the SSH distribution with the instrument impulse response distribution to produce the received distribution (rechist)

(E) Add random Poisson (or pulse) noise due to discrete nature of photon counts representative of what we might expect for a given bin size and total number of photon counts.

% -----

**% Begin Matlab code:**

% In this test program we will:

% (A) Establish the instrument impulse response distribution from Mabel data (XmitHist000)

% (B) Make a Gaussian mixture representing the ssh distribution (sshhist)

% (C) Compute noise (Noise) as the rms difference from the analytic gaussian mixture

% and sshist in the tails (+-2sig to +-3 sig)

% (D) Convolve the ssh ditribution with the instrument impulse response distribution to produce

% the received distribution (rechist)

% (E) Add random Poisson (or pulse) noise due to discrete nature of photon

% counts representative of what we might expect for a given binsize and

% total number of photon counts (NptsMix)

% photons.

%

% -----

% (A) load and plot Instrument impulse response Histogram

% -----

% -----

cd /Users/jamie/Documents/ICESat-2\_SDT/ICESat-

2\_OceanATBD\_Development/PhotonSourceDistribution

load XmitHist000

meanXmit00=sum(XmitHist000(:,1).\*XmitHist000(:,2))/sum(XmitHist000(:,2))

stdXmit00=sqrt(sum(XmitHist000(:,1).\*XmitHist000(:,1).\*XmitHist000(:,2))/sum(XmitHist000(:,2)))

% XmitHist000 is a raw histogram and XmitHist000(:,2) are the total number of photons in each

% 0.01-m bin convert. We convert it to a probability density function, the integral

```

% of which is 1.0. Binsize in all histograms/pdfs will be 0.01 m.
% XmitHist000 bins are relative to the mean delay is zero.
binsize=0.01;
totalxmit=sum(XmitHist000(:,2));
XmitHist_fraction=(XmitHist000(:,2)/totalxmit);
XmitHist000(:,2)=XmitHist_fraction/binsize;
checkintegralXMIT=sum(XmitHist000(:,2)*binsize);
meanXmit00=sum(XmitHist000(:,1).*XmitHist000(:,2))/sum(XmitHist000(:,2))
stdXmit00=sqrt(sum(XmitHist000(:,1).*XmitHist000(:,1).*XmitHist000(:,2))/sum(XmitHist000(:,2))))

% plot
figure
plot(XmitHist000(:,1),XmitHist000(:,2))
title('Xmit Pulse Delay Rel to Mean in Equiv Surface Height')
ylabel('Occurences as Fraction of Total per meter')
xlabel('Height Delay (m)')
print -dpng XmitHistogram_GM_8k.png

%-----
% (B) Make a sequence sea surface height consisting of a mix of two normally
% distributed random numbers with Means MuMix, standard deviations SigmaMix
% and percent mixing ratios RatioMix, and number of points total NptsMix
% -----
% -----
MuMix=[1,0]
SigmaMix=[2,1]
RatioMix=[50,50]
NptsMix=8000
ssh=makeGaussianMix(MuMix,SigmaMix,RatioMix,NptsMix);
meanssh=mean(ssh)
MeanfromMixValues=sum(RatioMix.*MuMix/sum(RatioMix))
stdssh=std(ssh)
StdfromMixValues=sqrt(sum(RatioMix.*(SigmaMix.^2)/sum(RatioMix)))
lssh=length(ssh)

% Compute histogram of ssh using bin size = 0.01 m running from -3 Std to +3
% Std of the ssh mix. The output of hist is a raw histogram and we convert it to
% a probability density function, the integral of which is 1.0 by dividing by the
% total number of points (=length of ssh) and the binsize
%
Nsigs=3;
sshx=round(meanssh)-Nsigs*round(stdssh):binsize:round(meanssh)+Nsigs*round(stdssh);
sshhist=hist(ssh,sshx);

```

```

sshhist_fraction=(sshhist/lssh);
sshhist=sshhist_fraction/binsize;
checkintegralSSH=sum(sshhist*binsize)
%
meansshhist=sum(sshx.*sshhist)/sum(sshhist)
stdsshhist=sqrt(sum((sshx-meansshhist).*(sshx-meansshhist).*sshhist)/sum(sshhist))
totalssh=sum(sshhist)
Nbins=length(sshhist);

% -----
% (C) Compute noise (Noise) as the rms difference from the analytic Gaussian mixture
% (gaussfit) and sshist in the tails (+-2sig to +-3 sig)
% -----
% -----

gaussfit=(1/stdssh)*(1/sqrt(2*pi))*exp(-0.5*((sshx-meanssh).^2)/stdssh^2);
NoiseAll=std(sshhist-gaussfit)

% because gaussfit is a pdf we divide histogram values by bin size for
% comparison. Noise values should probably be multiplied by bin size for
% computation as noise in histograms ?Noise=binsize*NoiseInTails?
DiffFromNorm=(sshhist)-gaussfit;
DiffFromNormInTails=[DiffFromNorm(1:round(0.5*Nbins/Nsigs)),DiffFromNorm(end-
round(0.5*Nbins/Nsigs))];
NoiseInTails=std(DiffFromNormInTails')

figure
plot(sshx,sshhist,sshx,gaussfit,'-g')
title(['Simulated True Sea Surface Height Distribution, 2-GaussMix ',num2str(NptsMix),'
Photons'])
ylabel('Occurrences as Fraction of Total per meter')
xlabel('Height (m)')
print -dpng Sim_SSH_Distriburtion_GM_8k.png

% -----
% (D) Convolve the instrument impulse response and simulated true height histograms
% to get a simulated received height ssh distribution rcvhist
% -----
% -----
% ----- Matlab Routine conv.m -----
% conv Convolution and polynomial multiplication.
% C = conv(A, B) convolves vectors A and B. The resulting vector is
% length MAX([LENGTH(A)+LENGTH(B)-1,LENGTH(A),LENGTH(B)]). If A and B are
% vectors of polynomial coefficients, convolving them is equivalent to

```

```
% multiplying the two polynomials.
%
% C = conv(A, B, SHAPE) returns a subsection of the convolution with size
% specified by SHAPE:
% 'full' - (default) returns the full convolution,
% 'same' - returns the central part of the convolution
%         that is the same size as A.
% 'valid' - returns only those parts of the convolution
%         that are computed without the zero-padded edges.
%         LENGTH(C)is MAX(LENGTH(A)-MAX(0,LENGTH(B)-1),0).
%-----
% NOTE: conv.m does a raw convolution, i.e., simple sums of products. To
% replicate a true convolution integral with proper scaling, the results of
% conv.m must be multiplied by the bin size so that the scale of the
% resulting convolution is of the same order as the scale on the two
% histograms convolved.
% Also the length of the convolution should equal length of the ssh
% histogram plus the length Xmit histogram minus 1
%-----
```

```
tic
rcvhist=conv(sshhist,XmitHist000(:,2))*binsize;
cleanrcvhist=rcvhist;
toc
```

```
lrcvhist=length(rcvhist)
lxmithist=length(XmitHist000(:,2))
lsshhist=length(sshhist)
halfwidthrcvhist=(lxmithist+lsshhist-2)/2
if 2*halfwidthrcvhist+1~=lrcvhist
    message=['length of rcvhist is consistent']
end
```

```
% If the impulse response distribution were symmetric conv.m would pad the length of the sshhist
% by (lxmithist-1)/2 at each end. The Xmit histogram is not symmetric. The minimum x-axis index
% of the received histogram should be the minimum index of the true surface height histogram plus
% the minimum negative bin index of the impulse response histogram and the maximum x-axis
% index of the received histogram should be the maximum index of the true histogram plus
% the maximum (positive) bin index of the Xmit histogram.
% Therefore, we find the index of the zero bin,zbin,
% of XmitHist000 (which is the old XmitHist00 histogram interpolated to even cm bin indices)and
% add the bins with index 0 to zbin-1 before the first bin of the ssh histogram and
% add the bins with index zbin+1 to end after the last bin of the ssh histogram
```

```
zbin=find(XmitHist000(:,1)==0);  
xaddend=XmitHist000(zbin+1:end,1)+sshx(end)*ones(1,length(XmitHist000(zbin+1:end,1)));  
xaddbegin=XmitHist000(1:zbin-1,1)+sshx(1)*ones(1,length(XmitHist000(1:zbin-1,1)));  
xrechist=[xaddbegin,sshx,xaddend];
```

```
figure
```

```
plot(xrechist,rcvhist)
```

```
title('Simulated Convolved Sea Surface Height Distribution')
```

```
ylabel('Occurrences as Fraction of Total per meter')
```

```
xlabel('Height (m)')
```

```
% -----
```

```
% -----
```

```
% -----
```

```
% (E) Add random Poisson (or pulse) noise due to discrete nature of photon
```

```
% counts representative of what we might expect for a given binsize and
```

```
% total number of photon counts (NptsMix)
```

```
% -----
```

```
sumrchhist=sum(rcvhist*binsize)
```

```
noisey=rcvhist;
```

```
% make Poisson distributed photon counts in histogram to represent received + pulse noise
```

```
for inoise=1:length(rcvhist)
```

```
    noisey(inoise)=randpoisson_JM(NptsMix*binsize*cleanrcvhist(inoise));
```

end

% NOTE %  
 %randpoisson\_JM.m is a Matlab subroutine to generate random numbers drawn  
 % from a Poisson distribution:

```
function X = randpoisson_JM(np)
x=1:round(np+1)*10;
p= poisspdf(x,np);
m=1;
X = zeros(m,1); % Preallocate memory
for i = 1:m
    u = rand;
    I = find(u < cumsum(p));
    if isempty(I)
        X(i)=0;
    else
        X(i) = min(I);
    end
end
end
```

% poisspdf Poisson probability density function.  
 % Y = poisspdf(X,LAMBDA) returns the Poisson probability density  
 % function with parameter LAMBDA at the values in X.  
 % The size of Y is the common size of X and LAMBDA. A scalar input  
 % functions as a constant matrix of the same size as the other input.  
 % Note that the density function is zero unless X is an integer.

```
% Convert back to PDF
Noise=std(noisey/(NptsMix*binsize)-rcvhist);
rcvhist=noisey/(NptsMix*binsize);
sumnoiseyrchhist=sum(rcvhist*binsize)
```

```
figure
plot(xrechist,rcvhist)
title(['Simulated Received Sea Surface Height Distribution + Pulse Noise= ',num2str(Noise)])
ylabel('Occurences as Fraction of Total per meter')
xlabel('Height (m)')
```

% -----  
 % rcvhist is the simulated received histogram at the histogram bins centered at xrechist. It  
 is shown in blue in Figure 17 for 8000 photons (left) and 800 photons (right).

## **5.8 Numerical Computation Considerations**

*TBD – as needed specific considerations on method of code computation*

## **5.9 Programmer/Procedural Considerations**

*TBD- provide information related to output parameters that were not in the algorithm description*

## **5.10 Calibration and Validation**

There are three types of open ocean calibration and validation:

- 1) Direct comparison of sea surface height or dynamic ocean topography with satellite radar altimetry from TOPEX/Poseidon and CryoSat-2. This may be possible to automate so that the project personnel can do it, but funding is being sought outside the ICESat-2 and NASA Cryosphere program for Cal/Val.
- 2) Comparison of changes in DOT with in situ measurements of dynamic heights from hydrography plus ocean bottom pressure from in situ gauges or GRACE-FO. This will have to be done for the open ocean perhaps funded outside the Cryosphere program.
- 3) Direct comparison to in situ precision GPS measurements. Buoys are being built with NOPP funding to do this as an add-on to similar measurements for NASA Oceanography's SWOT cal/val effort.

## **6.0 BROWSE PRODUCTS**

*These browse figures show images that allow user to easily evaluate if the data would be useful and of quality for their research and will aid in the quick approval or disapproval of products prior to public distribution.*

### **6.1 Data Quality Monitoring**

#### **6.1.1 Line plots** (each strong beam)

- a) mean sea surface height for each segment
- b) standard deviation of height distribution and associated SWH for each segment
- c) skewness of height distribution for each segment
- d) kurtosis of height distribution for each segment

#### **6.1.2 Histograms** (each strong beam)

- a) Line plots of parameters of 2-Gaussian fit for each segment
- b) TBD quality measure of each 2-Gaussian fit

## 7.0 DATA QUALITY

### 7.1 Statistics

Calculate the following statistics for each open ocean granule and broken down by strong beam ground track – so there is one set for each ground track.

- Aggregate histogram and mean/standard deviation of each of the following parameters

#### 7.1.1 Per orbit statistics

Table 7 ATL12 Output Variables for Per Orbit Statistics

| Product Label              | Description  | Symbol            |
|----------------------------|--|-------------------|
| <b>sea_surface_heights</b> |  |                   |
| h                          | Mean sea surface height  | <i>SSH</i>        |
| h_var                      | Variance of best fit probability density function (meters <sup>2</sup> )                           | <i>SSHvar</i>     |
| h_skewness                 | Skewness of photon sea surface height histogram  | <i>SSHskew</i>    |
| h_kurtosis                 | Excess kurtosis of sea surface height histogram  | <i>SSHkurt</i>    |
| mix_m1                     | Fraction of component 1 in 2-component Gaussian mixture  | <i>m1</i>         |
| mix_mu1                    | Mean of component 1 in 2-component Gaussian mixture  | <i>mu1</i>        |
| mix_sig1                   | Standard deviation of component 1 in 2-component Gaussian mixture                                  | <i>Sig1</i>       |
| mix_m2                     | Fraction of component 1 in 2-component Gaussian mixture  | <i>m2</i>         |
| mix_mu2                    | Mean of component 1 in 2-component Gaussian mixture  | <i>mu2</i>        |
| mix_sig2                   | Standard deviation of component 1 in 2-component Gaussian mixture                                  | <i>Sig2</i>       |
| delt_seg                   | Time duration segment  | <i>t_seg</i>      |
| lat_seg                    | Mean latitude of surface photons in segment  | <i>lat_seg</i>    |
| lon_seg                    | Mean longitude of surface photons in segment   | <i>lon_seg</i>    |
| length_seg                 | Length of segment (m)  | <i>length_seg</i> |
| P0                         | Constant of linear fit versus along-track distance to surface photon height over the ocean segment | <i>P0</i>         |
| P1                         | Slope of linear fit versus along-track distance to surface photon height over the ocean segment    | <i>P1</i>         |
| n_pulse_seg                | Number of laser pulses in segment  | <i>n_pls_seg</i>  |
| meanoffit2                 | Mean of linear fit removed from surface photon height  | <i>meanoffit2</i> |
| Y                          | Probability density function of photon surface height  | <i>Y</i>          |
| Ymean                      | Mean=first moment of Y, should be $\sim 0 = h - \text{meanoffit2}$                                 | <i>Ymean</i>      |
| Yvar                       | Variance = second moment (m <sup>2</sup> ) of Y  | <i>Yvar</i>       |
| Yskew                      | Skewness = (third moment of Y)/ $Yvar^{3/2}$   | <i>Yskew</i>      |

|                               |   |                                      |
|-------------------------------|---|--------------------------------------|
| <i>Ykurt</i>                  | Excess Kurtosis = (fourth moment of <i>Y</i> )/ <i>Yvar</i> <sup>2</sup> -3   | <b><i>Ykurt</i></b>                  |
| <i>binSSBias</i>              | Sea state bias estimated from the correlation of photon return rate with along track 10-m bin averaged surface height (4.3.1)   | <b><i>binSSBias</i></b>              |
| <i>SWH</i>                    | Significant wave height estimated as 4 times the standard deviation of along track 10-m bin averaged surface height   | <b><i>SWH</i></b>                    |
|                               |   |                                      |
| <b>Height_segment_stat</b>    |   |                                      |
| <i>n_ttl_photon</i>           | Number of photons in the ±15-m ocean downlink band  | <b><i>n_ttl_photon</i></b>           |
| <i>n_photons</i>              | Number of surface photons found for the segment   | <b><i>n_photon</i></b>               |
| <i>Photon_rate</i>            | Photon count rate, averaged over the segment  | <b><i>r<sub>surf</sub></i></b>       |
| <i>Photon_noise_rate</i>      | Noise photon count rate, averaged over the segment  | <b><i>r<sub>noise</sub></i></b>      |
| <i>backgr_seg</i>             | <i>backgrd_atlas/bckgrd_rate</i> from ATL03 averaged over the segment   | <b><i>backgr_seg</i></b>             |
| <i>first_pce_mframe_cnt</i>   | First Major Frame ID in the SSH segment   | <b><i>first_pce_mframe_cnt</i></b>   |
| <i>first_tx_pulse</i>         | First Transmit pulse in along-track segment   | <b><i>first_tx_pulse</i></b>         |
| <i>layer_flag_seg</i>         | The layer flag from ATL09 that is in effect over 50% of the ocean segment, 0 indicating absence of clouds and forward scattering, and 1 indicating possibility of forward scattering as in ATL09  | <b><i>layer_flag_seg</i></b>         |
| <i>depth_ocn_seg</i>          | The average of <i>depth_ocn</i> of geo-segments used in the ocean segment.  | <b><i>depth_ocn_seg</i></b>          |
| <i>orbit_number =</i>         | Unique identifying number for each planned ICESat-2 orbit   | <b><i>orbit_number</i></b>           |
| <i>ss_corr</i>                | Subsurface scattering correction, placeholder = zero pending further findings to the contrary   | <b><i>ss_corr</i></b>                |
| <i>ss_corr_stdev</i>          | Estimated error of subsurface scattering correction, placeholder = zero pending further findings to the contrary  | <b><i>ss_corr_stdev</i></b>          |
| <i>neutat_delay_total_seg</i> | Ocean segment average of total neutral atmosphere delay correction (wet + dry)  | <b><i>neutat_delay_total_seg</i></b> |
| <i>seg_dist_x_seg</i>         | Ocean segment average of the along-track distance from the equator crossing to the start of the 20-m geolocation segments included in the ocean segment   | <b><i>seg_dist_x_seg</i></b>         |
| <i>solar_azimuth_seg</i>      | Ocean segment average of the azimuth of the sun position vector from the reference photon bounce point position in the local ENU frame. The angle is measured from North and is positive towards East. The average is provided in degrees.                | <b><i>solar_azimuth_seg</i></b>      |
| <i>solar_elevation_seg</i>    | Ocean segment average of the elevation of the sun position vector from the reference photon bounce point position in the local ENU frame. The angle is measured from the East-North plane and is positive towards Up. The average is provided in degrees. | <b><i>solar_elevation_seg</i></b>    |
| <i>geoid_seg</i>              | Ocean segment average of geoid height above the WGS – 84 reference ellipsoid (range -107 to 86 m)   | <b><i>geoid_seg</i></b>              |
| <i>dac_seg</i>                | Ocean segment average of dynamic atmospheric  | <b><i>dac_seg</i></b>                |

|                             |   |                                    |
|-----------------------------|---|------------------------------------|
|                             | correction (DAC) includes inverted barometer (IB) affect  |                                    |
| <i>tide_earth_seg</i>       | Ocean segment average of solid earth tides in the tide-free system  | <b><i>tide_earth_seg</i></b>       |
| <i>tide_load_seg</i>        | Ocean segment average of local displacement due to ocean loading (-6 to 0 cm)   | <b><i>tide_load_seg</i></b>        |
| <i>tide_oc_pole_seg</i>     | Ocean segment average of oceanic surface rotational deformation due to polar motion (-2 to +2 mm)   | <b><i>tide_oc_pole_seg</i></b>     |
| <i>tide_ocean_seg</i>       | Ocean segment average of ocean tides including diurnal and semi-diurnal (harmonic analysis) and longer period tides (dynamic and self-consistent equilibrium)   | <b><i>tide_ocean_seg</i></b>       |
| <i>tide_equilibrium_seg</i> | Long period equilibrium tides   | <b><i>tide_equilibrium_seg</i></b> |
| <i>tide_pole_seg</i>        | Ocean segment average of solid pole tide - Rotational deformation due to polar motion (-1.5 to 1.5 cm)  | <b><i>tide_pole_seg</i></b>        |
| <i>surf_type_prcnt</i>      | The percentages of each <b><i>surf_type</i></b> of the photons in the ocean segment as a 5-element variable with each element corresponding to the percentage of photons from each of the 5 surface types | <b><i>surf_type_prcnt</i></b>      |

## **8.0 TEST DATA**

This section describes the test data sets that have been used to derive and verify the performance of the ATL12 code for surface finding, deconvolution of the instrument impulse response, and Gaussian mixture determination.

### **8.1 In Situ Data Sets**

**Table 8 ATL12 Test Data**

| Instrument | Date       | Location                      |
|------------|------------|-------------------------------|
| MABEL      | April 2012 | Fram Strait and Greenland Sea |
| MABEL      | July 2014  | North Pacific                 |

### **8.2 Simulated Test Data**

Development of ATL12 used the simulated data set described in Section 5.6 Synthetic Data. For these synthetic data we started with a synthetic sea surface height record comprised of a known 2-Gaussian mixture that we convolved with a known instrument impulse response and added random measurement noise. We exercised the developmental Matlab code and the ASAS PGE code on this data to see that they output the same 2-Gaussian mixture that was the basis of the synthetic ocean surface

## **9.0 CONSTRAINTS, LIMITATIONS, AND ASSUMPTIONS**

In this section, we list notable constraints, limitations, and assumptions important to ATL12 that affect the coverage, quality and interpretation of the sea surface height retrievals and our objectives for the ATL12. These topics have been discussed throughout the ATBD. In order to compare with other open ocean topography measures, the overarching objective for the ATL12 product is that it should be a solid description of sea surface height probability distribution over each strong beam ground track (and weak beam ground track where available). This objective and the constantly changing wave-covered character of the ocean surface impose the primary constraint on the ATL12 product. To achieve standard errors in mean sea surface height better than 1-cm under typical sea states, we accumulate the distributions over distances of 5 to 7 km. This is far longer than the ultimate spatial resolution of the ICESat-2 instrument, which we in fact use in the ATL12 analysis for sea state bias estimation. Users can aggregate the ATL 12 distributions to obtain greater statistical significance, and we do this to produce the ocean gridded product, ATL19. Where applicable we and other users can go back to ATL03 photon heights and derive specialized ocean products using ATL12 statistics as a guide and benchmark.

### **9.1 Constraints**

The following are constraints imposed by the inherent capability of the instrument.

- At 532 nm, clouds will affect visibility of the open ocean. First impressions looking at preliminary ICESat-2 data the lidar appears able detect the ocean surface through at least thin clouds better than expected.
- The reflectance of the ocean surface is lower than the other surfaces ICESat-2 operates over with the result that only on the order of one photon per pulse is returned from the surface. Thus, longer path lengths are required to accumulate desired statistical significance of ocean height measurements than would be required for other surfaces. On the other hand, we don't have to worry about detector saturation and first photon bias over the ocean.

### **9.2 Limitations**

These limitations stem from on our current understanding of the altimetric returns from the sea ice cover.

- Subsurface Scattering - Quantification of the impact of subsurface scattering on height retrievals due to multiple scattering from bubbles or particles in the water remains to be addressed. For the central parts of the deep ocean, these effects are likely reduced by the scarcity of scatterers in the water. We might also expect that just as surface waves reduce the reflectance of the surface, they may also reduce the transmittance of subsurface returns up through the ocean surface, a benefit offsetting the generation of bubbles by wind waves. Preliminary analysis of ICESat-2 deep ocean data suggests long, but low energy negative tails in the raw height distribution that are mainly removed in the trimming of the histogram in the fine surface finding step. Subsurface scattering will be most important in coastal regions where sediment and biological productivity increase the density of scatterers. Gaining a better understanding the subsurface return problem will be a high priority for future ICESat-2 oceanography.

- Sea State Bias – ICESat-2 will be unique in estimating what we think will be the main source of sea state bias by calculating the correlation of photon return rate and surface height at scales resolving the energy containing surface waves. This constitutes what is termed EM-bias in other altimeters. Because we don't use retracking in the traditional sense or assume a Gaussian surface distribution, we anticipate ICESat-2 will not suffer from sea state bias due to these factors, and the ICESat-2 sea state bias is wholly due to EM-bias. We will assess this assumption as part of the validation process.

### **9.3 Assumptions**

These are assumptions made by the retrieval routines that will have to be tested.

- Ocean Surface Height retrievals – As discussed above key assumptions are that our fine surface finding clips off the negative histogram tail due to subsurface return and that what is commonly termed EM-bias is the sole source of sea state bias in our analysis of ICESat-2 over the ocean.

## 10.0 REFERENCES

- Arnold, D. V., W. K. Melville, R. H. Stewart, J. A. Kong, W. C. Keller, and E. Lamarre (1995), Measurements of electromagnetic bias at Ku and C bands, *J. Geophys. Res.*, *100*(C1), 969-980.
- Carrère, L., and F. Lyard (2003), Modeling the barotropic response of the global ocean to atmospheric wind and pressure forcing - comparisons with observations.
- Chambers, D. P., S. A. Hayes, J. C. Ries, and T. J. Urban (2003), New TOPEX sea state bias models and their effect on global mean sea level, *J. Geophys. Res.*, *108*(C10), 3305.
- Chapron, B., V. Kerbaol, D. Vandemark, and T. Elfouhaily (2000), Importance of peakedness in sea surface slope measurements and applications, *J. Geophys. Res.*, *105*(C7), 17195-17202.
- Cox, C., and W. Munk (1954), Measurement of the Roughness of the Sea Surface from Photographs of the Sun's Glitter, *J. Opt. Soc. Am.*, *44*(11), 838-850.
- Elfouhaily, T., D. R. Thompson, B. Chapron, and D. Vandemark (2000), Improved electromagnetic bias theory, *J. Geophys. Res.*, *105*(C1), 1299-1310.
- Gaspar, P., F. Ogor, P.-Y. Le Traon, and O.-Z. Zanife (1994), Estimating the sea state bias of the TOPEX and POSEIDON altimeters from crossover differences, *J. Geophys. Res.*, *99*(C12), 24981-24994.
- Hausman, J., and V. Zlotnicki (2010), Sea State Bias In Radar Altimetry Revisited, , *Marine Geodesy*, *33*(S1), 336---347.
- Markus, T., et al. (2016), The Ice, Cloud, and land Elevation Satellite-2 (ICESat-2): Science 1 requirements concept, and implementation., *Remote Sensing of the Environment*, in press.
- Menzies, R. T., D. M. Tratt, and W. H. Hunt (1998), Lidar In-Space Technology Experiment Measurements of Sea Surface Directional Reflectance and the Link to Surface Wind Speed, *Appl. Opt.*, *37*(24), 5550-5559.
- Plant, W. J. (2015a), Short wind waves on the ocean: Wavenumber-frequency spectra, *J. Geophys. Res. Oceans*, *120*, 2147-2158.
- Plant, W. J. (2015b), Short wind waves on the ocean: Long-wave and windspeed dependences, *J. Geophys. Res. Oceans*, *120*, 6436-6444.
- Urban, T. J., and B. E. Schutz (2005), ICESat sea level comparisons, *Geophys. Res. Lett.*, *32*(23), L23S10.
- Vandemark, D., B. Chapron, T. Elfouhaily, and J. W. Campbell (2005), Impact of high-frequency waves on the ocean altimeter range bias, *J. Geophys. Res.*, *110*(C11), C11006.
- Wu, J. (1972), Sea-Surface Slope and Equilibrium Wind-Wave Spectra, *Physics of Fluids*, *15*(5), 741-747.

## **ACRONYMS**

### Acronym List

|              |  |
|--------------|--|
| ASA          | ATLAS Science Algorithm Software                 |
| ATLAS        | ATLAS Advance Topographic Laser Altimeter System |
| GSFC         | Goddard Space Flight Center                      |
| ICESat-2 MIS | ICESat-2 Management Information System           |
| IIP          | Instrument Impulse Response                      |
| MIZ          | Marginal Ice Zone                                |
| PSO          | Project Science Office                           |
| PSO          | ICESat-2 Project Support Office                  |
| SDMS         | Scheduling and Data Management System            |
| SIPS         | Science Investigator-led Processing System       |
| TEP          | Transmit Echo Pulse                              |

## **GLOSSARY**

**APPENDIX A: ICESat-2 Data Products**

ICESat-2 Data Products

| File ID/Level | Product Name   | Concept   | Short Description   | Frequency  |
|---------------|--|---|---|--|
| 00/0          | Telemetry Data   | Full rate Along-track with channel info   | Raw ATLAS telemetry in Packets with any duplicates removed  | Files for each APID for some defined time period     |
| 01/1A         | Reformatted Telemetry                                    | Full rate Along-track with channel info   | Parsed, partially reformatted, time ordered telemetry. Proposed storage format is NCSA HDF5.  | Uniform time TBD minutes (1 minute?)                 |
| 02/1B         | Science Unit Converted Telemetry                         | Full rate Along-track with channel info   | Science unit converted time ordered telemetry. Reference Range/Heights determined by ATBD Algorithm using Predict Orbit and s/c pointing. All photon events per channel per pulse. Includes Atmosphere raw profiles.  | Uniform time TBD minutes (1 minute?)                 |
| 03/2A         | Global Geolocated Photon Data                            | Full rate Along-track with channel info   | Reference Range/Heights determined by ATBD Algorithm using POD and PPD. All photon events per pulse per beam. Includes POD and PPD vectors. Classification of each photon by several ATBD Algorithms.   | Uniform time TBD minutes (1 minute?)                 |
| 04/2A         | Calibrated Backscatter Profiles                          | 3 profiles at 25 Hz rate (based on 400 pulse mean)                                  | Along-track backscatter data at full instrument resolution. The product will include full 532 nm (14 to -1.0 km) calibrated attenuated backscatter profiles at 25 times per second for vertical bins of approximately 30 meters. Also included will be calibration coefficient values for the polar region. | Per orbit  |
| 05/2B         | Photon Height Histograms                                 | Fixed distances Along-track for each beam   | Histograms by prime Classification by several ATBD Algorithms. By beam  | Uniform time TBD minutes (30 minutes?)               |
| 06/L3         | Antarctica Ice Sheet Height / Greenland Ice Sheet Height | Heights calculated with the ice sheet algorithm, as adapted for a dH/dt calculation | Surface heights for each beam, along and across-track slopes calculated for beam pairs. All parameters are calculated for the same along-track increments for each beam and repeat.   | There will be TBD files for each ice sheet per orbit |

| <b>File ID/Level</b> | <b>Product Name</b>   | <b>Concept</b>  | <b>Short Description</b>   | <b>Frequency</b>                                     |
|----------------------|---|---|--|--|
| 07/ L3               | Arctic Sea Ice Height/ Antarctic Sea Ice Height                   | Along-track heights for each beam ~50-100m (uniform sampling); separate Arctic and Antarctic products | Heights of sea ice and open water samples (at TBD length scale) relative to ellipsoid after adjusted for geoidal and tidal variations, and inverted barometer effects. Includes surface roughness from height statistics and apparent reflectance  | There will be files for each pole per orbit          |
| 08/ L3               | Land Water Vegetation Heights                                     | Uniform sampling along-track for each beam pair and variable footpath                                 | Heights of ground including inland water and canopy surface at TBD length scales. Where data permits, include estimates of canopy height, relative canopy cover, canopy height distributions (decile bins), surface roughness, surface slope and aspect, and apparent reflectance. (Inland water > 50 m length -TBD) | Per half (TBD) orbit                                 |
| 09/ L3               | ATLAS Atmosphere Cloud Layer Characteristics                      | Based on 3 profiles at a 25 hz rate. (400 laser pulses are summed for each of the 3 strong beams.)    | Cloud and other significant atmosphere layer heights, blowing snow, integrated backscatter, optical depth  | Per day  |
| 10/ L3               | Arctic Sea Ice Freeboard / Antarctic Sea Ice Freeboard            | Along-track all beams. Freeboard estimate along-track (per pass); separate Arctic/ Antarctic products | Estimates of freeboard using sea ice heights and available sea surface heights within a ~TBD km length scale; contains statistics of sea surface samples used in the estimates.  | There will be files for each polar region per day    |
| 11/ L3               | Antarctica Ice Sheet H(t) Series/ Greenland Ice Sheet H(t) Series | Height time series for pre-specified points (every 200m) along-track and Crossovers.                  | Height time series at points on the ice sheet, calculated based on repeat tracks and/or crossovers   | There will be files for each ice sheet for each year |
| 12/ L3               | Ocean Height  | Along-track heights per beam for ocean including coastal areas  | Height of the surface 10 Hz/700 m (TBD) length scales. Where data permits, include estimates of height distributions (decile bins), surface roughness, surface slope, and apparent reflectance   | Per half orbit                                       |
| 13/ L3               | Inland Water Height   | Along-track height per beam   | Along-track inland ground and water height extracted from Land/Water/Vegetation product. TBD data-derived surface indicator or mask. Includes roughness, slope and aspect.   | TBD files Per day                                    |

| <b>File ID/Level</b> | <b>Product Name</b>  | <b>Concept</b>  | <b>Short Description</b>  | <b>Frequency</b>  |
|----------------------|--|---|---|---|
| 14/L4                | Antarctica Ice Sheet Gridded/<br>Greenland Ice Sheet Gridded             | Height time series interpolated onto a regular grid for each ice sheet. Series (5-km posting interval)  | Height maps of each ice sheet for each year of the mission, based on all available ICESat-2 data.       | Per ice sheet per year  |
| 15/L4                | Antarctica Ice Sheet dh/dt Gridded/<br>Greenland Ice Sheet dh/dt Gridded | Images of dH/dt for each ice sheet, gridded at 5 km.  | Height-change maps of each ice sheet, with error maps, for each mission year and for the whole mission. | Per ice sheet for each year of mission, and for the mission as a whole  |
| 16/ L4               | ATLAS Atmosphere Weekly  | Computed statistics on weekly occurrences of polar cloud and blowing snow   | Polar cloud fraction, blowing snow frequency, ground detection frequency                                | Per polar region Gridded 2 x 2 deg. weekly  |
| 17/ L4               | ATLAS Atmosphere Monthly   | Computed statistics on monthly occurrences of polar cloud and blowing snow  | Global cloud fraction, blowing snow and ground detection frequency                                      | Per polar region Gridded 1 x 1 deg. Monthly   |
| 18/L4                | Land Height/<br>Canopy Height Gridded                                    | Height model of the ground surface, estimated canopy heights and canopy cover gridded on an annual basis. Final high resolution DEM generated at end of mission | Gridded ground surface heights, canopy height and canopy cover estimates                                | Products released annually at a coarse resolution (e.g. 0.5 deg. tiles, TBD). End of mission high resolution (~1-2km) |
| 19/ L4               | Ocean MSS  | Gridded monthly   | Gridded ocean height product including coastal areas. TBD grid size. TBD merge with Sea Ice SSH         | Monthly   |
| 20/ L4               | Arctic and Antarctic Gridded Sea Ice Freeboard/                          | Gridded monthly; separate Arctic and Antarctic products   | Gridded sea ice freeboard. (TBD length scale)   | Aggregate for entire month for each polar region  |

| <b>File ID/Level</b> | <b>Product Name</b>   | <b>Concept</b>  | <b>Short Description</b>   | <b>Frequency</b>   |
|----------------------|---|---|--|--|
| 21/ L4               | Arctic Gridded Sea Surface Height within Sea Ice/ Antarctic Gridded Sea Surface Height within Sea Ice | Aggregate for entire month (all sea surface heights within a grid) separate Arctic and Antarctic products                                 | Gridded monthly sea surface height inside the sea ice cover. TBD grid  | Aggregate for entire month for each polar region                                 |
| Experimental         | Arctic Sea Ice Thickness / Antarctic Sea Ice Thickness  | Per Pass Thickness samples (from 10-100m freeboard means) for every 10 km (TBD) segment (all beams) where leads are available; (per pass) | Sea ice thickness estimates derived from the sea ice freeboard product. External input: snow depth and density for each pass.  | There will be files for each polar region per day                                |
| Experimental         | Arctic Gridded monthly Sea Ice Thickness / Antarctic Gridded monthly Sea Ice Thickness                | Aggregate for entire month (all thickness observations within a grid) plus Thickness (corrected for growth)                               | Gridded sea ice thickness product; centered at mid-month. Include thickness with or without adjustment for ice growth (based on time differences between freeboard observation). | Gridded monthly (all thickness observations within a grid) for each polar region |
| Experimental         | Lake Height   | Along reference track per beam in Pan-Arctic basin (>50-60 deg N).  | Extracted from Product 08 and 13, for lakes >10 km <sup>2</sup> , with slope and aspect. Ice on/off flag. TBD water mask developed from existing masks.                          | Monthly along track product, no pointing   |
| Experimental         | Snow Depth  | Along reference track per beam for Pan-Arctic basin (>50-60 deg N).   | Extracted from Product 08 and 13 along track repeat heights, with slope and aspect. Snow detection flag.   | Monthly along track product, no pointing   |

## APPENDIX B: Sea State Bias Computations for a Photon Counting Lidar

For ICESat-2, we are looking over all the received surface photon heights to get a received height distribution and then deconvolving the instrument impulse response to get the surface height distribution. If we are getting a disproportionate share of photons back from the wave crests or troughs because of a difference in reflectance between crests and troughs, the correlation of height and reflectance (or in this case rate of photon returns) and the sea state bias it causes are unknown to us. However, if as a separate step we take advantage of the fine spatial resolution of ICESat-2 to obtain along-track distance bin average estimates of height and photon return rate unbiased by the number of photons in the bins, and over bins that are short compared to the dominate surface wavelength, we can estimate the sea state bias in the surface height distribution using the relation of *Arnold et al.* [1995]. To do this we need to consider the *Arnold et al.* relation in terms of bin averages rather than aggregate photon averages.

First we establish the relation between average height computed over all surface photons and the average taken over all photons grouped in  $K$  along-track distance bins. The photon average sea surface height is the sum the heights of  $N$  surface reflected photons divided by  $N$ :

$$H_{\text{photonavg}} = \frac{1}{N} \sum_{i=1}^N \eta_i \quad (\text{B1})$$

However, if we express  $N$  as the sum over all  $K$  along-track bins of the number of photons grouped into each bin,  $r_j$ , we see that:

$$N = \sum_{j=1}^K r_j \quad (\text{B2})$$

Similarly, we can group the heights into the contributions from each bin

$$\sum_{i=1}^N \eta_i = \sum_{j=1}^K \sum_{l=1}^{r_j} \eta_l \quad (14- \text{B3})$$

where  $\eta_l$  is the height of the  $l^{\text{th}}$  photon in a bin with a total of  $r_j$  photons in it. Therefore, the average height over all photon heights is equal to the bin average heights weighted by the relative share of photons in each bin, combining (12-14)

$$\frac{1}{N} \sum_{i=1}^N \eta_i = \frac{1}{N} \sum_{j=1}^K \sum_{l=1}^{r_j} \eta_l = \frac{\sum_{j=1}^K \sum_{l=1}^{r_j} \eta_l}{\sum_{j=1}^K r_j} \quad (15- \text{B4})$$

In the relation of *Arnold et al.*, [1995] (9), we replace the backscatter coefficient of  $\sigma_i^0$ , by the number of photons per bin  $r_l$  as an expression of the energy returned from the surface in each bin.

SSB is the photon average or photon weighted bin average minus the true average of surface heights over all the distance bins,  $\sum_{j=1}^K \eta_j / K$  :

$$SSB = \frac{1}{N} \sum_{i=1}^N \eta_i - \frac{\sum_{j=1}^K \eta_j}{K} = \frac{\sum_{j=1}^K \sum_{l=1}^{r_j} \eta_l}{\sum_{j=1}^K r_j} - \frac{\sum_{j=1}^K \eta_j}{K} \quad (B5)$$

where  $\eta_j$  is the true average of height in the  $j^{\text{th}}$  bin not biased by the number photons, and so the second term on the right is  $\mu_\eta$ , the true arithmetic mean of surface height averaged over  $K$  bins.

$$\mu_\eta = \frac{\sum_{j=1}^K \eta_j}{K} \quad (B6)$$

The number of samples in along-track bin  $j$ , is  $r_j$ , and though the sample rate with each sample,  $\rho_j$ , is potentially different for each sample, we take  $\rho_j$  as the average sample rate in each  $\delta_x$  wide bin such that

$$\delta_x \rho_j = r_j \quad (B7)$$

The average of photon heights in each bin is

$$\bar{\eta}_j = \frac{1}{r_j} \sum_{l=1}^{r_j} \eta_l \quad (B8)$$

So

$$r_j \bar{\eta}_j = \sum_{l=1}^{r_j} \eta_l \quad (B9)$$

and (B5) becomes

$$SSB = \frac{\sum_{j=1}^K r_j \bar{\eta}_j}{\sum_{j=1}^K r_j} - \frac{\sum_{j=1}^K \eta_j}{K} \quad (B10)$$

and with (B6), (B10) becomes

$$SSB = \frac{\sum_{j=1}^K r_j \bar{\eta}_j}{\sum_{j=1}^K r_j} - \mu_\eta = \frac{\sum_{j=1}^K r_j \bar{\eta}_j - \sum_{j=1}^K r_j \mu_\eta}{\sum_{j=1}^K r_j} = \frac{\sum_{j=1}^K r_j (\bar{\eta}_j - \mu_\eta)}{\sum_{j=1}^K r_j} \quad (B11)$$

This looks like the same relation as (9) by *Arnold et al.* [1995] but it is a little unclear if Arnold et al meant to use the backscatter coefficient in his equation or the variation in backscatter coefficient about the mean. To check this for our relation we break height and return rate in  $\frac{\sum_{j=1}^K \sum_{l=1}^{r_j} \eta_l}{\sum_{j=1}^K r_j}$  into mean, ( $\mu$ ) and time varying (primed) components. Speaking

of the along-track bin quantities,  $\bar{\eta}_j = \mu_\eta + \eta_j'$  and  $r_i = \mu_\rho + r_j'$ . From (B9):

$$\frac{1}{N} \sum_{i=1}^N \eta_i = \frac{1}{N} \sum_{j=1}^K \sum_{l=1}^{r_j} \eta_l = \frac{\sum_{j=1}^K \sum_{l=1}^{r_j} \eta_l}{\sum_{j=1}^K r_j} = \frac{\sum_{j=1}^K r_j \bar{\eta}_j}{\sum_{j=1}^K r_j} \quad (B12)$$

If the along-track bins are small enough so that the sea surface height variation within a bin is much smaller than the variation of height between bins (bins are small compared to the wavelength of the dominant waves), we can assume that the average of photon heights within bin,  $\bar{\eta}_j$ , equals the true average of height within a bin,  $\eta_j$ , and the true average height is equal to the average of  $\bar{\eta}_j$  over all bins.

$$\mu_\eta = \frac{\sum_{j=1}^K \eta_j}{K} = \frac{\sum_{j=1}^K \bar{\eta}_j}{K} \quad (B13)$$

This assumption is equivalent to saying the bias due to variation of the number of photons within bins is small compared to the bias due to the differences in the number of photons among bins. Similarly, the average photon rate,  $\mu_\rho$ , is

$$\mu_\rho = \frac{\sum_{j=1}^K r_j}{K} \quad (\text{B14})$$

Applying (B9) to (B4) and breaking into mean and varying parts

$$\begin{aligned} \frac{1}{N} \sum_{i=1}^N \eta_i &= \frac{\sum_{j=1}^K \sum_{l=1}^{r_j} \eta_l}{\sum_{j=1}^K r_j} = \frac{\sum_{j=1}^K r_j \bar{\eta}_j}{\sum_{j=1}^K r_j} = \frac{\sum_{j=1}^K r_j \eta_j}{\sum_{j=1}^K r_j} = \frac{\sum_{j=1}^K (r_j' + \mu_r)(\eta_j' + \mu_\eta)}{\sum_{j=1}^K r_j} \\ &= \frac{\sum_{j=1}^K (r_j' \eta_j' + r_j' \mu_\eta + \mu_r \eta_j' + \mu_r \mu_\eta)}{\sum_{j=1}^K r_j} \quad (\text{B15}) \\ &= \frac{\sum_{j=1}^K (r_j' \eta_j' + \mu_r \mu_\eta)}{\sum_{j=1}^K r_j} = \frac{\sum_{j=1}^K (r_j' \eta_j')}{\sum_{j=1}^K r_j} + \frac{K \mu_r \mu_\eta}{\sum_{j=1}^K r_j} = \frac{\sum_{j=1}^K (r_j' \eta_j')}{\sum_{j=1}^K r_j} + \mu_\eta \end{aligned}$$

So in fact the product in the SSB expression of *Arnold et al.* (1995) is the product of the variations in distance bin photon rate and photon height:

$$SSB = \frac{\sum_{j=1}^K (r_j' \eta_j')}{\sum_{j=1}^K r_j} \quad (\text{B16})$$

Alternatively, consider breaking down (B11)

$$SSB = \frac{\sum_{j=1}^K r_j \bar{\eta}_j}{\sum_{j=1}^K r_j} - \mu_\eta = \frac{\sum_{j=1}^K r_j \bar{\eta}_j - \sum_{j=1}^K r_j \mu_\eta}{\sum_{j=1}^K r_j} = \frac{\sum_{j=1}^K r_j (\bar{\eta}_j - \mu_\eta)}{\sum_{j=1}^K r_j} \quad (\text{B17})$$

with,  $\bar{\eta}_j = \mu_\eta + \eta_j'$  and  $r_j = \mu_r + r_j'$ .

$$SSB = \frac{\sum_{j=1}^K r_j \bar{\eta}_j}{\sum_{j=1}^K r_j} - \mu_\eta = \frac{\sum_{j=1}^K (r_j' + \mu_r)(\eta_j' + \mu_\eta)}{\sum_{j=1}^K r_j} - \mu_\eta = \frac{\sum_{j=1}^K (r_j' \eta_j')}{\sum_{j=1}^K r_j} + \mu_\eta - \mu_\eta = \frac{\sum_{j=1}^K (r_j' \eta_j')}{\sum_{j=1}^K r_j} \quad (B18)$$

consistent with (B16).

We propose that there is a sea state bias in the higher moments also. If we consider higher sample  $n^{\text{th}}$  moments of height

$$M(n) = \frac{\sum_{j=1}^K (\eta_j - \mu_\eta)^n}{K} = \frac{\sum_{j=1}^K g_j(n)}{K} \quad (B19)$$

As with (B15):

$$\begin{aligned} M(n) &= \frac{1}{N} \sum_{i=1}^N g_i(n) = \frac{\sum_{j=1}^K \sum_{l=1}^{r_j} g_j(n)}{\sum_{j=1}^K r_j} = \frac{\sum_{j=1}^K r_j \bar{g}_j(n)}{\sum_{j=1}^K r_j} = \frac{\sum_{j=1}^K r_j g_j(n)}{\sum_{j=1}^K r_j} = \frac{\sum_{j=1}^K (r_j' + \mu_r)(g_j(n)' + \mu_g)}{\sum_{j=1}^K r_j} \\ &= \frac{\sum_{j=1}^K (r_j' g_j(n)' + r_j' \mu_g + \mu_r g_j(n)' + \mu_r \mu_g)}{\sum_{j=1}^K r_j} \\ &= \frac{\sum_{j=1}^K (r_j' g_j(n)' + \mu_r \mu_g)}{\sum_{j=1}^K r_j} = \frac{\sum_{j=1}^K (r_j' g_j(n)')}{\sum_{j=1}^K r_j} + \frac{K \mu_r \mu_g}{\sum_{j=1}^K r_j} = \frac{\sum_{j=1}^K (r_j' g_j(n)')}{\sum_{j=1}^K r_j} + \mu_g \end{aligned}$$

Thus, the  $(\eta_j - \mu_\eta)^n$ ,  $n^{\text{th}}$  moment, would have a similar derivation for their sea state bias,  $SSBM(n)$ :

$$SSBM(n) = \frac{\sum_{j=1}^K r_j ((\eta_j - \mu_\eta)^n - avg(\eta_j - \mu_\eta)^n)}{\sum_{j=1}^K r_j} \quad (B20)$$

## APPENDIX C: Expectation-Maximization (EM) Procedure

From Appendix E of ATBD ATL07

EM algorithm for estimating the parameters of two-component normal mixtures  
 The EM algorithm estimates the parameters of a two-component normal mixture that best describe a distribution of random variables (*Dempster et al., 1977; Bilmes, 1998*).  
 The two-component mixture model:

$$f(x_i) = \alpha\phi_1(x_i; \mu_1, \sigma_1) + (1 - \alpha)\phi_2(x_i; \mu_2, \sigma_2)$$

$$\phi_i(x; \mu_i, \sigma_i) = \frac{1}{\sqrt{2\pi\sigma_i}} e^{-\frac{(x-\mu_i)^2}{2\sigma_i^2}} \quad (\text{Normal Distribution})$$

The EM steps to compute the parameters of the mixture model with  $T$  random variates  $x_t(\alpha, \mu_1, \sigma_1, \mu_2, \sigma_2)$  are:

1. Initialize with:  $\alpha, \mu_1, \sigma_1, \mu_2, \sigma_2$
2. Expectation (E) step: compute:

$$\gamma_t = \frac{\alpha\phi_1(x_t; \mu_1, \sigma_1)}{\alpha\phi_1(x_t; \mu_1, \sigma_1) + (1 - \alpha)\phi_2(x_t; \mu_2, \sigma_2)}$$

for  $t = 1, \dots, T$ .

3. Maximization (M) step. compute:

$$\mu_1 = \frac{\sum_{t=1}^T \gamma_t x_t}{\sum_{t=1}^T \gamma_t}, \quad \sigma_1^2 = \frac{\sum_{t=1}^T \gamma_t (x_t - \mu_1)^2}{\sum_{t=1}^T \gamma_t}$$

$$\mu_2 = \frac{\sum_{t=1}^T (1 - \gamma_t) x_t}{\sum_{t=1}^T (1 - \gamma_t)}, \quad \sigma_2^2 = \frac{\sum_{t=1}^T (1 - \gamma_t) (x_t - \mu_2)^2}{\sum_{t=1}^T (1 - \gamma_t)}, \text{ and}$$

$$\alpha = \sum_{t=1}^T \frac{\gamma_t}{T}$$

Iterate E and M steps until parameters converge.

## APPENDIX D: Fitting a Plane to Spatially Distributed Data

To evaluate the average DOT at the center of a grid cell we fit a plane to all the samples within the grid cell and evaluate the height of the plane at the center of the grid cell. To do this we first have to make a least squares fit of a plane to DOT at  $N$  locations within the grid cell. Following *Eberly* (2019), given data (DOT) as a function of  $x$  and  $y$ ,  $h_i = f(x_i, y_i)$  at  $i=1$  to  $N$  locations, find a least squares fit of a plane, coefficients  $a$ ,  $b$ , and  $c$ , to  $h_i$  with

mean,  $\bar{h} = \sum_{i=1}^N h_i$ . (Also note  $\bar{x} = \sum_{i=1}^N x_i$  and  $\bar{y} = \sum_{i=1}^N y_i$ )

$$h_i \approx ax_i + by_i + c \quad (1)$$

And we want to choose  $a$ ,  $b$ , and  $c$  such that the error,  $E$ ,

$$E(a, b, c) = \sum_{i=1}^N ((ax_i + by_i + c) - h_i)^2$$

is minimized. According to *Eberle* (2019) the solution is more robust and the equations are simpler if we initially eliminate the need to determine  $c$  by taking the average of (1) and subtracting it from (1), to get:

$$h_i - \bar{h} \approx a(x_i - \bar{x}) + b(y_i - \bar{y})$$

and so for the deviations  $h'_i = h_i - \bar{h}$ ,  $x'_i = x_i - \bar{x}$ , and  $y'_i = y_i - \bar{y}$

$$h'_i \approx ax'_i + by'_i \quad (3)$$

and we will choose  $a$  and  $b$  to minimize:

$$E(a, b) = \sum_{i=1}^N ((ax'_i + by'_i) - h'_i)^2 \quad (4)$$

Then  $c$  will be given by  $c = \bar{h} - (a\bar{x} + b\bar{y})$ . To minimize  $E$  with respect to  $a$  and  $b$  we find  $a$  and  $b$  for which:

$$\begin{aligned} \frac{\partial E(a, b)}{\partial a} &= 2 \sum_{i=1}^N x'_i ((ax'_i + by'_i) - h'_i) = 2 \sum_{i=1}^N ax'_i x'_i + bx'_i y'_i - x'_i h'_i = 0 \\ \frac{\partial E(a, b)}{\partial b} &= 2 \sum_{i=1}^N y'_i ((ax'_i + by'_i) - h'_i) = 2 \sum_{i=1}^N ay'_i x'_i + by'_i y'_i - y'_i h'_i = 0 \end{aligned}$$

or

$$a \sum_{i=1}^N x'_i x'_i + b \sum_{i=1}^N x'_i y'_i = \sum_{i=1}^N x'_i h'_i$$

$$a \sum_{i=1}^N y'_i x'_i + b \sum_{i=1}^N y'_i y'_i = \sum_{i=1}^N y'_i h'_i$$

Letting

$$L_{xx} = \sum_{i=1}^N x'_i x'_i$$

$$L_{yy} = \sum_{i=1}^N y'_i y'_i$$

$$L_{xy} = \sum_{i=1}^N y'_i x'_i$$

$$R_{xh} = \sum_{i=1}^N x'_i h'_i$$

$$R_{yh} = \sum_{i=1}^N y'_i h'_i$$

(5)

a, b, and c are given by

$$a = \frac{R_{xh}L_{yy} - R_{yh}L_{xy}}{L_{xx}L_{yy} - L_{xy}^2}$$

$$b = \frac{R_{yh}L_{xx} - R_{xh}L_{xy}}{L_{xx}L_{yy} - L_{xy}^2}$$

$$c = \bar{h} - (a\bar{x} + b\bar{y})$$

(6)

Eberly, D., 2019, Least Squares Fitting of Data by Linear or Quadratic Structures

David Eberly, Geometric Tools, Redmond WA 98052

<https://www.geometrictools.com/>

This work is licensed under the Creative Commons Attribution 4.0 International License.

To view a copy

of this license, visit <http://creativecommons.org/licenses/by/4.0/> or send a letter to

Creative Commons,

PO Box 1866, Mountain View, CA 94042, USA.

Created: July 15, 1999

Last Modified: February 14, 2019

<https://www.geometrictools.com/Documentation/LeastSquaresFitting.pdf>

## APPENDIX E: Hierarchy of ATL12 and ATL10 Variables

### ATL12 Inputs to ATL19

Segment Averages: *SSH-geoid\_seg, lat\_seg, lon\_seg, bin\_ssbias, geoid\_seg, depth\_ocn\_seg, length\_seg*, and *surf\_type\_prcnt*.

Segment Moments: *SSHvar, SSHskew, SSHkurt, SWH*

Segment Histogram: *Y, n\_photons*

Segment Degrees-of-Freedom: *NP\_effect*

### 5.6.4.1.1 Output ATL19 Averaging Over *n\_segsinbin* Bins

Grid Cell Averages: *dot\_avg, grid\_lat, grid\_lon, ssb\_avg, geoid\_avg, depth\_avg, length\_avg, surf\_avg*

Grid Cell Average Moments: *dot\_sigma\_avg, dot\_skew\_avg, dot\_kurt\_avg, SWH\_avg*

Grid Cell Total Histogram: *dot\_hist\_grid*

Grid Cell Totals: *n\_segsinbin, n\_photons\_gridttl, length\_sum*

### 5.6.4.1.2 Output ATL19 Averaging Weighted by Degrees-of-Freedom

Grid Cell Degree-of-Freedom Weighted Averages *dot\_dfw, grid\_lat\_dfw, grid\_lon\_dfw, , ssb\_dfw, geoid\_dfw, depth\_dfw, length\_dfw, surf\_dfw*,

Grid Cell Degree-of-Freedom Weighted Moments *dot\_sigma\_dfw, dot\_skew\_dfw, dot\_kurt\_dfw, SWH\_dfw*

Grid Cell Degrees-of-Freedom and DOT Uncertainty: *dof\_grid, dot\_dfw\_uncertain*

### 5.6.4.2.1 Output ATL19 Interpolated to Bin Centers (*gridcntr lon* and *gridcntr lat*)

Average DOT at Grid Cell Center: *dot\_avgcntr*

### 5.6.4.2.2 Output ATL19 Interpolated to Bin Centers (*gridcntr* and *gridcntr lat*)

DOF Weighted Average DOT at Grid Cell Center: *dot\_dfwcntr*

### 5.6.4.5.1 Output ATL19 Merging All 3 Strong Beams of DOT Averaged by *n\_segsinbin*

Average DOT at Grid Cell Center: *dot\_allbeam*

### 5.6.4.5.2 Output ATL19 Merging All 3 Strong Beams of DOT Averaged by *dof\_grid*

Degree-of-Freedom Weighted Average DOT at Grid Cell Center: *dot\_dfwallbeam*

Degree-of-Freedom Weighted Average DOT at Grid Cell Center: *dot\_sigma\_dfwalbm*

Degree-of-Freedom Weighted Average DOF and Uncertainty at Grid Cell Center:

*dof\_grid\_allbeam, , dot\_dfwalbm\_uncrtn*

## 11.0 REFERENCES

- Arnold, D. V., W. K. Melville, R. H. Stewart, J. A. Kong, W. C. Keller, and E. Lamarre (1995), Measurements of electromagnetic bias at Ku and C bands, *J. Geophys. Res.*, *100*(C1), 969-980.
- Carrère, L., and F. Lyard (2003), Modeling the barotropic response of the global ocean to atmospheric wind and pressure forcing - comparisons with observations.
- Chambers, D. P., S. A. Hayes, J. C. Ries, and T. J. Urban (2003), New TOPEX sea state bias models and their effect on global mean sea level, *J. Geophys. Res.*, *108*(C10), 3305.
- Chapron, B., V. Kerbaol, D. Vandemark, and T. Elfouhaily (2000), Importance of peakedness in sea surface slope measurements and applications, *J. Geophys. Res.*, *105*(C7), 17195-17202.
- Cox, C., and W. Munk (1954), Measurement of the Roughness of the Sea Surface from Photographs of the Sun's Glitter, *J. Opt. Soc. Am.*, *44*(11), 838-850.
- Elfouhaily, T., D. R. Thompson, B. Chapron, and D. Vandemark (2000), Improved electromagnetic bias theory, *J. Geophys. Res.*, *105*(C1), 1299-1310.
- Gaspar, P., F. Ogor, P.-Y. Le Traon, and O.-Z. Zanife (1994), Estimating the sea state bias of the TOPEX and POSEIDON altimeters from crossover differences, *J. Geophys. Res.*, *99*(C12), 24981-24994.
- Hausman, J., and V. Zlotnicki (2010), Sea State Bias In Radar Altimetry Revisited, , *Marine Geodesy*, *33*(S1), 336---347.
- Markus, T., et al. (2016), The Ice, Cloud, and land Elevation Satellite-2 (ICESat-2): Science 1 requirements concept, and implementation., *Remote Sensing of the Environment*, in press.
- Menzies, R. T., D. M. Tratt, and W. H. Hunt (1998), Lidar In-Space Technology Experiment Measurements of Sea Surface Directional Reflectance and the Link to Surface Wind Speed, *Appl. Opt.*, *37*(24), 5550-5559.
- Plant, W. J. (2015a), Short wind waves on the ocean: Wavenumber-frequency spectra, *J. Geophys. Res. Oceans*, *120*, 2147-2158.
- Plant, W. J. (2015b), Short wind waves on the ocean: Long-wave and windspeed dependences, *J. Geophys. Res. Oceans*, *120*, 6436-6444.
- Urban, T. J., and B. E. Schutz (2005), ICESat sea level comparisons, *Geophys. Res. Lett.*, *32*(23), L23S10.
- Vandemark, D., B. Chapron, T. Elfouhaily, and J. W. Campbell (2005), Impact of high-frequency waves on the ocean altimeter range bias, *J. Geophys. Res.*, *110*(C11), C11006.
- Wu, J. (1972), Sea-Surface Slope and Equilibrium Wind-Wave Spectra, *Physics of Fluids*, *15*(5), 741-747.